THE EFFECT OF GEOLOGICAL ALTERATIONS ON PILLAR STRENGTH

by

PAUL MICHAEL COUTO

Presented in fulfilment of the requirements for the degree

M.Sc. Applied Science (Mining Engineering)

In the Faculty of Engineering, Built Environment and Information Technology

Department of Mining Engineering

21 March 2022

DECLARATION OF ORIGINALITY

I hereby declare that this project is my own unaided work and I have referenced all the sources I have used. It is being submitted in fulfilment of the requirements for the degree M.Sc. Applied Science (Mining Engineering) at the University of Pretoria, Pretoria. It has not been submitted before for any degree or examination at any other university. This document represents my own opinion and interpretation of information received from research or / and interviews. I thus accept the rules of assessment of the University and the consequences of transgressing them.

_____

Paul Michael Couto

14062586

21 March 2022

UNIVERSITY OF PRETORIA
FACULTY OF ENGINEERING, BUILT ENVIRONMENT AND INFORMATION TECHNOLOGY
DEPARTMENT OF MINING ENGINEERING

The Department of Mining Engineering places great emphasis upon integrity and ethical conduct in the preparation of all written work submitted for academic evaluation. While academic staff teach you about systems of referring and how to avoid plagiarism, you too have a responsibility in this regard. If you are at any stage uncertain as to what is required, you should speak to your lecturer before any written work is submitted.

You are guilty of plagiarism if you copy something from a book, article or website without acknowledging the source and pass it off as your own. In effect you are stealing something that belongs to someone else. This is not only the case when you copy work word-by-word (verbatim), but also when you submit someone else's work in a slightly altered form (paraphrase) or use a line of argument without acknowledging it. You are not allowed to use another student's past written work. You are also not allowed to let anybody copy your work with the intention of passing if of as his/her work.

Students who commit plagiarism will lose all credits obtained in the plagiarised work. The matter may also be referred to the Disciplinary Committee (Students) for a ruling. Plagiarism is regarded as a serious contravention of the University's rules and can lead to expulsion from the University. The declaration which follows must be appended to all written work submitted while you are a student of the Department of Mining Engineering. No written work will be accepted unless the declaration has been completed and attached.

I (full names): Paul Michael Couto

Student number: 14062586

Topic of work: The effect of geological alterations on pillar strength.

Declaration

1. I understand what plagiarism is and am aware of the University's policy in this regard.
2. I declare that this thesis is my own original work. Where other people's work has been used (either from a printed source, internet, or any other source), this has been properly acknowledged and referenced in accordance with departmental requirements.
3. I have not used another student's past written work to hand in as my own.
4. I have not allowed and will not allow anyone to copy my work with the intention of passing it off as his or her own work.

Signature _____

Abstract

THE EFFECT OF GEOLOGICAL ALTERATIONS ON PILLAR STRENGTH

Paul Michael Couto

Supervisor: Prof DF Malan

Department: Mining Engineering

University: University of Pretoria

Degree: M.Sc. Applied Science (Mining Engineering)

This study investigated the problem of determining hard rock pillar strength when geological alterations are present in the pillars. These alterations substantially weaken the pillars, and a better understanding of pillar strength will allow for improved designs to be implemented in future. The dissertation includes a literature review and describes three valuable case studies of pillar collapses in Southern Africa. This includes a Zimbabwean operation in the Great Dyke, the Wonderkop Mine in the Western Bushveld and Everest Platinum Mine in the Eastern Bushveld. Access to the Everest Platinum Mine was still possible and most of the work in this study focusses on the pillar behaviour at this mine. A geological alteration is present between the hanging wall and top reef contact at this location, and this resulted in a mine-wide collapse and closure of the mine.

Empirical methods are still popular in the rock engineering fraternity to determine pillar strength. The Hedley and Grant formula, which was derived for Canadian uranium pillars, has been used extensively in the South Africa hard rock pillar designs. Surprisingly, very few collapses of hard rock bord and pillars mines have been reported in the country. This pillar strength formulation therefore seems to be mostly conservative, but its application at the three mines mentioned above did not prevent the collapses of the underground workings.

This study proposed an alternative numerical modelling approach to determine the stability of bord and pillar layouts where alteration layers are present. The displacement discontinuity code, TEXAN, proved to be suitable to analyse and simulate the pillar failure. The capability of the code to simulate irregular-shaped

pillars on a large scale was indispensable for this kind of study. Furthermore, the built-in limit equilibrium model allows the pillar scaling and failure to be simulated. The model contains an interface at the hangingwall and footwall contacts and this appears to be suitable to simulate the effect of geological alterations. For the Everest Mine, two areas were simulated, namely part of the collapsed area and a second area, with larger pillars, that is still stable. This allowed for a first order calibration of the limit equilibrium model.

The calibrated model was subsequently used to explore alternative layout designs for these ground conditions. Barrier pillars will clearly be necessary to compartmentalise the mine. The numerical modelling predicted that the barrier pillars will remain stable, even for large scale collapses, provided their width exceeds 25 m. Main access routes into the mine can be protected by a double row of pillars of at least 15 m wide to provide for a safe travelling way.

In summary, a key finding of the study is that geological alterations substantially reduce the strength of hard rock pillars and a revised design methodology is required. The traditional South African design methodology of using the empirical Hedley and Grant formula does not work in these cases. A displacement discontinuity numerical model using a limit equilibrium model appears to be useful to simulate this pillar behaviour on a mine-wide scale. After calibration of the model, this can be used to explore appropriate layouts and aspects such as the required width of barrier pillars. Further work includes additional calibration of the model and underground monitoring of future layouts to verify the stability of the barrier pillars. A drawback of the current limit equilibrium model is that it is a symmetrical model with partings at both the hangingwall and footwall contacts. In contrast, the pillars at Everest Mine only has a weak alteration layer at the top reef contact and there is a need to extend the limit equilibrium model to better match this mechanism of pillar failure. The time-dependent failure of the pillars was beyond the scope of this study, and this also needs to be explored in future.

Keywords:
Pillar design, pillar strength, geological alteration, limit equilibrium model, displacement discontinuity numerical modelling

ACKNOWLEDGEMENTS

The author would like to acknowledge the assistance given by Willie Theron for allowing the collection of data from Everest Platinum.

A special word of thanks is extended to Mr Jacques Pretorius (General Manager – Eland Platinum Mine), previously Mine Manager of Everest Platinum, and Mr Noel Fernandes, Group Rock Engineer for their personal insight in the case studies. Mr Pretorius' knowledge of Everest was valuable to understand the sequence of events before the collapse. Mr Fernandes personal experience with the mine in Zimbabwe was also beneficial to this study.

Mr Jannie Maritz, Senior Lecturer, University of Pretoria, has not only contributed with academic advice during this study, but has given me valuable moral support.

Dr Michael Du Plessis, Group Rock Engineer, Gold Fields, produced numerous publications on pillars during the past decade. He also provided kind assistance on this topic. His valuable time spent discussing this topic with me is greatly appreciated.

I would like acknowledge Ms Paula Preston, Chief Geologist, for her time in assisting with geological representations.

Thank you to, Prof Francois Malan for all his guidance both academically and personally throughout the duration of this study. The mentorship of such an extra-ordinary person alone is a huge honour and will be cherished forever. The constant motivation and guidance to continue working hard is a motivation for future studies.

Thank you to my family Michael Couto, Marisa Couto and Arthur Couto for sacrificing throughout my lifetime to provide me with a solid foundation and a good education to achieve what I have achieved so far.

Finally, a huge word of thanks to my immediate family. To my wife, Stacey-Lee Couto, son Rowan Couto and daughter Eva Couto, thank you for your patience, sacrifice and support during the time used for this study.

"Hard work will always pay off, perhaps not now but when the time is right."

CONTENT

LIST OF FIGURES

LIST OF TABLES

LIST OF ABBREVIATIONS

APS	Average Pillar Stress
BC	Bushveld Complex
CMRCC	Coal Mines Research Controlling Council
COMRO	Chamber of Mines Research Organisation
COP	Code of Practice
CSIR	Council for Scientific and Industrial Research
DMRE	Department of Mineral Resources and Energy
DRMS	Design Rock Mass Strength
FLAC	Fast Lagrangian Analysis of Continua
FoG	Fall of Ground
FoS	Factor of Safety
GSI	Geological Strength Index
LoM	Life of Mine
mbs	meters below surface
RLS	Rustenburg Layered Suite
RMR	Rock Mass Rating
TAT	Tributary Area Theory
TCS	Triaxial Compressive Strength
TRC	Top Reef Contact
UCS	Uniaxial Compressive Strength
UG2	Upper Group 2

1 INTRODUCTION

The strength of hard rock pillars has been studied extensively and a large number of publications are available on this topic (see for example Martin and Maybee, 2000; Malan and Napier, 2011). Pillar design in the Southern African hard rock industry is mostly still based on the Hedley and Grant (1972) pillar strength formulation developed for different rock types. In comparison, extensive research on pillar strength in the coal industry, following the Coalbrook Colliery disaster (Van der Merwe, 2006), has resulted in a much better understanding of coal pillar strength in South Africa. Historically, behaviour of the rock mass in the gold mining sector in the Witwatersrand Basin has also been extensively studied and many research studies were conducted. The key driver for these studies was the importance of gold production in the South African economy. Research on layouts and pillar strength for the chrome and platinum mining sector in South Africa has unfortunately not received the same attention. Owing to a lack of pillar strength formulae, the Hedley and Grant power-law strength formula, as given below in equation (1.1), was adopted. The K-value is typically modified to suit local conditions.

$$P_s = K\left(\frac{w^{\alpha}}{h^{\beta}}\right) \quad (1.1)$$

where:

P_s = Pillar strength

K = in situ strength of the rock mass (typically a down-rated value of the UCS)

w = pillar width

h = pillar height

α = 0.5

β = 0.75

Extensive work was conducted for different orebodies and commodities to determine the most appropriate value of K as described in Chapter 2 (also see Malan and Napier, 2011). The Hedley and Grant exponents has nevertheless always remained as the basis for these various “calibrated” equations. Almost no work has been conducted when a geological alteration or other weak layers are present in the pillars. Pillar

failures for these conditions have occurred in UG2 pillars in the platinum industry in South Africa and in Zimbabwe for mines in the Great Dyke.

Hartzenberg et al (2020) defines alteration layers as follows: "*The hangingwall contact of the UG2 Chromitite Reef at these sites consists of pyroxenite. The pyroxenite layers have been exposed to hydrothermal fluid flow, serpentinization and layer-parallel shearing. The resulting clay-like material (weak partings) is defined as the alteration zone*." This definition of alteration zones in the last sentence of the quote is also adopted for this study.

A study by Malan and Napier (2011) has shown that geological alterations may be present in the pillars in both the Western and Eastern Bushveld. These have a detrimental effect on pillar strength and on overall mine stability. Any weak layers in the pillars need to be carefully considered when mine designs are conducted. Figure 1-1 illustrates such a weak layer in a pillar and the resulting failure of a pillar with such a layer is shown in Figure 1-2.

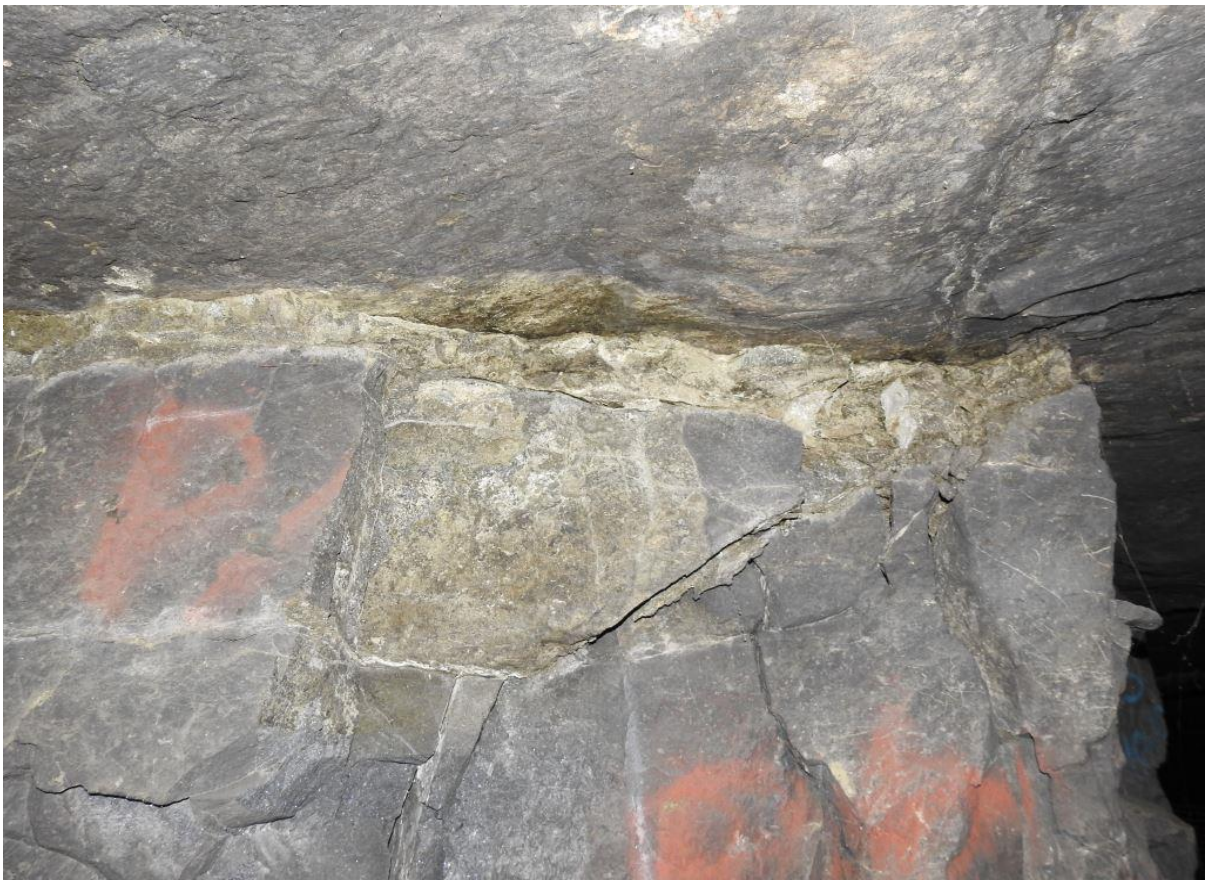

Figure 1-1. A weak alteration layer visible at the contact between the pillar and the hangingwall.

Figure 1-2. Typical pillar failure in areas where weak alteration zones are present.

This study investigated the underground conditions at three mines where failure has occurred due to this geological alteration. This is a valuable reference for rock engineering practitioners as these case studies have never been recorded in literature that is readily available. The collapse at Everest Mine was studied in detail. The TEXAN numerical modelling code was used for this case study to investigate if the pillar failures can be successfully simulated with a limit equilibrium model. The TEXAN code was also utilised to investigate modified layouts for future mine designs in similar ground conditions in the Bushveld Complex.

1.1 Research background

As discussed above, an understanding of the effect of geological alterations on pillar strength is important for future mine designs. The approach followed in this study was to collect as much information as possible on historic pillar failures in mines in the Bushveld Complex, South Africa and in the Great Dyke, Zimbabwe. Additional focus was placed on one particular case study, Everest Platinum Mine, as information on this collapse was readily available and access to the operation, both underground and on surface, was still possible. The data collected was used as input for the TEXAN numerical modelling code. This code was particularly useful to simulate the pillar failure on a large scale. A key aspect of this study was to investigate the applicability of a limit equilibrium model constitutive model for pillars containing weak alteration layers. Following a calibration of the model, the TEXAN code was used to conduct an analysis of layouts using barrier pillars to determine if these barrier pillars can arrest large scale collapses.

1.1 Problem statement

Currently, there is not a suitable methodology available to design a pillar system where a prominent geological alteration layer is present. To develop such a methodology, the effect of the geological alteration on pillar strength needs to be quantified and a better understanding of the failure mechanism must be obtained. As indicated in the literature study, such a study has never been conducted in South Africa. A conservative pillar design is one of the current options for future mine designs. This, however, reduces the extraction ratio of the orebody substantially and stability is still not guaranteed. It is therefore clear that an improved design approach for pillars with geological alterations is required for hard rock chrome and platinum mines. The objective of this study is to investigate the effect of a weak geological alteration layer on the pillar strength. Data collection from Everest Platinum Mine and TEXAN numerical modelling were used to understand the pillar strength.

1.2 Methodology

This topic was studied by conducting a literature survey and by collecting underground data and observations from the Everest Platinum Mine. Two other case studies were also included in the study as these provided additional insight into the problem. Unfortunately, for these two additional case studies, access to the underground workings was not possible. An extensive description of the Everest Platinum Mine is given in the document to provide the necessary geological and mining background. This is a valuable case study as the sequence of events leading to the collapse is available. The original pillar designs for the three case studies were studied to determine what methodology and parameters were used.

Numerical modelling was utilised to determine if the failure of the pillars and the collapse of the mine can be simulated using a limit equilibrium model (TEXAN Code). This was the first attempt ever to simulate these types of pillars with a limit equilibrium model. The advantages and disadvantages of the model is described in this dissertation. The difficulty of calibrating the model is also discussed in the document. This approach provided a methodology that can be utilised in the future for mines that have similar geological conditions.

2 LITERATURE REVIEW

2.1 Introduction

On 21 January 1960, 437 coal mine workers lost their lives when a large number of pillars collapsed at Coalbrook Colliery in South Africa. The collapse covered an estimated area of 324 hectares. This disaster led to the establishment of the Coal Mines Research Controlling Council (CMRCC). Following this disaster, the Council for Scientific and Industrial Research (CSIR) and the Chamber of Mines Research Organisation (COMRO) also commenced with larger scale in-situ testing programs and other studies to determine the strength of coal pillars.

Salamon and Munro (1967) conducted a key study on coal pillar strength. They developed their famous equation by assuming a power-law strength equation and calibrated the parameters using a database of collapsed pillars with the maximum likelihood method. The "power-law formula" for the strength of the pillars was proposed much earlier by Greenwald et al (1941). The Salamon and Munro formula was therefore an empirical equation based on a database of 125 cases which included 27 pillar collapses. Important to note was that the authors stated:

"*The work described in the paper is essentially empirical and the results, therefore, should not be extrapolated beyond the range of data which were used to derive them*."

The formula is given by:

$$Strength_{(coal)} = 7.2\ MPa\ \frac{w^{0.46}}{h^{0.66}} \qquad (2.1)$$

where

7.2 MPa = in situ strength of 1 m³ of coal

w = pillar width

h = pillar height

Wagner and Madden (1984) reported that since 1967 approximately 1100 million tonnes of coal had been mined in South Africa and they estimated that 1.2 million pillars were left underground during this period. During the same period, only 13 cases of pillar collapses were reported, involving a total of 4000 pillars. This corresponded to a probability of failure of only 0.003 (Malan and Napier, 2011).

Jager and Ryder (1999) illustrated data from laboratory and field tests that the width-height strengthening curve has a positive upwards curvature, however this was for rock materials. In spite of this wide adoption, criticism has been raised regarding this coal pillar formula as well. In contrast, the formula given in equation (2.1) forces downwards curvature. Bieniawski and Hustrulid (1976) also raised objections in relation to the volumetric size effect and they proposed the “linear” equation as an alternative. The linear equation does not consider the volumetric size effect. This equation is shown below:

$$Strength\ (Coal) = K\ (0.64 + 0.36\ \frac{w}{h}) \tag{2.2}$$

where

K = the strength of a unit cube of coal

w = pillar width

h = pillar height

A more general form of the linear formula is given by Bieniawski and Van Heerden (1975):

$$P_{Strength} = K\ \left[B + (1 - B)\frac{w}{h}\right] \tag{2.3}$$

where

K = the strength of a unit cube of coal;

B = constant

w = pillar width

h = pillar height

The database used by Salamon and Munro only contained pillars with a w:h < 3.8. Beyond a critical width to height ratio, it seemed as if the pillar strength exceeds that predicted by equation (2.1). Salamon (1982) therefore proposed that when the width to height ratio exceeds a critical ratio, the “squat pillar” formula needs to be used. From data collected in the mines, it seemed as if there were no collapses of pillars with a width to height ratio greater than four. The critical width to height ratio to use the squat pillar formula was selected as five (Salamon, 1982). A form of the squat pillar is

$$P_{S\_coal} = KV^{-0.0667}R_o^{0.5933}\ \left\{\frac{0.5933}{\varepsilon}\left[\left(\frac{R}{R_o}\right)^{\varepsilon} - 1\right] + 1\right\} \tag{2.4}$$

where

K = the strength of a unit cube of coal

V = Pillar volume (m^3)

R = Pillar w:h ratio

R_o = the critical width to height ratio

ε = rate of pillar strength increase

Further work on coal pillar strength was conducted by workers such as Van der Merwe, (2006) and (2019), but it is beyond the scope of this study and the reader is referred to these references for additional information. In conclusion, Ryder and Jager (1999) stated:

> *"The power law and its derivatives are perhaps too entrenched in coal engineering to warrant withdrawal from them at this time, but in hard rock engineering, the simpler and probably more realistic linear forms are advocated for general use."*

Owing to the large economic contribution of the gold mining industry in South Africa and the role the coal industry played in the required power generation, these two commodities received the bulk of the research funding. Other mining industries never received the same focus and funding in terms of research (Malan and Napier, 2011). This resulted in the pillar strength formulae and information from overseas mines being used to design pillars in the hard rock Bushveld Complex mines.

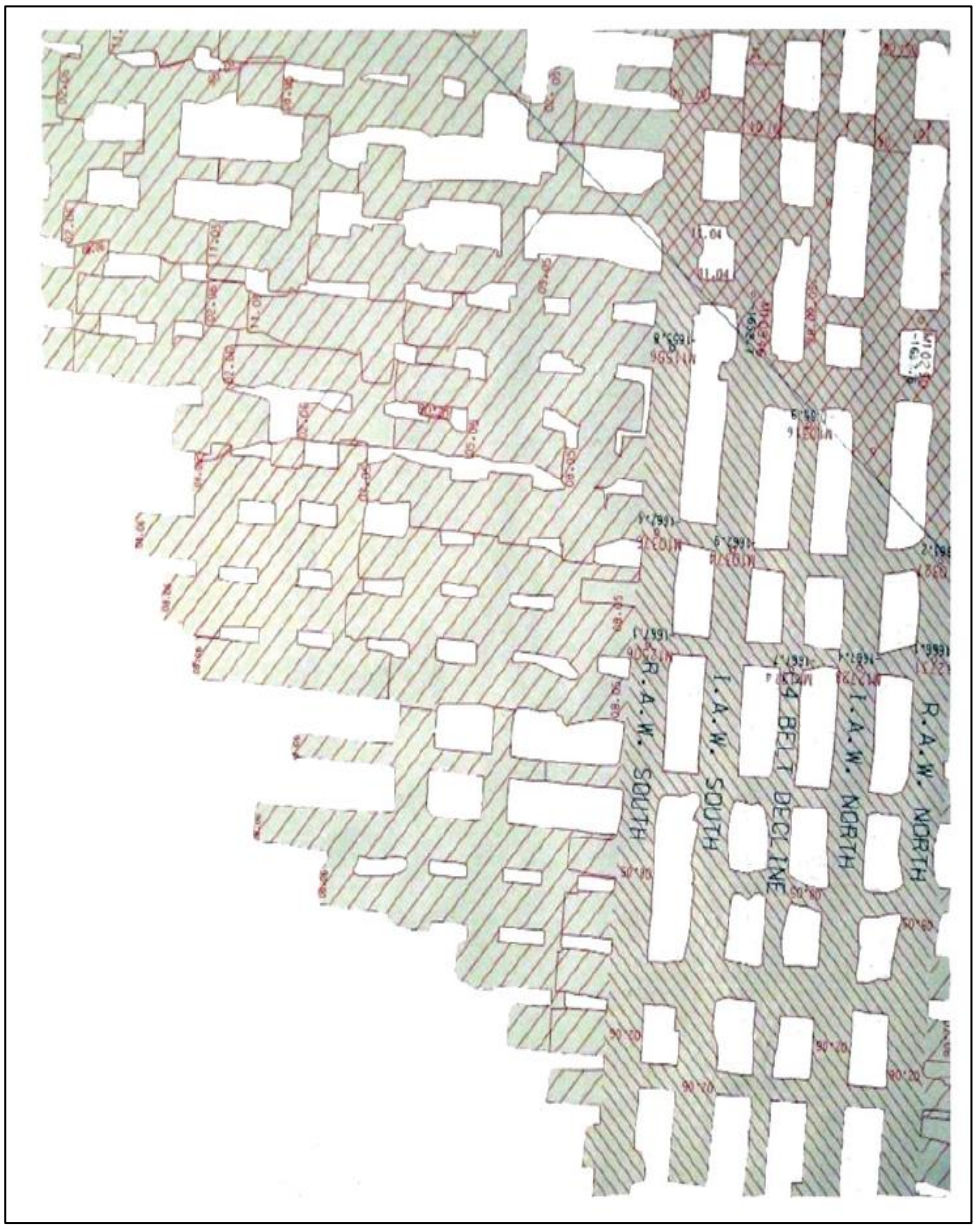

Figure 2-1. Poor pillar cutting in an underground platinum mine in the Bushveld Complex (after Malan and Napier, 2011).

Figure 2-1 illustrates a plan view of typical pillar shapes at a mine in the Bushveld Complex. Typically, the pillar cutting is poor, and the pillars have a range of shapes. Furthermore, Gay et al. (1982) stated:

> *"The design of pillar layouts in shallow to medium depth chromium and platinum mines has not reached the same advanced stage as has the design of pillars in coal mines"*

Three reasons were given for this namely:

- There is no information on the strength of pillars consisting of chromitite and Merensky Reef ore.
- There are competent and stiff strata in the hangingwall, and it may cause problems when attempting to determine the pillar load.
- The shear component along near geological discontinuities can alter the loading condition from a stiff displacement-controlled system to a soft load-controlled system.

The Hedley and Grant pillar formula was adopted by the mines in the Bushveld Complex in the 1970's as no other suitable formula was readily available. The origin of this formula is described below.

As described in Hedley and Grant (1972), the Ontario Department of Mines appointed a committee in 1958 to study the accidents and the mining methods in the Elliot Lake District. The report of this committee described the existing methods for mine design, pillar support and determining stable roof spans. It is concluded in this report:

"There is much about pillar loading and pillars strength that we do not know. This gap with the present facilities can be greatly narrowed for the stronger rock types. Stress measurements as a practice are in their infancy but making progress. A better knowledge of stress distribution in mines in the prerequisite for improved mine designs…." and *"at the present time scientific knowledge can be applied to the problems of ground control only in a quantitative manner. Quantitatively the answers must still be confirmed by actual practice. In many cases, this will probably continue to be so, but in many other, a better organisation and application of data that has been and can be made available to the industry would greatly reduce dependence on trial and error methods".*

The data collected to develop the Hedley and Grant pillar formula was from the uranium mines in the Elliot Lake district. These mines used rib pillars. The data collected was sparse, as seen below in Figure 2-2 and Figure 2-3. Of concern regarding the current wide-scale adoption of the formula in South Africa is that there were only three failed pillars in the database. The authors estimated the stress on the pillars using tributary area theory and this was probably not accurate owing to abutments being present. The value for $\alpha = 0.5$ was adopted as this value was commonly used in literature and the three failed pillar cases were used to back-calculate the β–value. A value of 0.75 was obtained. This was a crude approach, and it is therefore surprising that this formula is still widely used in the South African mining industry. This aspect was also highlighted by Malan and Napier (2011) more

than a decade ago. The formula has already been shown in Chapter 1 as equation (1.1) and it is not repeated here.

TABLE 2 — Comparison of Measured and Estimated Pillar Stresses

Depth ft	Extraction %	Measured Stress, psi		Estimated Stress, psi	
		Range	Average	Average	+ 5% Extraction
920	85	5500 — 13700	8700	8000	6000 — 12000
970	85	6300 — 12300	8100	8300	6200 — 12500
1050	85	7900 — 10600	9600	8900	6600 — 13300
1050	40	1500 — 3200	2400	2000	1800 — 2200
1180	85	4800 — 6800	5600	9700	7300 — 14600

Figure 2-2. Comparison of measured and estimated pillar stresses in the famous Hedley and Grant (1972) paper.

TABLE 3 — Dimensions and Estimated Stress and Strength of Pillars

Depth ft	Dip deg.	Extraction %	Pillar Width ft	Pillar Height ft	Estimated Pillar Stress psi	Estimated Pillar Strength psi
Stable Pillars						
500	17	85	10	10	5000	14600
700	17	85	10	10	6400	14600
800	26	65	20	18	3800	13300
850	20	85	10	10	7600	14600
950	11	85	10	10	7500	14600
1000	22	65	20	18	4000	13300
1050	15	85	10	10	8500	14600
1200	18	85	10	10	9400	14600
1300	20	65	20	20	4600	12300
1600	20	60	20	18	4800	13300
1600	20	65	18	18	5400	12600
1600	22	75	20	14	7600	16000
1700	22	65	40	20	5800	17400
1700	22	60	22	20	5000	12900
1700	12	75	20	14	7600	16000
1800	5	75	20	14	8000	16000
1900	23	65	19	18	6400	13000
2200	25	65	20	20	7200	12300
2400	11	65	20	8	7600	24400
2500	9	65	20	8	7900	24400
2700	13	65	20	8	8600	24400
2900	12	70	15	9	10500	19400
2900	12	75	20	9	12600	22400
Partially Failed Pillars						
1400	20	85	10	10	11400	14600
2400	18	80	10	9	13400	15800
Crushed Pillars						
2800	12	80	10	9	15200	15800
2900	12	80	10	9	15700	15800
3400	5	80	15	10	18500	17900

Figure 2-3. Dimensions and estimated strength and stresses of pillars as given in the Hedley and Grant (1972) paper.

The geotechnical conditions and layouts at Elliot Lake do not have any resemblance to the current mining layouts and pillar geometries in South Africa. Surprisingly, this has not prevented the adoption of this formula throughout the industry and it was used for numerous mine designs.

Apart from the Hedley and Grant formula, other empirical equations have been developed to predict pillar strength. A good overview of these can for example be found in Martin and Maybee (2000). The strengths predicted by these formulae are illustrated in Figure 2-4. Furthermore, Figure 2-5 shows a comparison of the predicted rib-pillar strength using numerical modelling versus the observed rib pillar behaviour in the Elliot Lake uranium mines.

These alternative empirical pillar strength formulae will not be explored further in this document as, similar to the Hedley and Grant formula, these were developed for different rock types and cannot take the effect of a weak alteration layer into account.

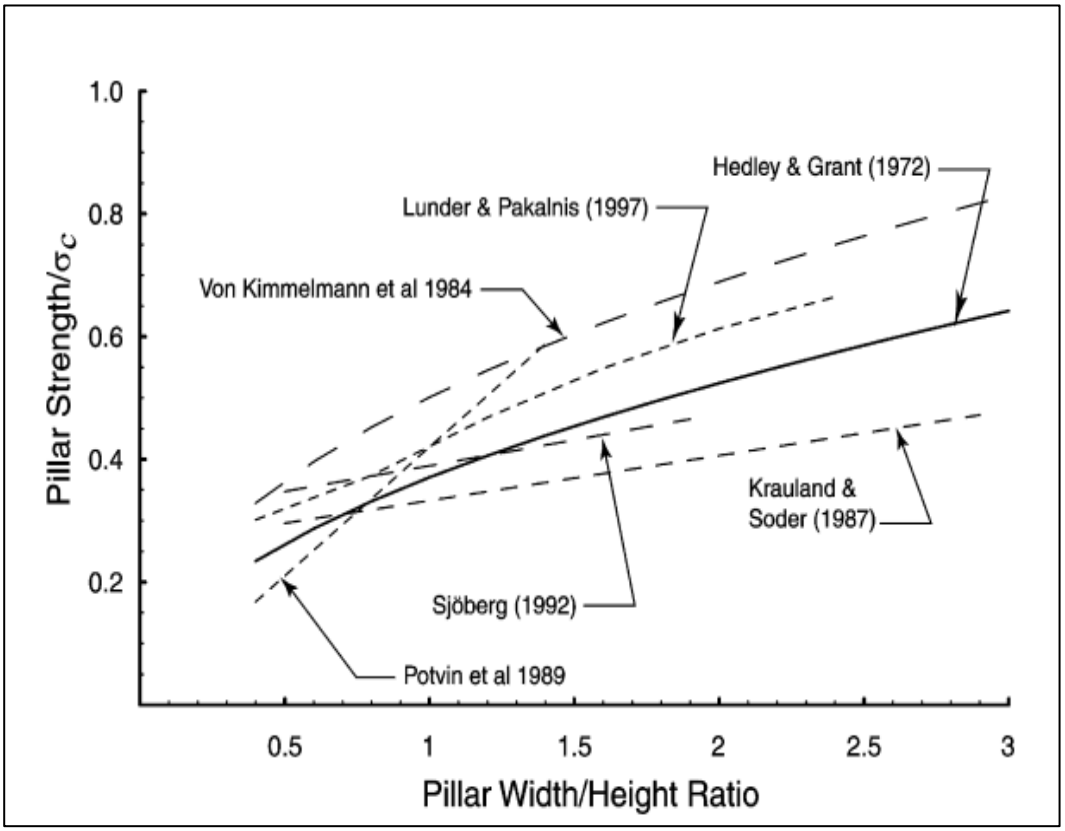

Figure 2-4. A comparison of the different empirical pillar strength formulas (after Martin and Maybee, 2000).

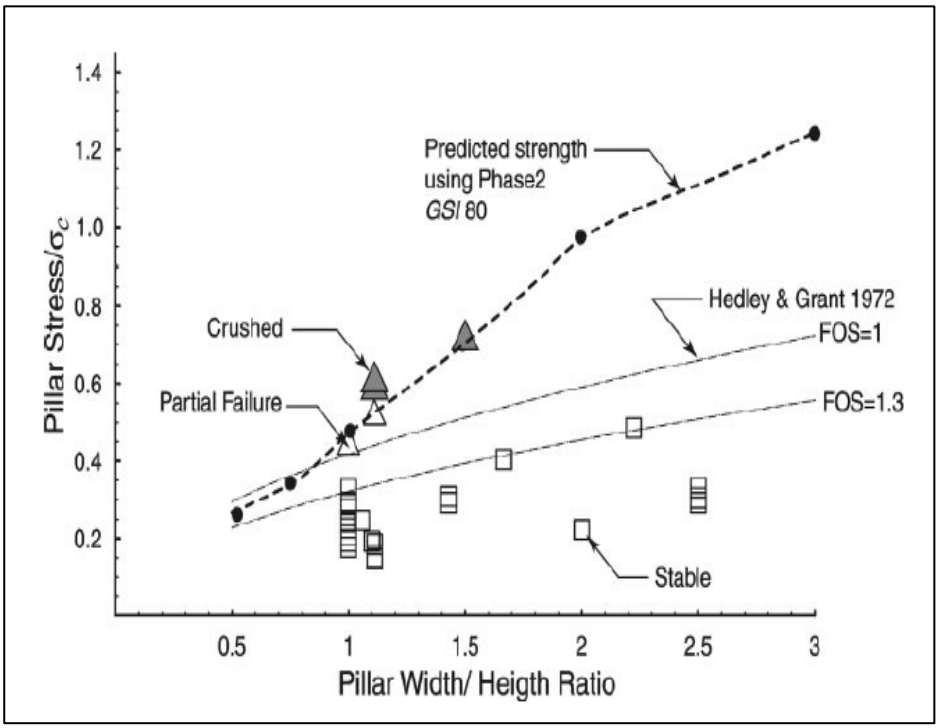

Figure 2-5. A comparison of the predicted rib pillar strength versus the observed rib pillar behaviour in the Elliot Lake uranium mines (Martin and Maybee, 2000).

Regarding developments in South Africa, to reflect local rock strengths, the K-value of the Hedley and Grant formula was modified by rock engineering practitioners and mining consultants. This approach seemed to work well if no geological alteration layers were present and it has now become firmly entrenched. As state by Malan and Napier (2011), it is currently the industry accepted "*method for designing pillars in shallow hard rock mines in South Africa*." The K-values used in South African mines for pillar designs typically ranges between one third and two thirds of the laboratory uniaxial compressive strength of the rock material.

As a proposed improved method of calibration, Stacey and Page (1986), Laubscher (1990) and Stacey and Swart, (2001) proposed that the value of K should be the DRMS (Designed Rock Mass Strength) value. The DRMS takes into consideration the rock quality, unfavourable geological discontinuities, and the method of excavation. Unfortunately, subjective decisions still need to be made to assign parameter values when calculating DMRS and it is not entirely satisfactory. The pillar strength, $P_{Strength}$, is then given by:

$$P_{Strength} = DRMS\ \frac{w^{\alpha}}{h^{\beta}} \qquad (2.5)$$

Interestingly, Swart et al. (2000) conducted a study on LG6 chromitite pillars and concluded that for the exponent, it is more applicable to use $\alpha = \beta = 1$. This would then be a modification of the linear equation given in equation (2.3).

Watson et al. (2008) derived new values for the power law formulation for Merensky reef pillars in a PlatMine project. This formula is (the parameters are similar to those described below equation (1.1) and only the exponents differ)

$$P_s = K \frac{w^{0.76}}{h^{0.36}} \tag{2.6}$$

A maximum likelihood evaluation similar to that of (Salamon and Munro, 1967) was used. A total of 179 pillars were assessed of which 109 were stable. The pillars had a w:h ratio ranging between 1 and 8. The values derived from the research were K = 86 MPa, α = 0.76 and β = 0.36.

The PlatMine formula predicts a much greater pillar strength than the Hedley and Grant formulation for which it is typically assumed that $K = \frac{1}{3}UCS$. Malan and Napier (2021) illustrated that for power-law formula where $\alpha > \beta$, the formula predicts an increasing strength for larger pillar volumes if the w:h ratio remains constant. This is illustrated in Figure 2-6. This increase in strength is counterintuitive.

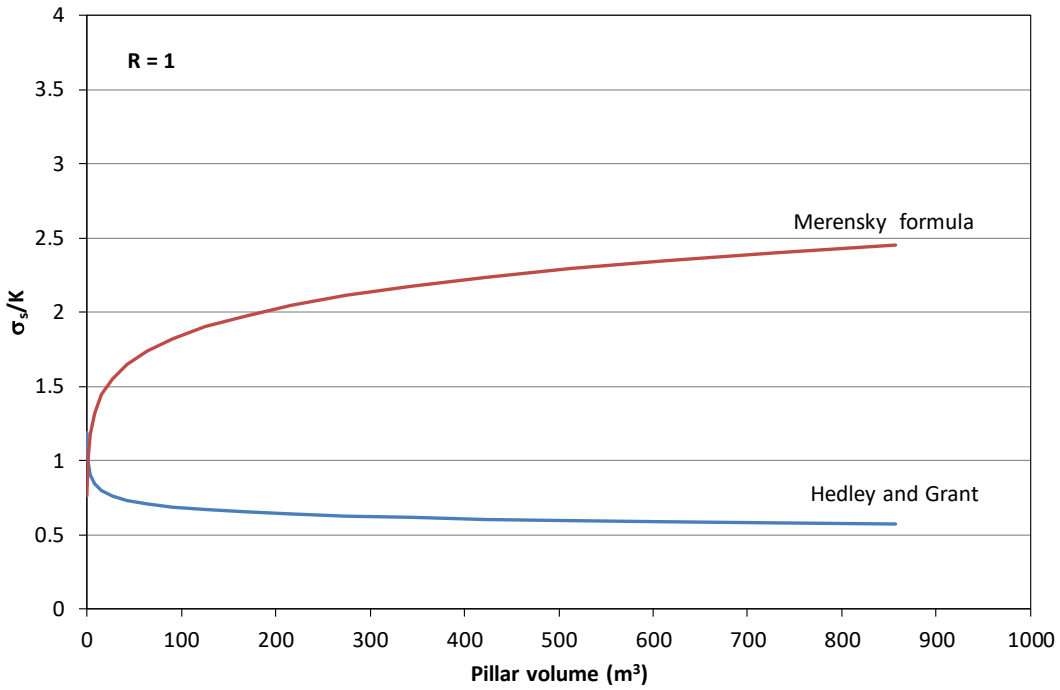

Figure 2-6. Diagram illustrating the effect of pillar volume on strength for a constant w:h ratio of $R = 1$ (after Malan and Napier, 2021).

From the available literature, it is currently not clear what the best method is to estimate pillar strength. Some workers favour empirical solutions, while others advocate the use of

numerical models with appropriate failure criteria such as Hoek and Brown (see, e.g., Malan and Napier, 2011). Calibration of complex inelastic models, however, is challenging and this method is therefore not necessarily always an improvement when compared to empirical pillar strength equations. A good example is given in Chapter 3 in equations (3.1) to (3.4). After the Everest Mine collapse, as an alternative to the Hedley and Grant pillar strength equation, numerical modelling using a Hoek-Brown strength criterion was proposed. Equations (3.1) to (3.4) are empirical equations, developed for other rock types, which used to calibrate the parameters used in the Hoek-Brown criterion at Everest Mine. In summary Malan and Napier (2011) state the following in the conclusion of their paper:

> *"In conclusion, it appears that neither empirical techniques nor numerical modelling can be used solely to provide a solid basis to predict pillar strength."* and *" The need for additional research into pillar strength should also be emphasized strongly as this problem has clearly not yet been solved! ".*

Regarding average pillar stress (APS), tributary area theory (TAT), which divides the overburden load equally on individual pillars for a regular, infinite layout, is commonly used. Using TAT, the average pillar stress (APS) is given by:

$$APS = \frac{\sigma_v}{(1-e)} \qquad (2.7)$$

where

σ_v = Virgin vertical stress

e = Extraction ratio

Numerical simulations of pillar stress are preferable, however, as the effect of abutments and different pillar sizes can be easily accounted for (Napier and Malan, 2011).

2.2 Effect of geological alterations on pillar strength

The literature study revealed that almost no information is available on the effect of weak alteration layers on pillar strength. Malan and Napier (2011) investigated the reduction in pillar strength caused by weak layers. They describe FLAC numerical modelling of a pillar containing weak interfaces. The rock material was simulated using a strain-softening model with parameters which were obtained from studies in the Bushveld Complex. The model used symmetry for both the vertical and horizontal centrelines as shown in Figure 2-7. A grid size of 0.1 m × 0.1 m was used. The complete stress-strain response was modelled as shown in Figure 2-8. The presence of a weak interface inside the pillar had virtually no effect,

even if the friction angle was as low as 6°. In contrast, the friction angles on the hangingwall contact (interface 2) had a strong effect. Varying this parameter reduced the peak strength of the pillar by reducing the confinement and reducing the residual strength (Figure 2-9).

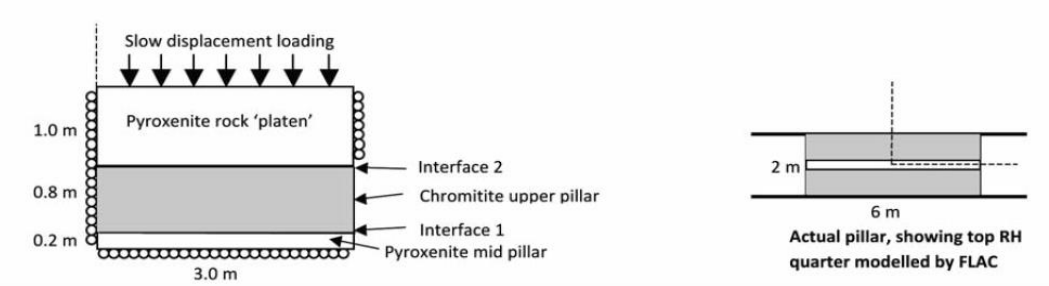

Figure 2-7. The geometry used in the FLAC modelling to simulate the effect of weak interfaces in a pillar (after Malan and Napier, 2011).

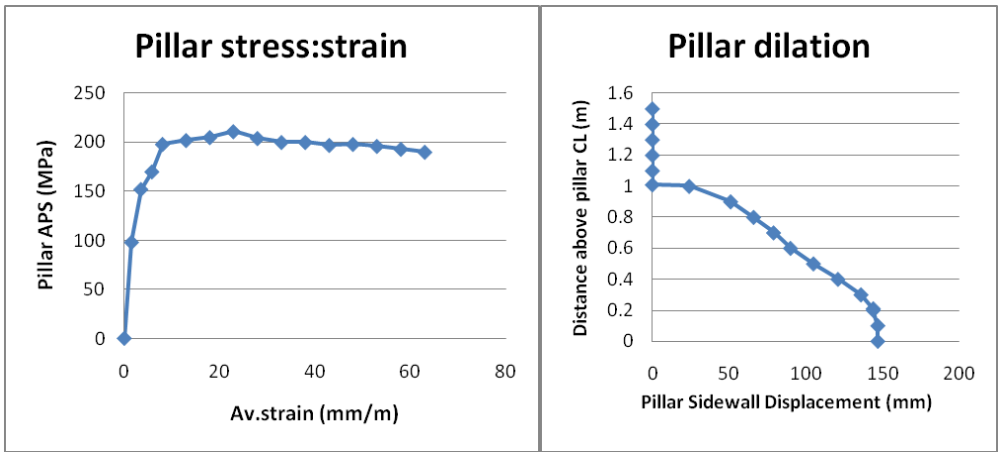

Figure 2-8. Pillar stress as a function of strain (left) and sidewall dilation (for the peak strength) (right) when the interface friction angle is 30° (after Malan and Napier, 2011).

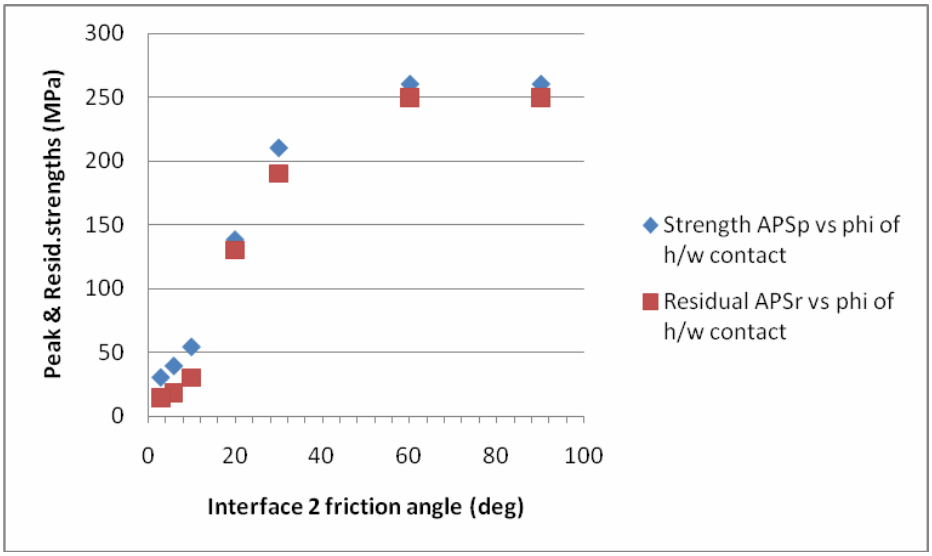

Figure 2-9. Changes in the peak and residual pillar strength for various values of hangingwall contact friction angle (after Malan and Napier, 2011).

Iannacchione (1990) investigated the effect of interfaces with a low friction angle in coal pillars. He concluded that the interface slip affected the rate at which the failure zone develops in the pillar. The interface slip mechanism allows the failed coal pillar to move into the mine opening. He concluded that the effect of interface slip should be considered when designing large coal pillars as ignoring these layers may result in an overestimation of the pillar strength.

Esterhuizen and Ellenberger (2007) investigated the effect of weak bands on pillars in stone mines in the United States. From numerical modelling and field observations, it was concluded that an extrusion-tensile failure mode initiates at the perimeter of a pillar and progresses inwards. This reduces the effective width of the pillar. Weak bands can cause rib failure to initiate when the average pillar stress is only about 10% of the limestone strength. Slender pillars are more severely affected by the presence of weak bands than wider pillars and pillar strength is adversely affected as the thickness of the weak zones increases. Furthermore, the investigation illustrated that single weak bands could have a significant effect on pillar strength if their thickness exceeds about 2% of the pillar height.

Maritz and Malan (2011) studied the shear stresses acting on weak partings in pillars. Numerical modelling was conducted using the TEXAN code and a number of bord and pillar layouts at various dip angles were simulated. The modelling indicated that the shear stress on the partings increases when the dip of the reef increases and the tendency for slip therefore becomes greater. Instability may occur if the contact does not have a “critical” minimum friction angle. More O’Farrell and Malan (2012) also investigated the effect of weak layers on pillars strength. This research mainly served the purpose of highlighting the problem and did not present any solutions to better estimate the strength of pillars containing these layers. Hartzenberg et al. (2020) highlighted that the stability of pillars is compromised by the presence of a weak geological alteration layer. This affects the ability of the pillars to function according to the planned design. It is clear from this paper that only a limited understanding of the effect of weak geological alteration layers is available.

2.3 Laboratory test work

As discussed above, it is well known that a weak geological layer between the hangingwall and pillar contact could possibly reduce pillar strength ability and overall strength. Wagner (1980) commented on this issue and noted that the friction and cohesion in the contact plane between the pillar and hangingwall will affect the overall performance of the pillar. Peng (1978) illustrated during a series of laboratory tests that the strength can vary by as much

as 100% depending on the conditions of the rock-sample and the testing machine interface. This was also reported by Wagner (1980). Wagner's tests results showed that the presence of a weak geological layer between the rock and testing machine platen interface reduces the strength of the rock sample and changes the mode of failure of the specimen as shown in Figure 2-10. Unfortunately, a better photograph could not be found, but it is included in the dissertation to illustrate the effect. The mode of failure changes from "hour glassing" and scaling on the edges for the higher friction angles to axial splitting for the lower contact friction angles.

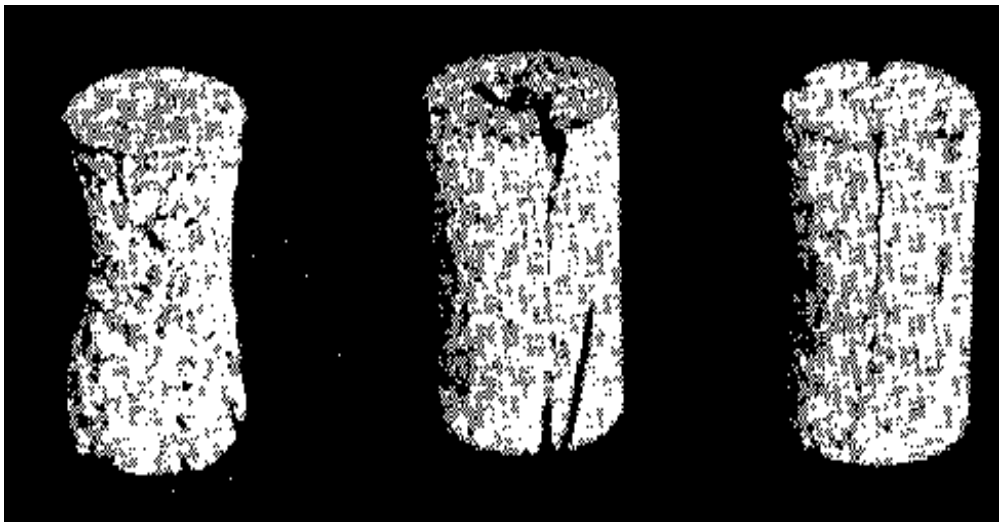

Figure 2-10. The effect of end constraints on the mode of failure of rock samples. This shows: An interface between rock and platen with no "infilling" (left). Thin lead sheath on both contacts (centre). Thin lead sheath on top contact only (right) (after Wagner, 1980).

Prophetically, Wagner (1980) emphasised that the method of predicting pillar strength must take the effect of the hangingwall and footwall contacts into account. He emphasised that this is often ignored and numerous pillar failures could be attributed directly to the application of empirical pillar strength formulae for simulations that were not comparable with those for which the formulae was derived.

To illustrate the different modes of actual underground pillar failure, Figure 2-11 shows the typical failure observed for pillars with "frozen" (high friction angle) pillar and hangingwall contacts. Figure 2-12 shows the same mode of failure mode observed at Hossy Shaft where UG2 was mined. Hossy shaft is a shallow platinum mine on the western bushveld near Wonderkop Mine.

Figure 2-11. An example of pillar scaling in areas where there is a “frozen” interface between the pillar and the hangingwall. The typical “hour-glass” failure mode is evident (photograph courtesy F. Malan).

Figure 2-12. An examples of pillar scaling in areas where there is a “frozen” interface between the pillar and the hangingwall at Hossy shaft. Again, this results in the typical “hour-glass” failure mode (photograph courtesy F. Malan).

2.4 Summary

From the literature study, it is clear that pillar design for hard rock bord and pillar operations in South Africa is mostly done using the Hedley and Grant empirical strength formula. This formula has been mostly used with success for many decades. Recent examples of large-scale pillar collapses highlighted the role of weak alteration zones that were present in the failed pillars. Currently to estimate the strength of pillars using appropriate failure criteria in South Africa a range of methods with varying complexities are used. For the empirical equations, care should be exercised that these calibrated equations and numerical models are not used for geotechnical areas beyond the environments in which they were developed for. This is also applicable to the Hedley and Grant formula that was derived for the Canadian uranium mines. Surprisingly, almost no collapses have been reported in South Africa for pillar layouts designed using this formula. It may therefore give estimates of pillar strength that are too conservative. This is clearly not the case, however, if weak geological alteration layers are present.

The literature survey highlighted that almost no information is available on appropriate design methodologies if weak geological alteration layers are present in the pillars. This is an area where numerical modelling can be used to determine pillar stresses accurately and to simulate specific pillar failure mechanisms, such as the influence of weak partings on pillar strength.

This study explores the use of a specialised numerical modelling code, TEXAN, with a limit equilibrium model, to simulate the effect of weak geological alteration layers on pillar strength. To further illustrate the detrimental effect of weak layers on pillar strength, three case studies of large mine collapses are discussed in the next chapter.

3 CASE STUDIES OF PILLAR FAILURES

3.1 Introduction

The three case studies described in this chapter, Mine A, Wonderkop Chrome Mine and Everest Platinum Mine, provide a valuable record of incidences where large-scale pillar collapses occurred. In all three cases, a weak geological alteration layer was present and the layouts were designed using the Hedley and Grant pillar strength formula. Mine A is situated in the Great Dyke and the following quote from Roberts and Clark-Mostert (2010) is therefore relevant:

"Fault gouge can be associated with flexural slip thrust faults and, if the bord and pillar mining method is employed and fault gouge is present in the vicinity of the reef, the integrity of the mining operations can be severely compromised and, in some cases, have been abandoned. Following recent work on the Great Dyke, the authors put forward some evidence that flexural slip thrust faults are also present in the Great Dyke. If this premise is correct, then mining methods and support strategies for mining operations on the Great Dyke will be required to be modified to take into account the presence of these geological structures."

The sections below give addition details of the three case studies. The information for the first case study is not in the public domain and therefore the mine is simply referred to as "Mine A".

3.2 Mine A - Platinum Mine – (Zimbabwe)

Mine A is situated on the southern edge of the Hartley Geological Complex that forms part of the Zimbabwean Great Dyke. It is located halfway between Harare and Gweru as shown in Figure 3-1.

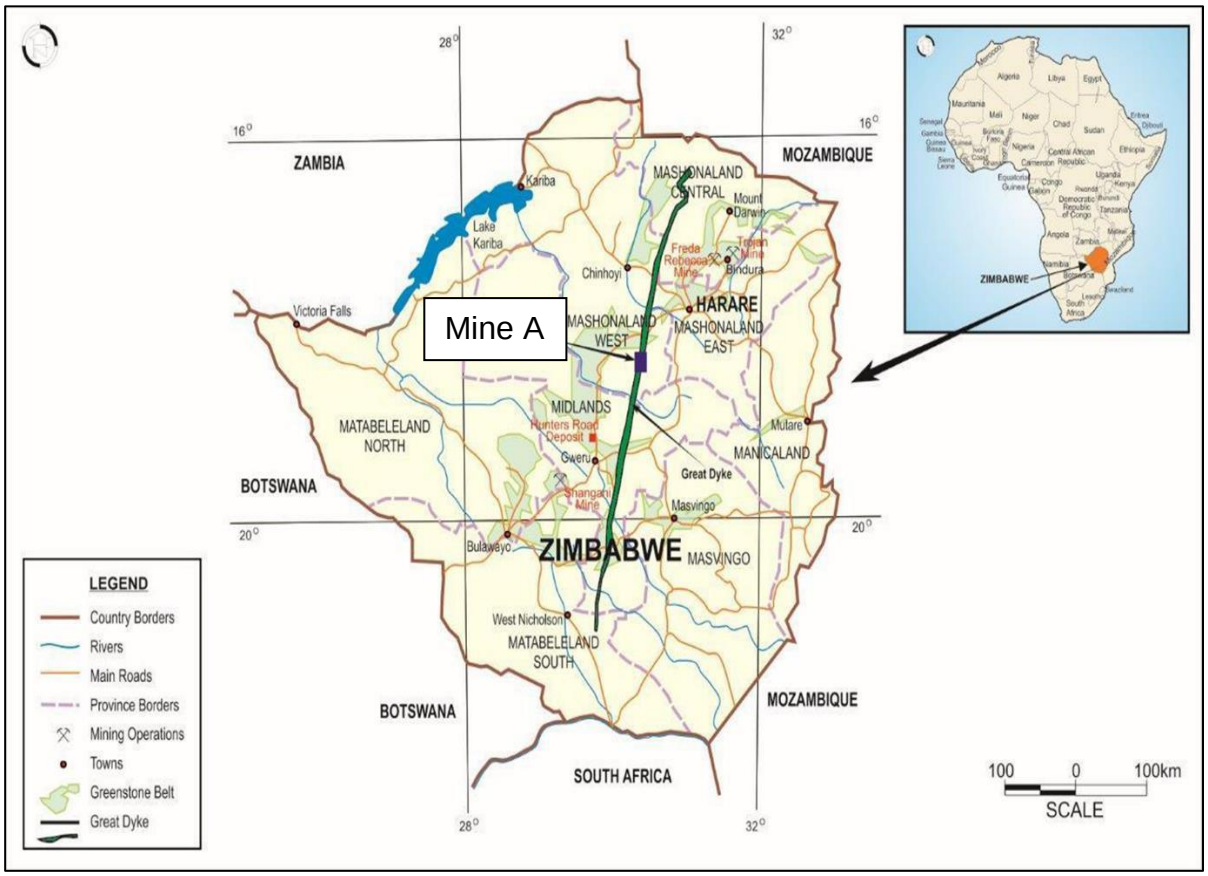

Figure 3-1. Location of Mine A between Harare and Gweru.

The Great Dyke is a 550 km long layered mafic-ultramafic igneous intrusion. Geometrically, the dyke is a narrow linear structure, has an NNE trend and varies from 4 km to 12 km wide. The country rock into which the dyke intruded are the granitoid and greenstone belts of the Archean Zimbabwe Craton. At the Hartley Complex, the Main Sulphide Zone is preserved (as shown in Figure 3-2 and Figure 3-3). The Main Sulphide Zone is the host rock for the platinum deposit at Mine A.

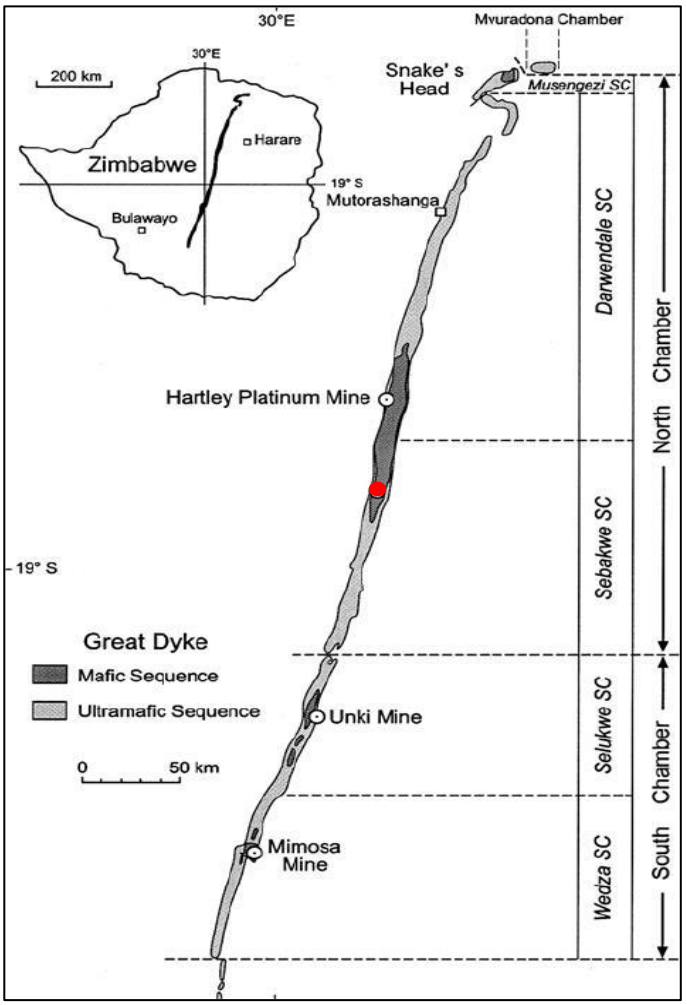

Figure 3-2. Location of Mine A (red dot) in relation to the North and South chambers of the Great Dyke (courtesy N. Fernandes).

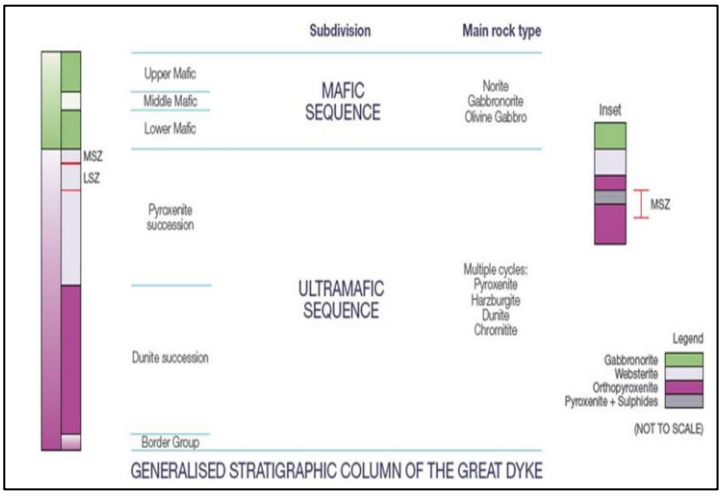

Figure 3-3. Generalized stratigraphy of the Great Dyke (courtesy N. Fernandes).

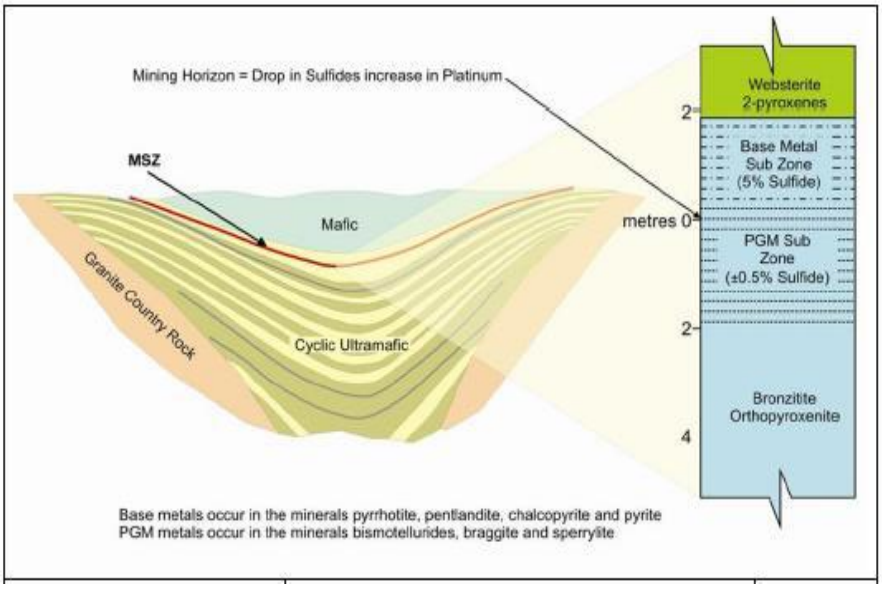

Figure 3-4. Geological structure of Mine A (courtesy N. Fernandes).

Figure 3-5. Satellite view of the Great Dyke (Google Earth, 2020).

The underground workings are located in a “shallow mining environment” and are less than 500 m below surface. Stress measurements have not been conducted at the mine. Based on underground observations, however, it is assumed that the k-ratio is unity.

From the original data set of the 143 exploration holes logged, geological alterations have been observed in 27 holes. As described in the previous chapter, the geological alterations significantly reduce the strength of the rock mass.

The observations below were made during the large-scale pillar failure that occurred in 2014 (see Figure 3-6 to Figure 3-13). Figure 3-6 to Figure 3-9 illustrate the underground observations of the geological alterations in the pillars. Figure 3-10 to Figure 3-13 illustrate the borehole cores, as well as the characteristics of the geological alteration.

Figure 3-6. A pillar at Mine A showing the typical condition of the rock mass (courtesy N. Fernandes).

Figure 3-7. A close-up view of the alteration layer at Mine A illustrating the “slickenside” material (courtesy N. Fernandes).

Figure 3-8. A close-up view of the alteration layer at Mine A (courtesy N. Fernandes).

Figure 3-9. View of the alteration layer when weathered following exposure to moisture (courtesy N. Fernandes).

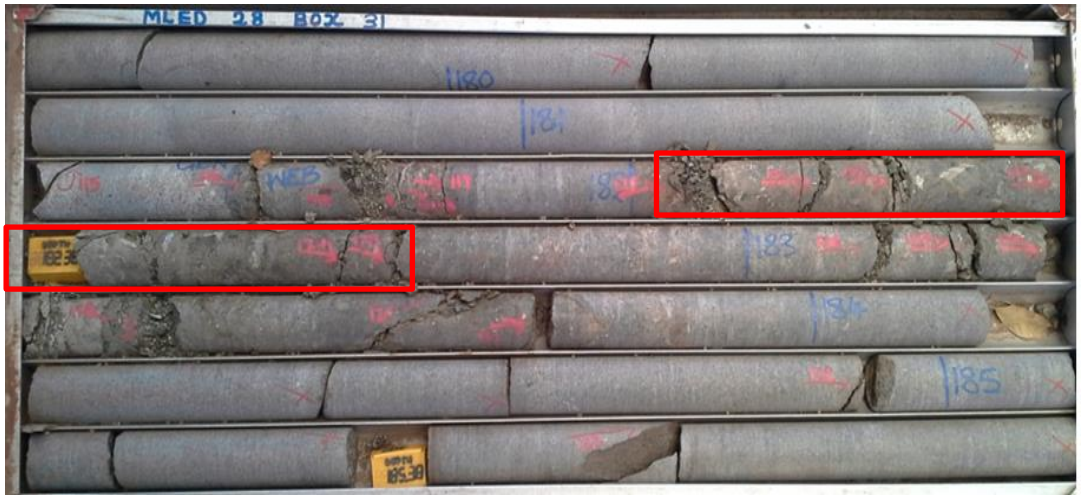

Figure 3-10. The alteration layer present in borehole core at Mine A (courtesy N. Fernandes).

Figure 3-11. Core showing the striations that assist with the identification of the alteration layer during core logging (courtesy N. Fernandes).

Figure 3-12. Alteration zone in borehole core with infilling and striations (courtesy N. Fernandes).

Figure 3-13. Mud-like texture and composition of the alteration zone from core drilling (courtesy N. Fernandes).

In 2013, Mine A experienced pillar failure as indicated below in Figure 3-14 to Figure 3-20. The failure zone gradually extended over several months. This is an interesting aspect of this collapse as it occurred in a time-dependent fashion. The time-dependent failure mechanism needs to be simulated in future but was considered beyond the scope of this current study. The mechanism is different to for example the Coalbrook collapse that occurred in a short period of time. This seems to be a characteristic of large-scale collapses caused by weak alteration zones in the pillars. The eventual pillar failure was extensive and Mine A had to be closed. From the figures below, it appears that no major regional pillars were left, either on geological losses, or in a systematic pattern according to a predetermined design.

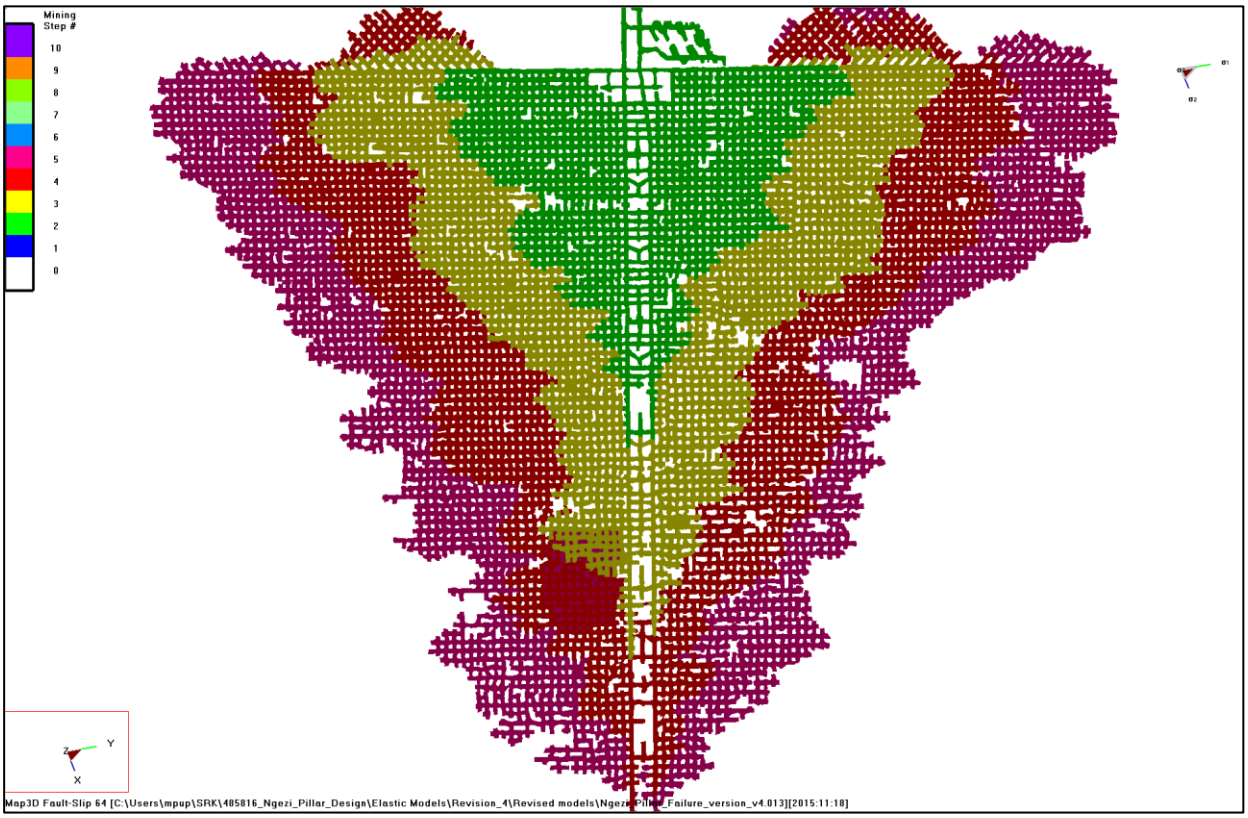

Figure 3-14. Schematic of the mined-out workings in 2013 when the initial pillar collapses were identified. This initial area of failure is indicated by the solid red area (courtesy N. Fernandes).

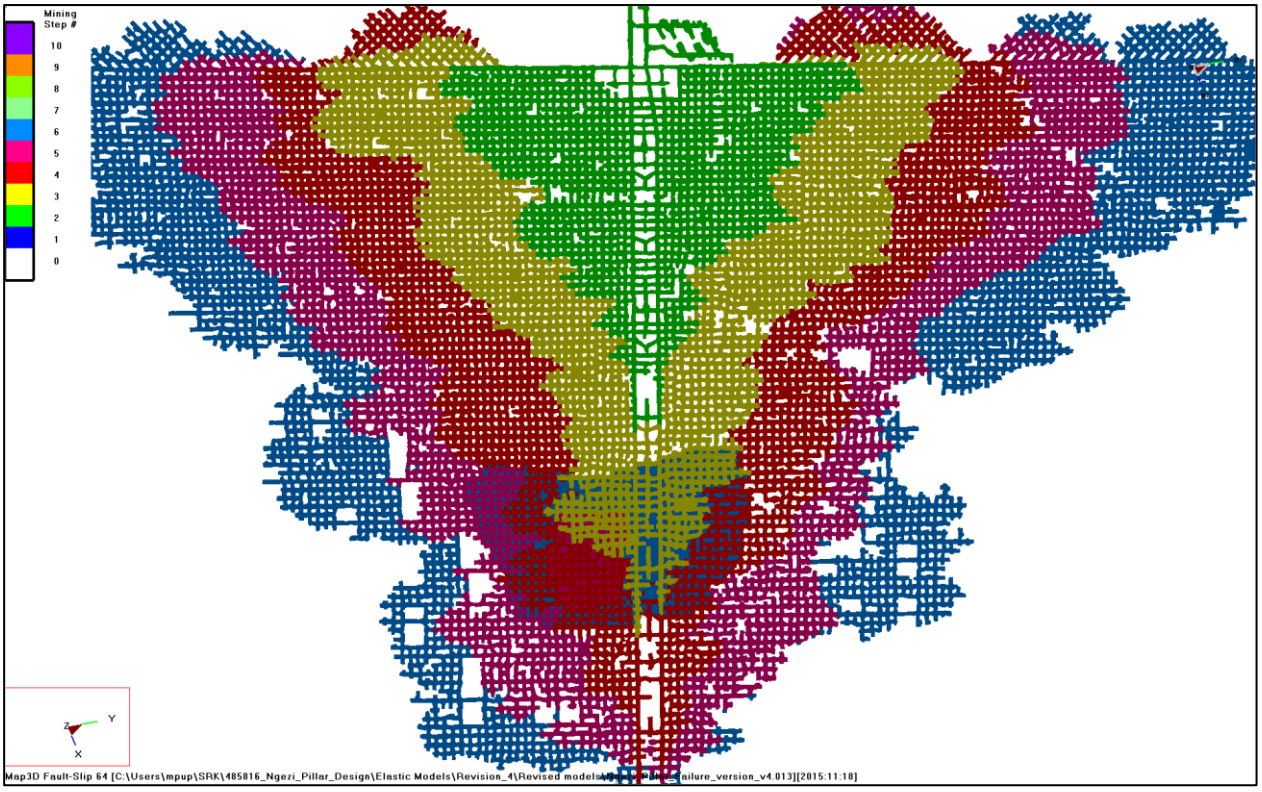

Figure 3-15. The area of pillar failure as recorded during January 2014 (courtesy N. Fernandes).

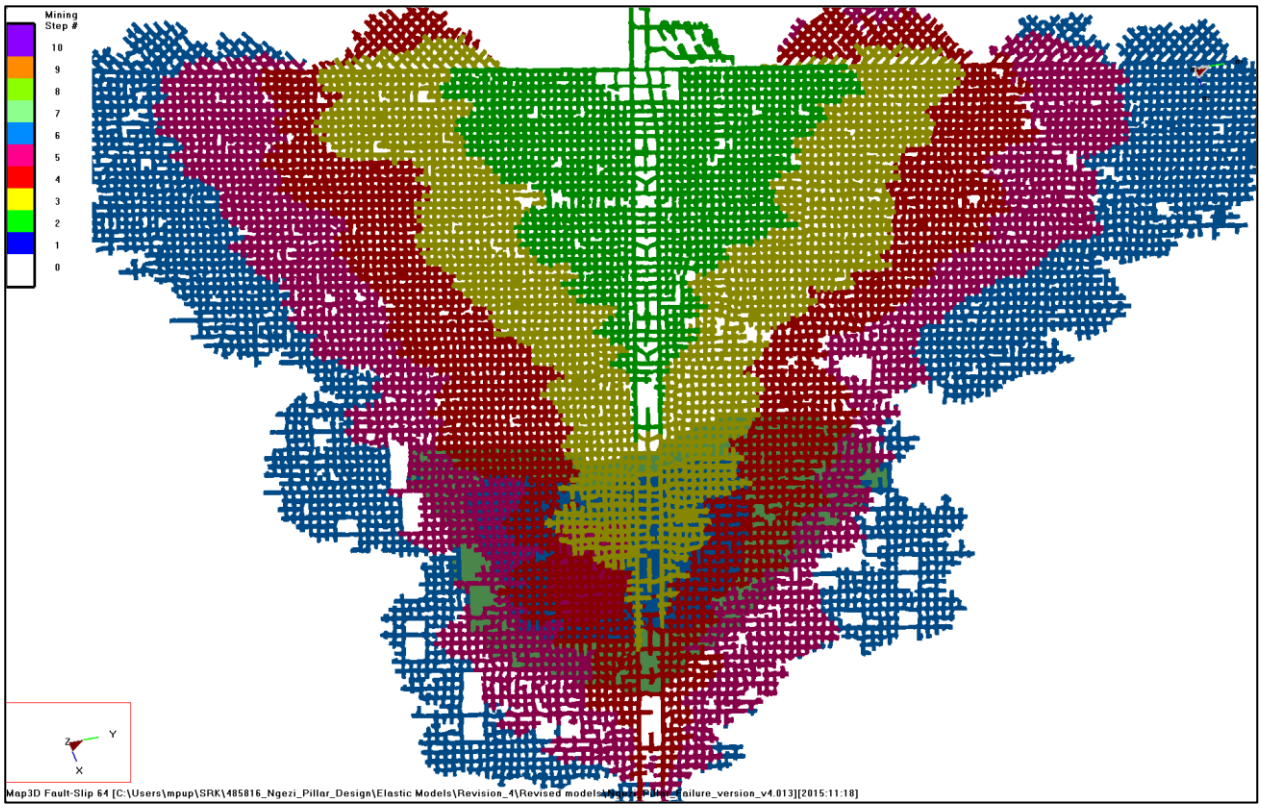

Figure 3-16. The area of pillar failure as recorded during June 2014 (courtesy N. Fernandes).

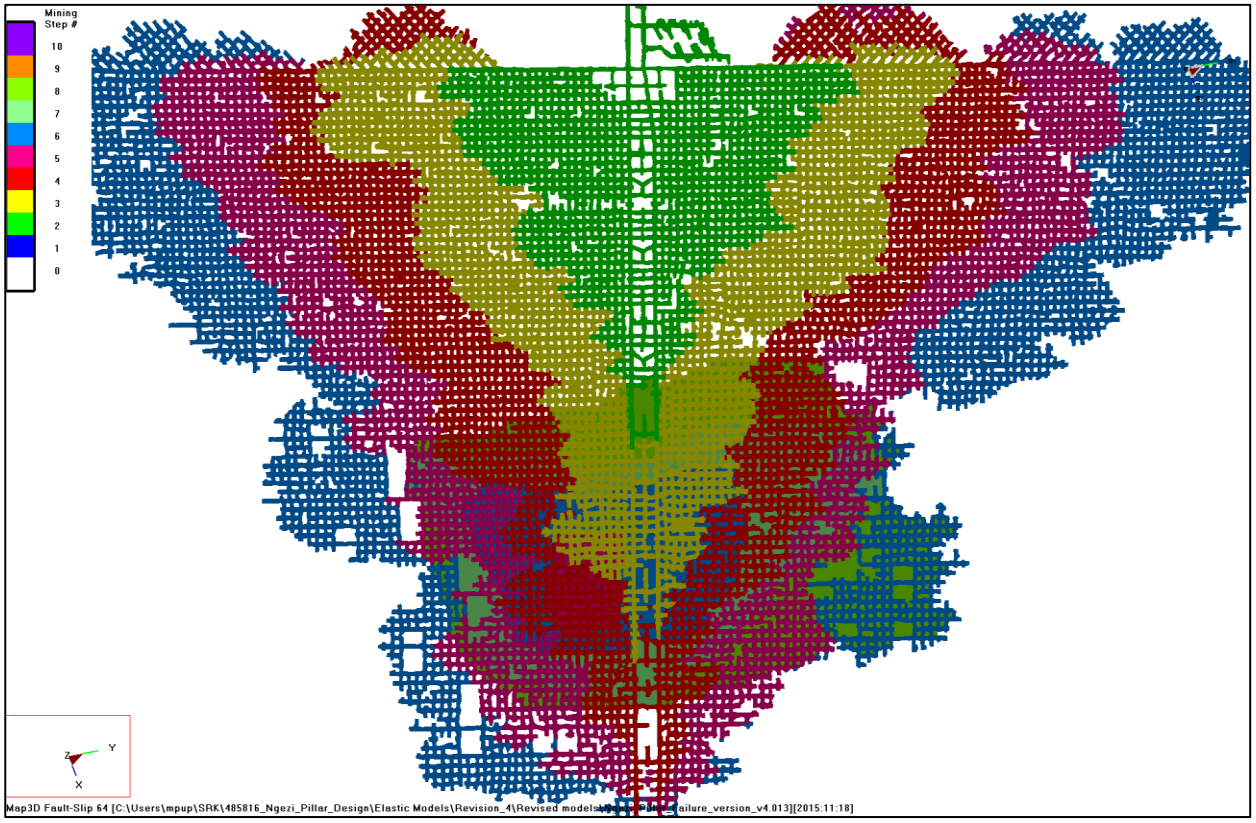

Figure 3-17. The area of pillar failure as recorded during July 2014 (courtesy N. Fernandes).

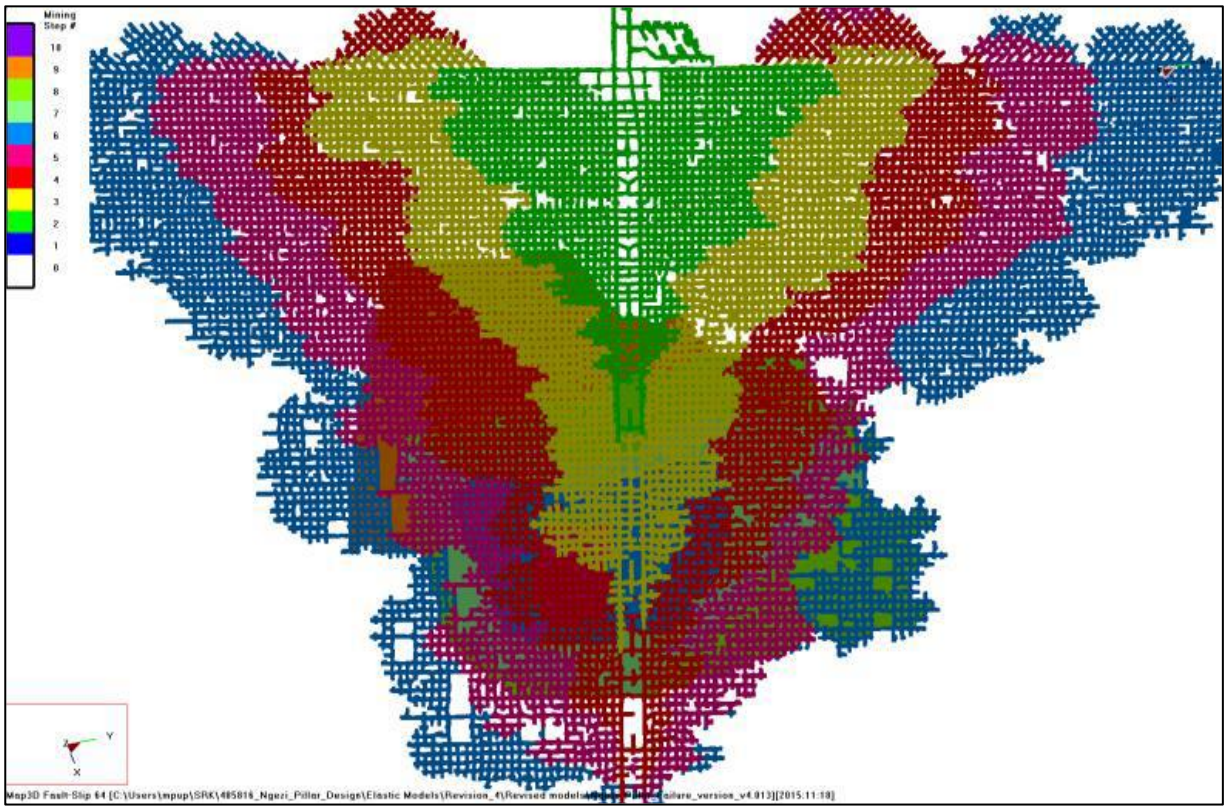

Figure 3-18. The area of pillar failure as recorded during August 2014 (courtesy N. Fernandes).

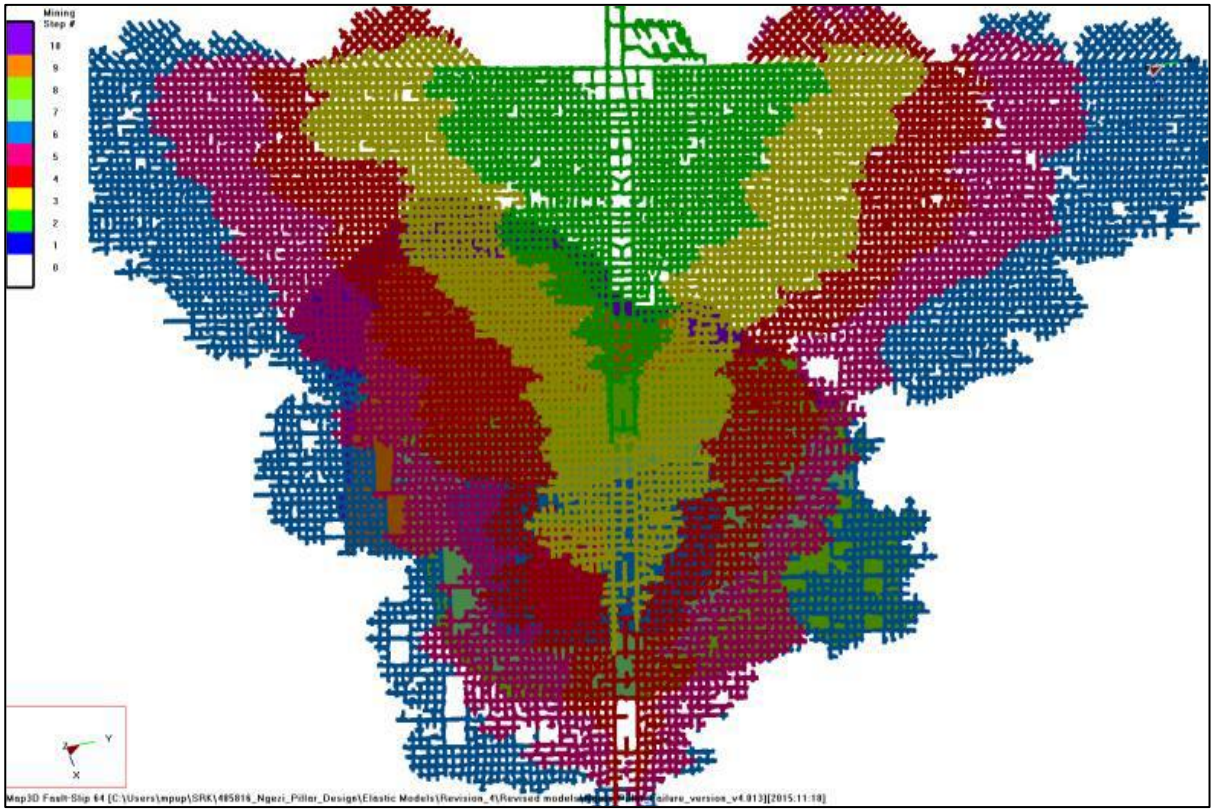

Figure 3-19. The area of pillar failure as recorded during December 2014 (courtesy N. Fernandes).

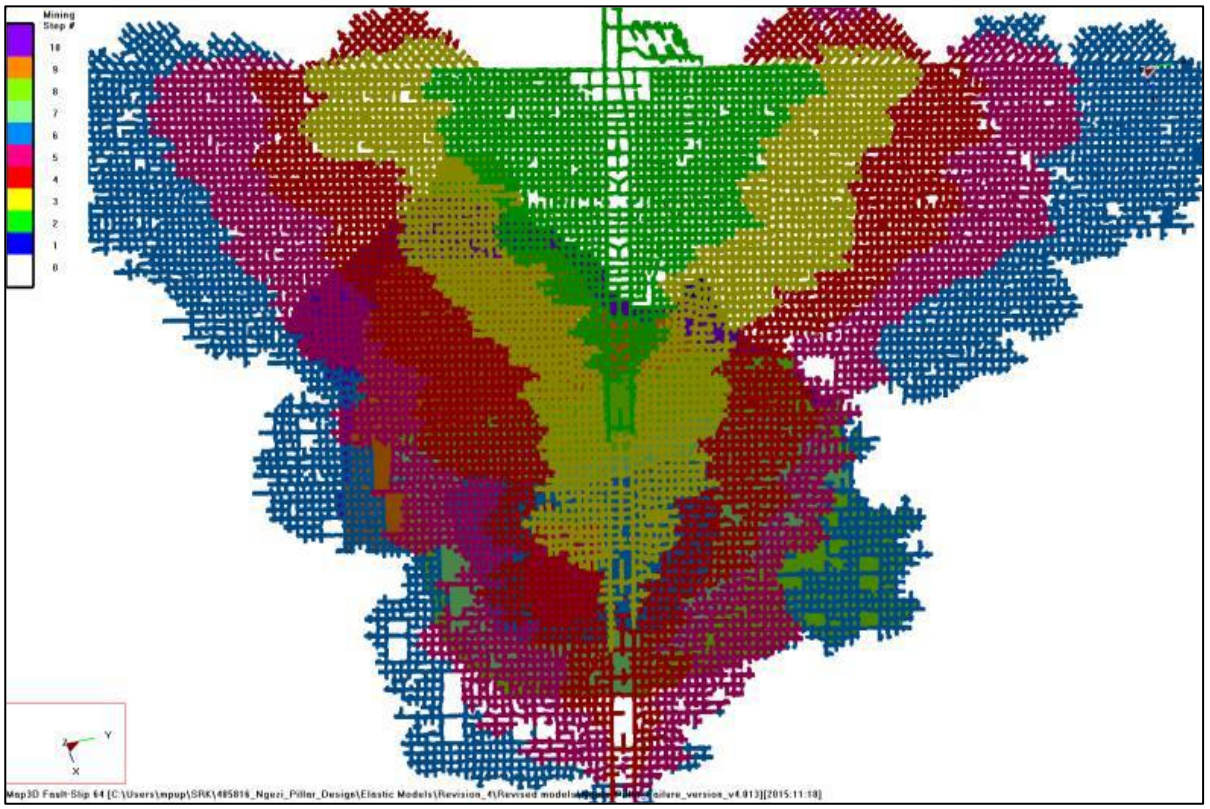

Figure 3-20. The area of pillar failure as recorded during May 2015 (courtesy N. Fernandes).

Mine A conducted a study of the pillar behaviour and the following were the important findings:

- An underground survey indicated that the pillars in the area classified as the geotechnical area with better ground conditions, currently still appear to be stable. This is not the case in the geotechnical area where the pillars contain the weak geological alteration layers. A numerical modelling back analysis indicated that K-values of 56-59 MPa should be adopted for the pillars in the better geotechnical area, while it should be reduced to 34 – 36 MPa in the areas with the alteration layers.
- Of significant concern is that many of the pillars examined underground were cut smaller than the specifications. One of the contributing factors to the large-scale mine collapse at Everest Platinum Mine (described below) was also that the pillars were cut smaller than the specified sizes.
- The effect of water on the weak geological alteration layers within the pillars was a contributing factor in some of the pillar failures.

3.3 Wonderkop Chrome Mine – Western Bushveld Complex

Chromecorp (Pty) Ltd. began sinking its decline system at Wonderkop Chrome Mine during November 1995, and in September 1996, commenced with underground stoping. It is situated in the Western Bushveld Complex in the Northwest Province of South Africa. (Spencer, 1999). The mining layout during March 1998 is shown in Figure 3-21.

Wonderkop mined the LG6 and LG6a chromitite seams at an average depth of 270 mbs with an average dip of 12°. The orebody lends itself to a mechanised bord and pillar operation. Drilling was carried out using conventional hand-held equipment. The original pillars were 6 m wide on dip and 12 m long on strike. The panels were 10 m wide with 4 m wide ventilation holings. An underground inspection of the pillars by Spencer during July 1997 is documented in his paper. He noted that joints started opening at the corners of some pillars. Some joints also opened up at the sides of the pillars and in some occasional cases, sliding along the weak clay layer was noted. Following these observations, an arrangement of barrier pillars with a width to height ratio of 10:1 was introduced. These barrier pillars failed to solve the problem as the deterioration continued over the next nine months. To strengthen the pillars along the declines, waste stowing and meshing and lacing of the pillars were introduced. The progress of this programme was too slow and it seemed as if the water introduced by drilling into the pillars made matters worse. During May 1998, the mine was closed owing to these deteriorating conditions (Spencer, 1999 and 2008).

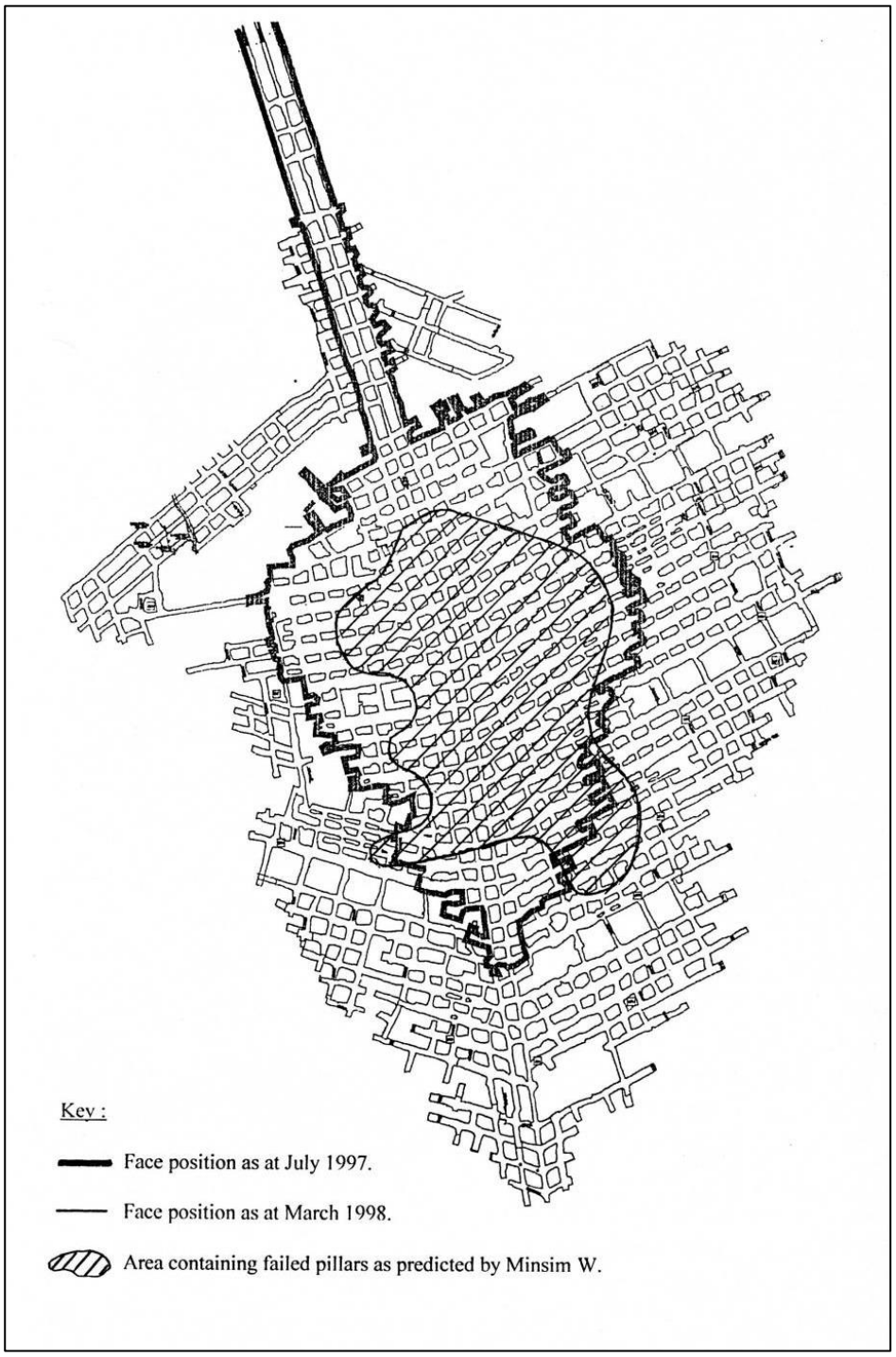

Figure 3-21. Extent of mining at Wonderkop Mine during March 1998 (after Spencer, 1999).

The composition of the layers that made up the pillars is shown in Figure 3-22. The wording “clay layer” is used to refer to the geological alteration layer. Figure 3-23 shows the area where the geological alteration was present in the Wonderkop property in relation to the mining. From the exploration boreholes, it was found that the geological alteration was not present at the greater depths.

The original pillar design was conducted using the Hedley and Grant formula with a K-value of 35 MPa. This K-value was based on data that was obtained much earlier when the

feasibility study was conducted for the proposed mining operation. The UCS of the pillar material was approximately 110 MPa. Owing to the low price of chrome, no additional testing was done for the mine design and the classical value of $K = \frac{1}{3}UCS$ was used for the pillar design. The pillars were designed at 12 m by 6 m with an effective width of 8 m based on Wagner's perimeter rule. An average stoping width of 2 m, giving a w:h ratio of at least 3, was adopted (Malan and Napier, 2011).

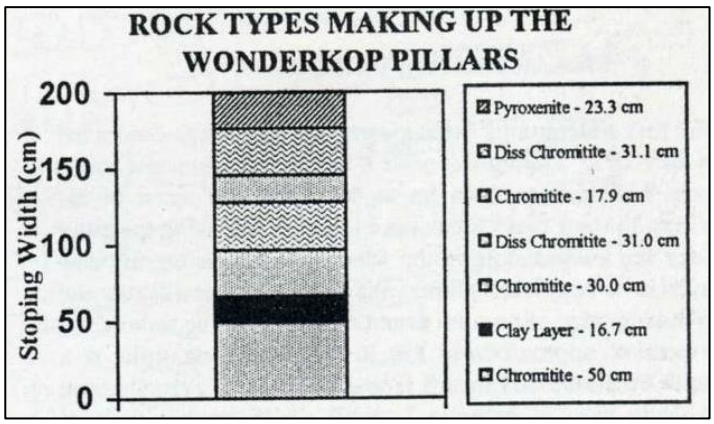

Figure 3-22. Rock types present at Wonderkop Mine in the pillars. The legend is in the same sequence as the stratigraphic column (after Spencer, 1999).

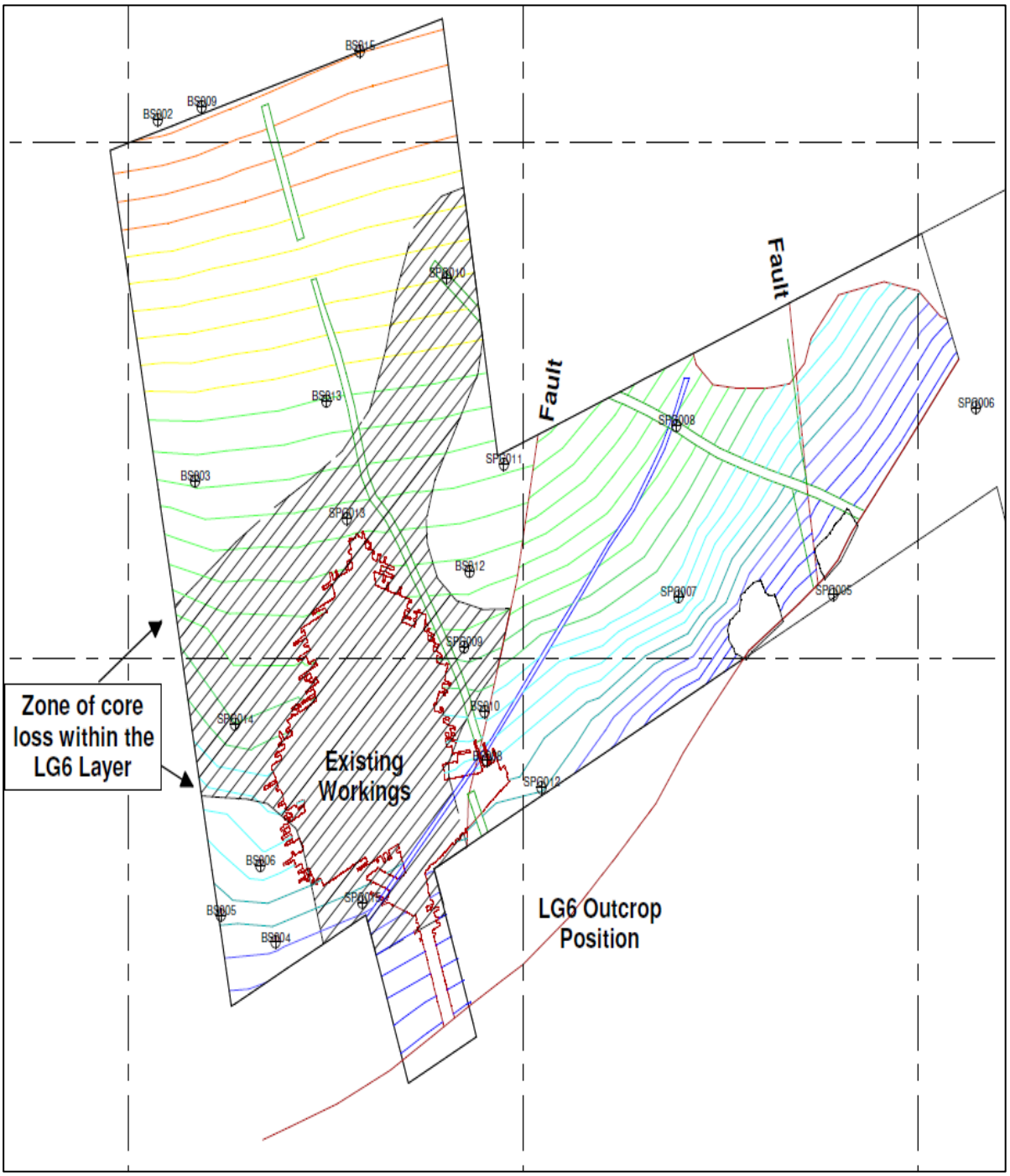

Figure 3-23. Geological plan of the core loss area (indicating where the alteration zone is present) in relation to the mine workings at Wonderkop Mine (courtesy F. Malan).

Figure 3-24 and Figure 3-25 illustrate the typical geological alteration at Wonderkop Mine. The initial failure of the pillars as recorded by Spencer (1999) is illustrated in Figure 3-26.

Figure 3-24. Presence of a weak alteration in the pillars at Wonderkop Mine. This photograph clearly illustrates the presence of the clay layer (Malan and Napier, 2011).

Figure 3-25. Presence of weak clay layers in proximity to the LG6/LG6A chromitite reefs at Wonderkop Mine (Malan and Napier, 2011).

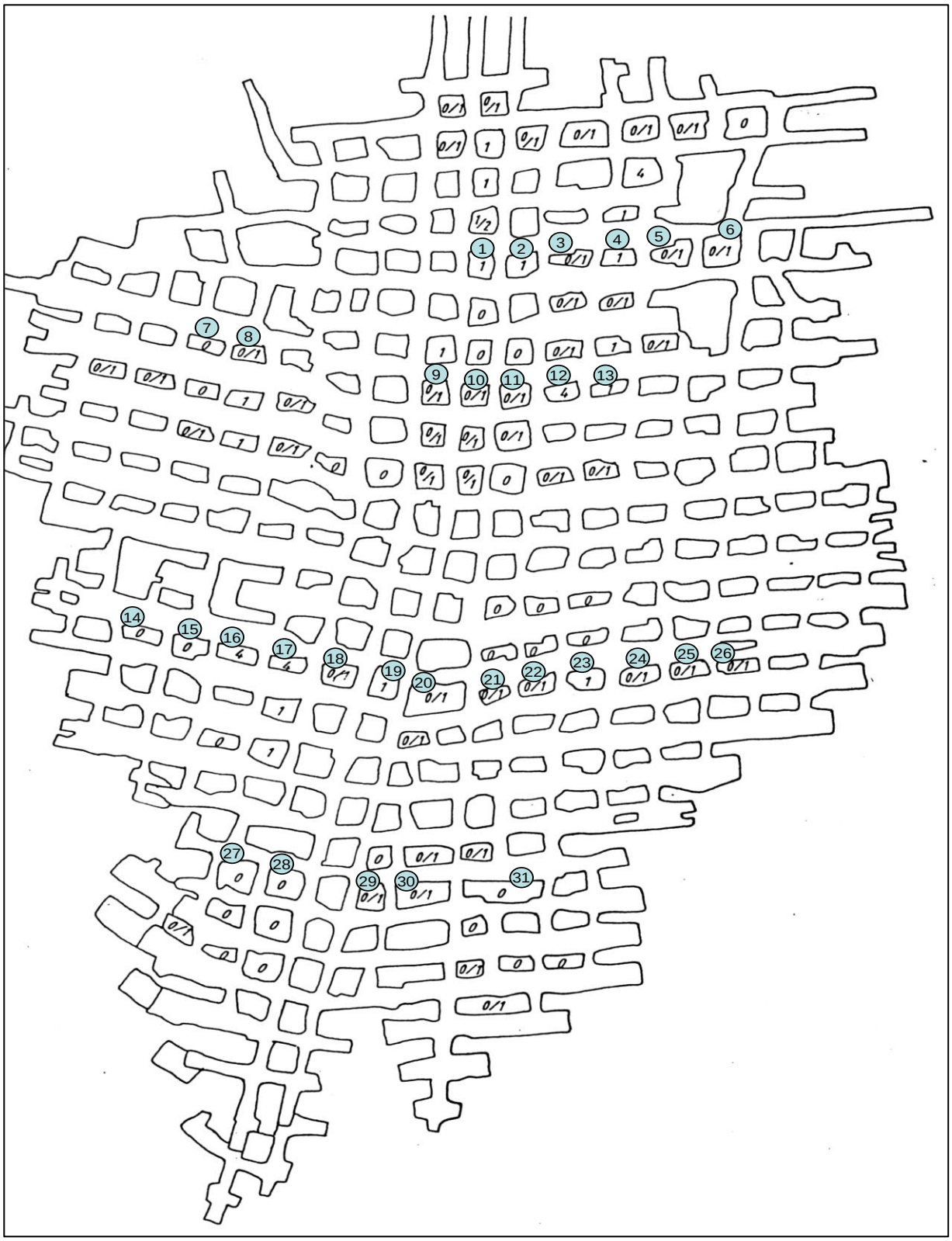

Figure 3-26. Failure condition of the pillars and the extent of mining during July 1997 (after Spencer, 1999). The failure codes used in this figure are as follows: 0 - No failure, 1 - opening of joints at the corners, 2 - opening of joints at the corners and along the sides, 3 - material slabbing off the corners and sides, 4 - horizontal movement occurring along the clay layer (Spencer, 1999).

The main finding of a numerical modelling back analysis was that the pillars had a peak strength of 7 MPa. This is based on a system of 6 m wide, 12 m long and 2 m high pillars. This strength was used to back-calculate the K-value for the Hedley and Grant formula and a value of 4.64 MPa was obtained. This gives a strength value of 9 MPa for a 10 m square pillar. Therefore, for design purposes in these ground conditions, the load on a 10 m square pillar should not exceed 6 MPa to maintain a FoS of 1.5 (Spencer, 1999).

No observations of the underground working at Wonderkop could be obtained for this study because of the closure of the mine. Photographs of pillar failure in a mine adjacent to Wonderkop, where the same weak geological alteration layer is present, can be seen in Figure 3-27.

Figure 3-27. Mechanism of pillar failure at a mine adjacent to Wonderkop. For this pillar, a geological alteration was found between the upper LG6A chrome and the pyroxenite below it. This layer facilitates the fracturing of pyroxenite, causing it to scale out (left). The failures led to large amounts of convergence as can be seen in the photograph on the right (after Malan and Napier, 2011).

From a practical point of view, it is possible that the pillar instability was inadvertently accelerated through the following two actions:

- Water, from the meshing and lacing support operations of the pillars, probably percolated along the fractures towards the centre of the pillar. This mobilised the alteration layer and reduced the friction angle (Malan and Napier, 2011).
- The scraping action of the LHD buckets, whilst loading broken ore and using weak, scaling pillars as backstops, contributed to the pillar deterioration (Spencer, 1999).

As a final summary for the Wonderkop case study, the effect of the 30 cm alteration layer weakened the peak pillar strength from an estimated 43 MPa to 7 MPa (Spencer, 1999). This is a substantial reduction in pillar strength (84 %) and will make the design of a stable and profitable mechanised bord and pillar operation in these ground conditions extremely difficult.

3.4 Everest Platinum Mine – Eastern Bushveld Complex

The Everest Platinum Mine is of particular interest for this study as more information was available on this collapse compared to the other two case studies. The mine is situated in the Eastern Bushveld Complex. The sections below give detailed geological information of the area where the mine is located and it is included here as important background for the following chapters.

The Bushveld Complex (BC) is the world's largest layered igneous intrusion. It hosts the world's single largest deposit of platinum group metals (PGMs). The BC consists of a 7 to 9 km thick sequence of mafic to ultramafic cyclic units. The Eastern lobe is located predominately in the Limpopo Province, but also in the Mpumalanga Province of South Africa (see Figure 3-28).

The mafic rocks of the BC are known as the Rustenburg Layered Suite (RLS) that sub-outcrop around the periphery of the complex and dip towards its center. The RLS is subdivided into five zones, of which the Critical Zone (CZ) is the most important as it contains the economically important horizons that include the PGM's and chromitite. The two mineralized layers, which contain the economically important PGM's, are the Merensky reef and the Upper Group 2 (UG2) chromitite layer. Only the UG2 reef was mined at Everest Platinum Mine. Everest Platinum Mine is located 35 km west of the town Lydenburg in the Mpumalanga Province (Everest Platinum Mine COP, 2007).

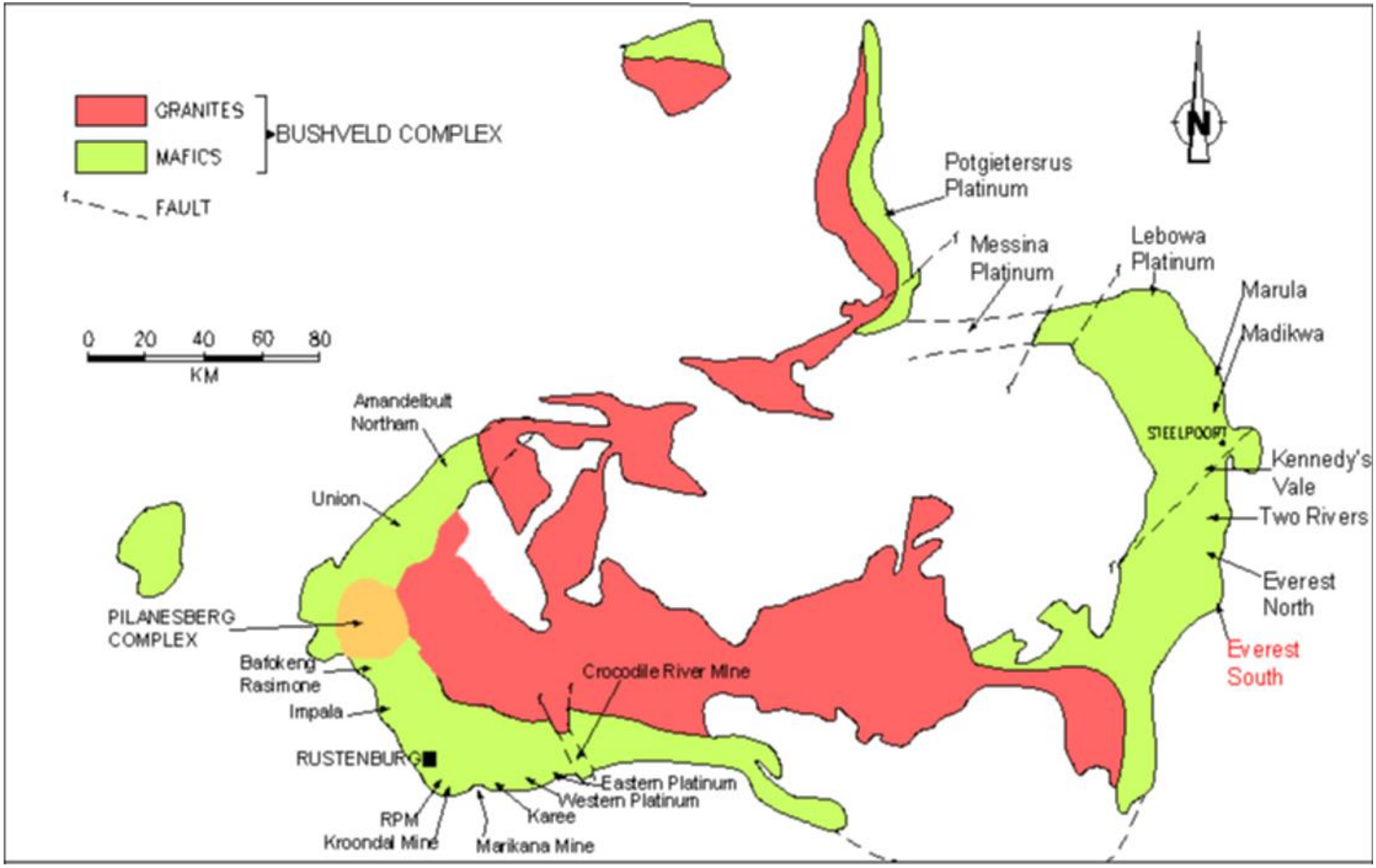

Figure 3-28. Location of the Everest Platinum Mine in the Bushveld Complex (Everest Platinum COP, 2007).

3.4.1 Stratigraphic sequence and geology

The general stratigraphic sequence of the UG2 and its immediate hangingwall and footwall, as found at the Everest Platinum Mine, is depicted in Figure 3-29. The stratigraphy on the left is typically what is expected in the north mining area (known on the mine as bords north). The one on the right is found in the south mining area (known on the mine as bords south).

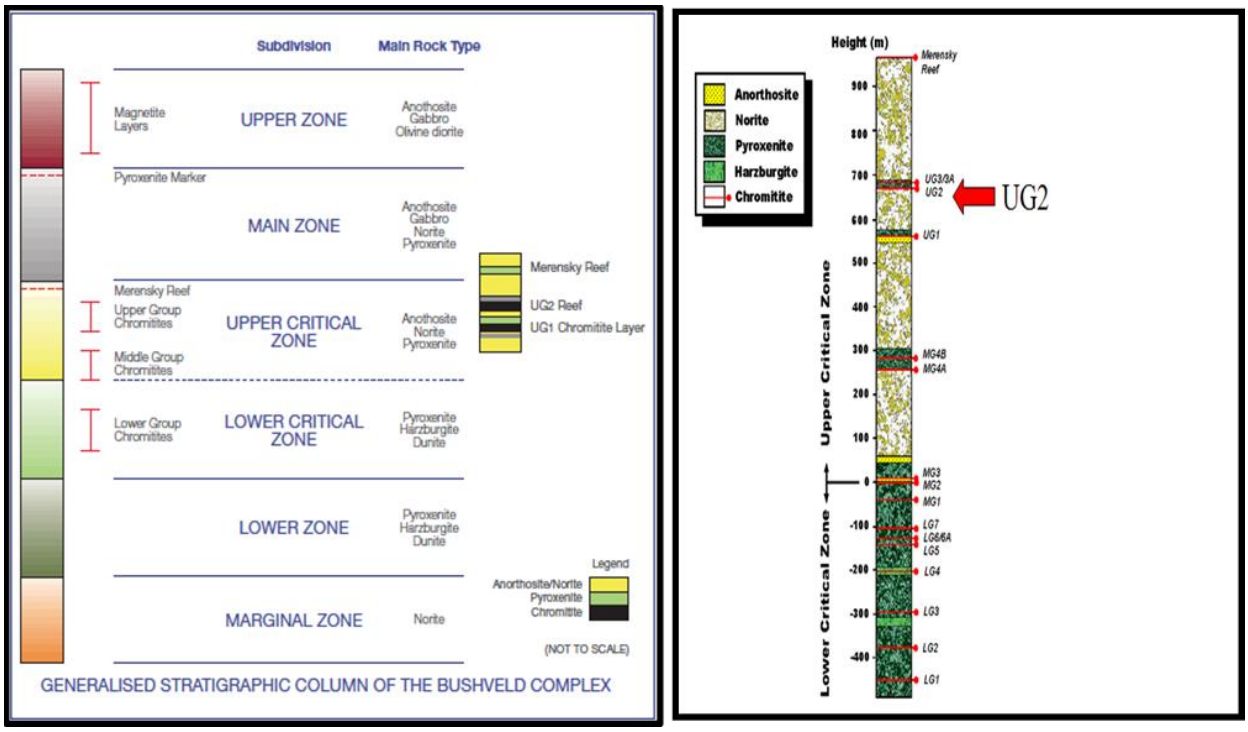

Figure 3-29. Everest Platinum Mine stratigraphy sections (Preston, 2020).

The UG2 Reef lies at the base of an approximately 0.3 m to 10 m thick, equi-granular feldspathic pyroxenite unit. A gentle transgressive shear zone, which is broadly parallel to the reef plane, extends within the hangingwall pyroxenite layer and up to approximately 5 m above the top reef contact (TRC), depending on the thickness of the pyroxenite layer.

The depth of surface weathering in norites and anorthosites (overburden and footwall series) depends on the density of local jointing. The more densely jointed rock tends to be more deeply weathered. Groundwater can be expected to accumulate in weathered rock mass layers, from where it can percolate into underground workings along pre-existing discontinuities (joints, shears, fault zones and dyke margins). The top elevation of such groundwater depends on the rate of natural or pumped water drainage rate versus the water

recharge rate. Based on measurements from boreholes drilled in the region, groundwater depths vary from 0.5 mbs to 63 mbs, with the average being around 5 mbs to 17 mbs.

The UG2 reef tends to be resistant to surface weathering, unless the plagioclase matrix is weakly developed. This often acts as an efficient aquiclude. The result is that the depth of reef plane oxidation can be less than the up-dip limit for safe and stable stoping, with the former varying in the 10 mbs to 30 mbs range. On average, reef plane weathering extends to approximately 10 mbs to 30 mbs at Everest Platinum Mine with locally increased depths of weathering prevalent along the reef parallel alteration zone (shear zone) (Figure 3-30).

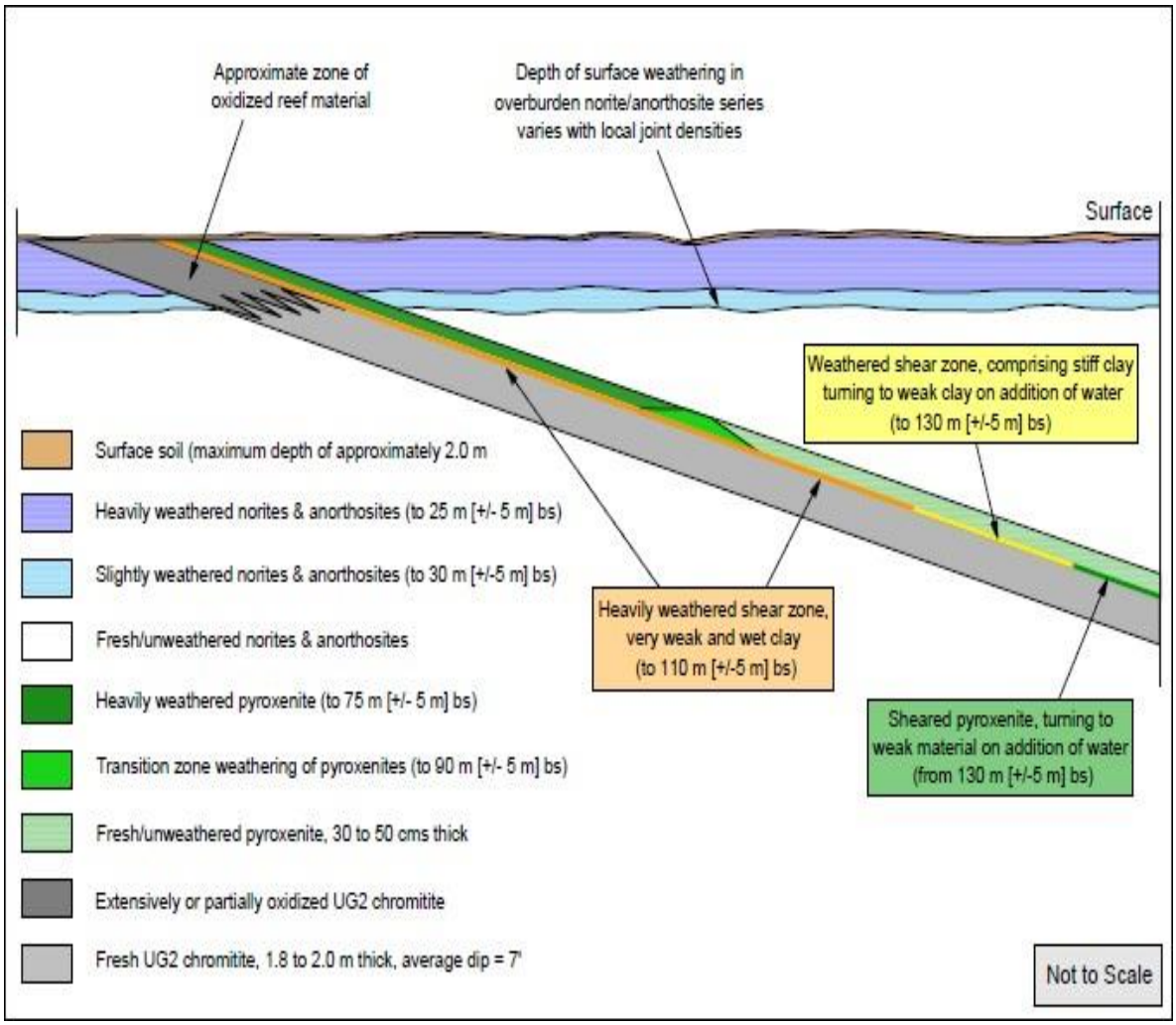

Figure 3-30. Typical surface weathering profile for the historic working areas at Everest Platinum Mine (Godden, 2010). The weak geological alteration layer is referred to as the "shear zone" in the figure.

A reef-parallel alteration zone undulates close to the TRC across the Everest Platinum Mine orebody. The material making up the alteration zone is weathered, wet and muddy to the

touch closer to surface, but more competent and solid at greater depths underground. It undulates from the TRC to 0.9 m along the South bords and from about 0.5 m to larger than 5 m in the North bords.

3.4.2 Material Properties

The mine conducted laboratory testing on reef samples and the average properties of the UG2 is summarized in Table 3-1 and in Figure 3-31. The results compare favourably with the upper and lower strength envelopes (Hoek and Brown criterion) for typical UG2 chromitite (Figure 3-31).

Table 3-1. Uniaxial and triaxial test results (UCS and TCS) for UG2 reef chromitite (after Godden, 2009)

Confining Stress (MPa)	Peak Strength (MPa)	Density (kg/m^3)	Young's Modulus (GPa)	Poisson's Ratio
0	139.3	3,800	115.4	0.499
0	94.3	3,610	55.2	0.152
0	138.7	3,840	98.8	0.342
10	177.2	3,800	-	-
10	217.8	3,470	-	-
20	256.2	3,830	-	-
20	334.1	3,810	-	-

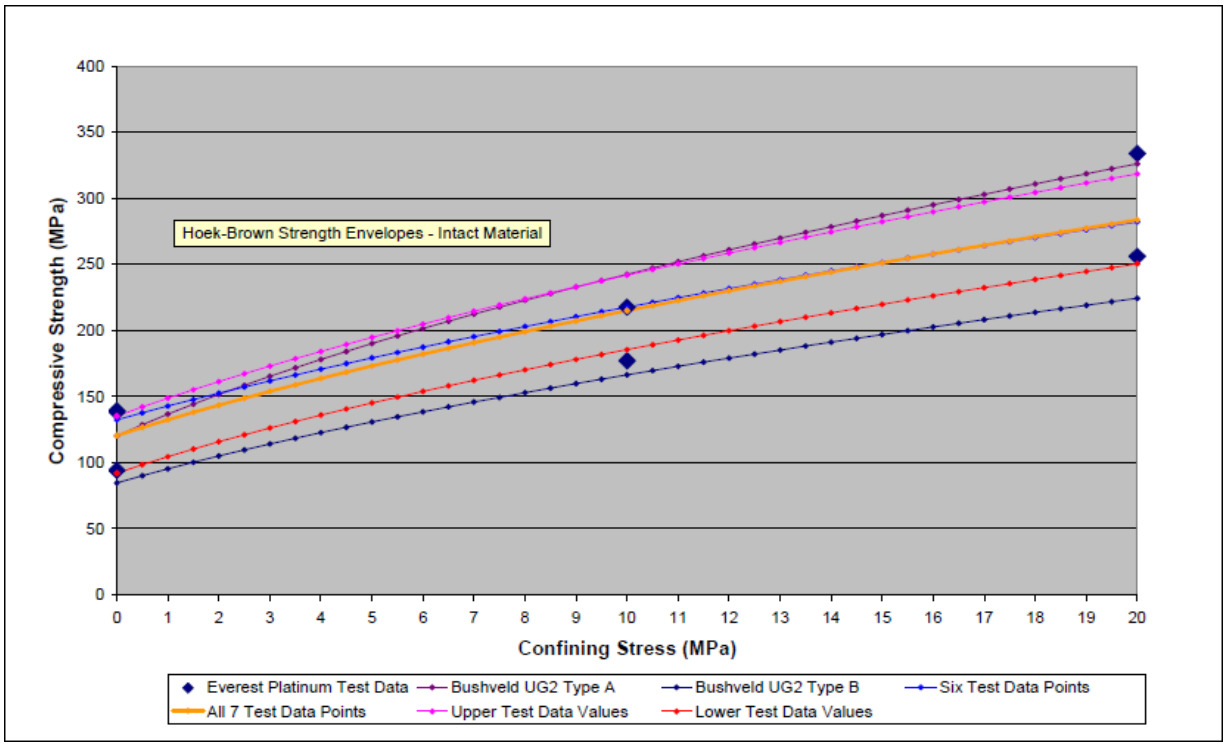

Figure 3-31. Typical Hoek-Brown strength envelopes for UG2 chromitite compared to the Everest Platinum Mine data (after Godden, 2009).

3.4.3 Sequence of events leading to the collapse

In March 2007, a consultant recommended a change in pillar layout as well as additional support based on the observed pillar scaling. These changes were implemented and FLAC3D modelling was used to investigate the new designs. This modelling work illustrated that the alteration zone does have an impact on the strength of the pillars.

By August 2008, the area of pillar scaling increased in size and a further assessment was conducted by external consultants. They recommended that closure meters be installed and that backfill should possibly be used to prevent further deterioration. During November 2008, the shaft rock engineer recorded 5 mm of closure in the unstable area. Contributing to the problem was that in 2008, 220 mm of rain fell within a short period of time. The water pumps in the surface mine were inundated with the excessive water flow and water seepage along the alteration zone (shear zone) occurred. This became a significant contributing factor to the large collapse that occurred on 8 December 2008. Figure 3-32 shows the initial area of affected pillars (scaling). The monitoring positions is shown in Figure 3-33. A detailed sequence of events is given in Table 3-2.

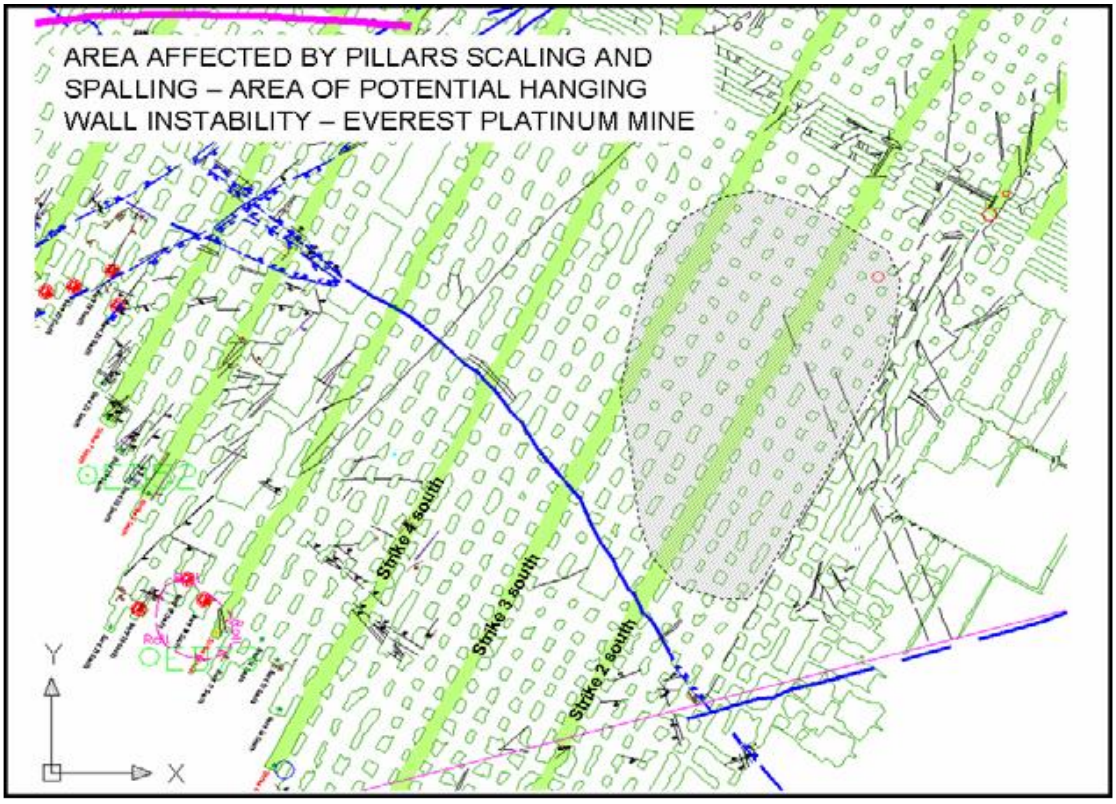

Figure 3-32. The extent of observed pillar instability during late March 2008 at Everest Platinum Mine (after Lombard, 2008).

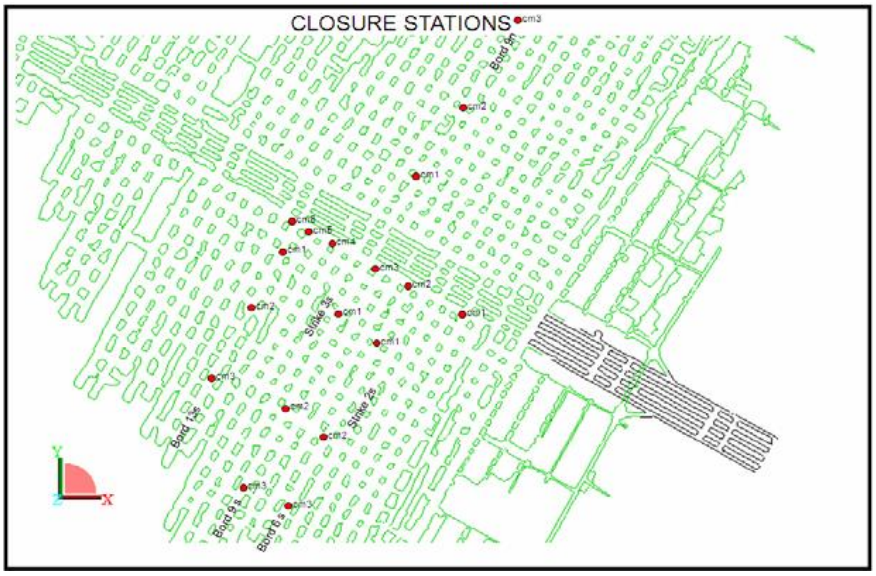

Figure 3-33. The positions of the closure monitoring stations installed during September 2008 at Everest Platinum Mine (after Lombard, 2008).

Table 3-2. Sequence of events leading up to the large-scale pillar failure (after Godden, 2009).

Event	Date	Responsible Party	Outcome/Result
Extensive mud layer & weathered pyroxenite observed above first cut pillars	Sept. 29, 2005	Mine Rock Engineer (report RED 25/05)	Potential impact of shear zone identified, FLAC^{3D} analyses, fibrecrete recommended
FLAC^{3D} modelling of pillar behaviour, inclusive of mud layer and weathered pyroxenite, to test for pillar strength reducing effects	Jan. 2006	IndiRoc cc (report NDA03, rev. 1.1)	Results indicated long-term impact of shear zone 'not significant'. Minor changes to pillar layouts and a thin shotcrete layer recommended where shear plane exposed.
High closure rates noted in near surface breast stopes	Aug. 28, 2006	Mine Rock Engineer (report RED 80/06)	Conventional mining stopped, pillar fibrecreting and monitoring implemented.
Change to pillar layout strategy	Aug. 30, 2006	Mine Rock Engineer (report RED 82/06)	Regional stability pillars along fault intersection recommended
Hangingwall failure over near surface breast stoped area	Nov. 30, 2006	Mine Rock Engineer (report RED 111/06)	Regional stability pillars confirmed, fibrecreting confirmed, additional monitoring implemented
Hangingwall closure stations installed in South and North Side workings	Feb. 2007	Mine Rock Engineer (report RED 76/07)	Very small initial movements recorded
Mine visit to assess pillar issue	March 05/06, 2007	D. Spencer, SRMC (March 08, 2007 report)	Reviews and recommendations as regards pillar layouts and pillar support
Pillar dimensions increased & bords decreased	March 25, 2007	Mine Rock Engineer (report RED 39/07)	Standard pillar layouts changed, additional FLAC^{3D} analyses recommended
No additional movement in North Side, minor additional movement in South Side	July 04, 2007	Mine Rock Engineer (report RED 76/07)	No additional action recommended, focus remains on fibrecreting pillars
Minor additional pillar spalling reported	Oct. 11, 2007	Mine Rock Engineer (report RED 116/07)	Routine safety measures implemented
FLAC^{3D} modelling of pillar behaviour	Nov. 2007	Itasca Africa (Pty) Ltd (November 2007 report)	Results show shear has significant influence on pillar behaviour, use of fibrecrete confirmed
Minor increase in hangingwall closure and pillar spalling in South Side workings.	March 20, 2008	Mine Rock Engineer (report RED 33/08)	No additional actions recommended, current actions confirmed
Hangingwall instability reported in South Side workings, immediately downdip of November 2006 collapse area	May 28, 2008	Mine Rock Engineer (report RED 52/08)	Current actions confirmed, local safety measures implemented
Growth in area of minor pillar spalling reported, now close to the decline system	Aug. 11, 2008	Mine Rock Engineer (report RED 62/08	Fibrecreting of decline pillars and site visits by external consultants recommended
Mine visit to assess pillar issue	Sept. 02, 2008	D. Spencer, SRMC (Sept. 02, 2008 report)	Progressive degradation of workings suggested, workshop recommended along with installation of additional closure monitoring stations and pillar design review
Mine visits to assess pillar issue	Sept. 17, 2008	B. Kotze, RockEng cc (Sept. 17, 2008 report) D. Spencer, SRMC (Sept. 18, 2008 report)	Progressive degradation of workings expected, backfilling recommended and a mining method and pillar layout review suggested
Additional closure monitoring stations installed	Sept. 2008	Mine Rock Engineer	Additional closure monitoring over an increased area of interest
Mine visit to assess pillar issue	Oct. 09, 2008	M.K.C. Roberts (Oct. 09, 2008 report)	Risk of decline collapse identified – backfill and/or new decline suggested. Risk analysis recommended.
Backfilling considered, cost estimates compiled, samples for testing taken	Oct. 14, 2008	Mine Rock Engineer (report RED 82/08)	Update report
Backfill options update, alternative solutions considered	Oct. 31, 2008	Mine Rock Engineer (report RED 88/08)	Update report
Hangingwall closure update, decline pillar support recommended, capital vote application for sidewall support submitted, money made available	Nov. 19, 2008	Mine Rock Engineer (report RED 97/08)	5 mm of hangingwall closure recorded in Decline No. 2, pillar support and possible time line for implementing amelioration/prevention strategies compiled with D. Spencer of SRMC
Abnormal rainfall event	Nov. 23, 2008	Mine personnel	220 mm of rain falls in one day (mine site readings, later used by VSA Leboa Consulting)
Significant closure monitored across declines	Nov. 24, 2008	Mine Rock Engineer (reports RED 100/08)	Onset of accelerated hangingwall closure near the declines, follow-up in report RED 103/08
First significant damage occurs over the declines. Repairs attempted but accelerated pillar spalling led to the declines being closed	Dec. 05/06, 2008	Mine Rock Engineer (report RED 103/08)	Post-event reporting
Mine cleared of all personnel	Dec. 07, 2008	Mine Management	Concerns over growing rockmass activity
Mine visit to assess on-going pillar spalling	Dec. 07, 2008	D. Spencer, SRMC (Sept. 02, 2008 report)	Stabilisation of pillar sidewalls, re-routing the decline system and backfilling recommended
Subsidence event occurs	Dec. 08, 2008	-	-

Subsequent to the collapse, a pillar design review was conducted during April 2009 (Godden, 2009). The following key points were highlighted:

The pillar design at Everest Platinum Mine was originally conducted by using the empirical strength equation developed by Hedley and Grant (1972) and modified by Stacey and Page (1986). Similar to standard industry practice, a factor of safety of 1.5 was adopted. Some of the design parameters are given in Table 3-3. For the UG2 pillar design, the *K*-value at Everest Platinum Mine was estimated to be 35 MPa.

Table 3-3. Some of the design parameters for the pillars (after Godden, 2009).

Condition	Material Properties	Min./Max. RMR_{eff}	Minimum pillar w:h	Minimum pillar FoS	Maximum nominal e%	Groundwater control
Shear zone undercut	As defined	96	1.5	2.0	85%	N/A
Shear zone exposed in the stoping horizon	As defined	92	2.0	2.5	80%	YES

For the purpose of the revised pillar design, the rock mass strength was modelled using a strain-softening Hoek-Brown failure criterion. This was in contrast to previous inelastic modelling done for the mine which approximated the rock mass strength using a strain-softening Mohr Coulomb criterion. Elastic properties for the in-situ rock mass were estimated using the following empirical formulae:

$$E = \sqrt{\frac{UCS}{100}} + 10^{\frac{GSI-10}{40}} \quad (3.1)$$

where

E = Young's Modulus

UCS = Uniaxial Compressive Strength of material

GSI = Geological Strength Index

and

$$\nu = 0.32 - (0.0015 \times GSI) \quad (3.2)$$

where

ν = Poisson's ratio

The values calculated from these formulae are significantly lower than those derived from laboratory tests on intact rock samples and represent the weakening effect of joints and other discontinuities.

In situ rock strength for the numerical modelling was defined in terms of a Hoek-Brown strength criterion:

$$\sigma_1 = \sigma_3 + UCS\left(m_b \frac{\sigma_3}{UCS} + s\right)^{0.5} \quad (3.3)$$

where

σ_1 and σ_3 are the major and minor principal stresses

m_b and s define the shape of the failure envelope.

The parameters m_b and s are related to GSI, and the initial, m_i, as follows:

$$\frac{m_b}{m_i} = exp\left(\frac{GSI-100}{28}\right) \text{ and } s = exp\left(\frac{GSI-100}{9}\right) \quad (3.4)$$

The rock mass properties adopted as “best-fit estimates” for the various rock materials in the models are listed in

Table **3-4**, below.

Table 3-4. Rock properties used in the numerical model (after Godden, 2009).

Property	Shear - Parting	UG2 - Pyroxenite	Chromitite and Leader	Footwall Norite
Base properties				
UCS (MPa)	2 MPa	168 MPa	129 MPa	212 MPa
m_i	15	14	19	15
GSI	60	60	60	60
Density (ρ)	3200 kg/m^3	2850 kg/m^3	4150 kg/m^3	3200 kg/m^3
Elastic properties				
Young’s Modulus (E)	60 GPa	60 GPa	60 GPa	60 GPa
Poisson’s Ratio (υ)	0.2	0.2	0.4	0.2
Bulk Modulus (k)	36 GPa	36 GPa	100 GPa	43 GPa
Shear Modulus (G)	25 GPa	25 GPa	21 GPa	24 GPa
In situ strength properties				
m_b	3.595	3.355	4.553	3.595
S	0.012	0.012	0.012	0.012

Simulations in FLAC3D were conducted by Dlokweni and Leach (2007). Their results are shown in Figure 3-34 to Figure 3-36. The peak strength reduces as the thickness of the alteration zone increases (Figure 3-36 and Table 3-5).

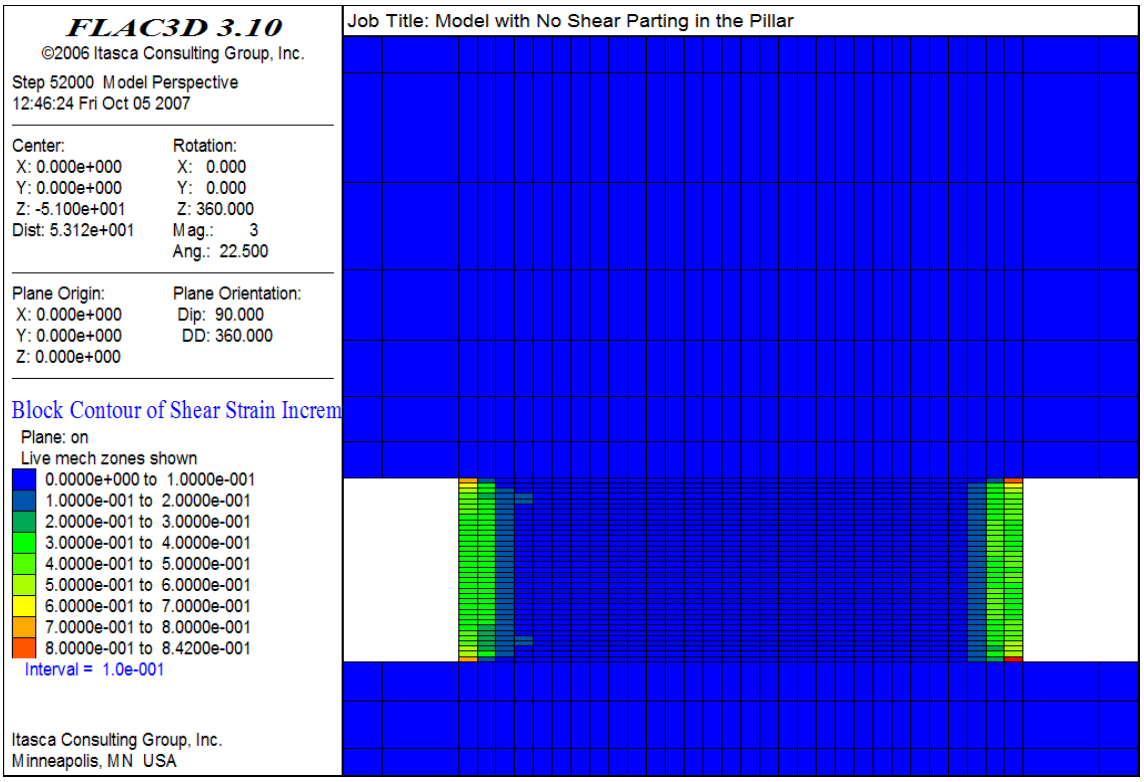

Figure 3-34. Model with no shear parting in the pillar (after Dlokweni and Leach, 2007).

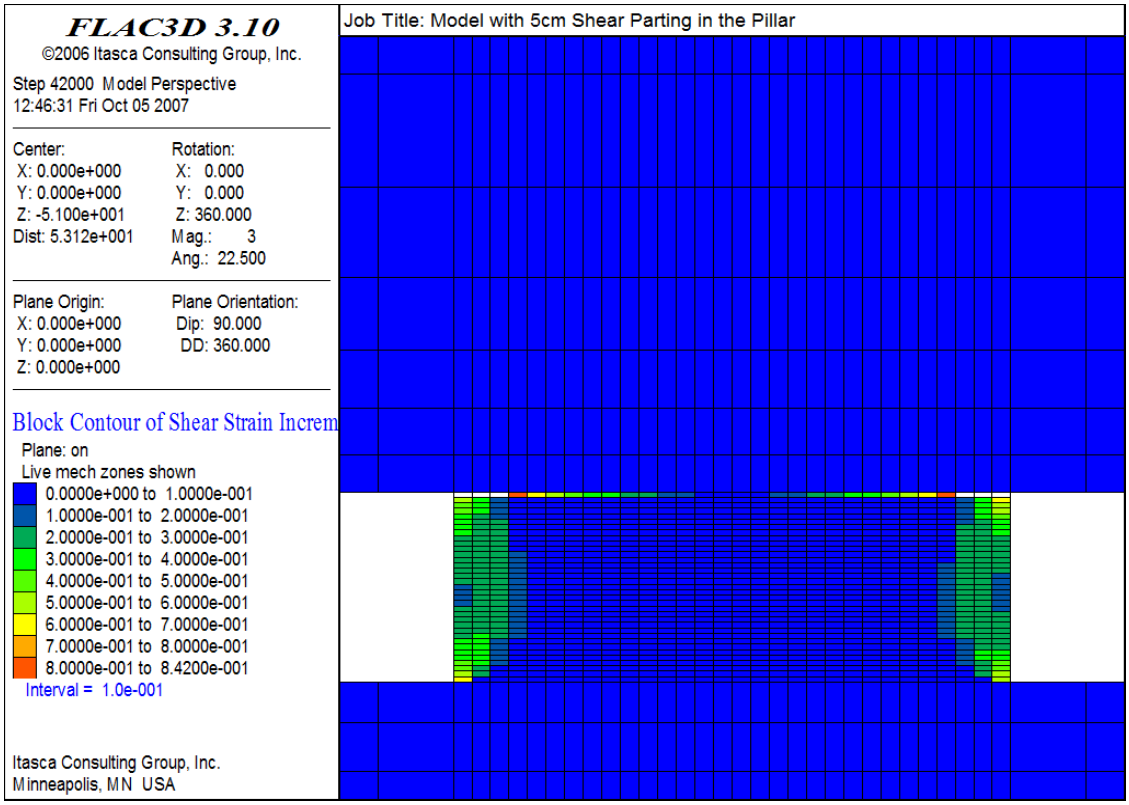

Figure 3-35. Model with 5 cm thick shear parting in the pillar (after Dlokweni and Leach, 2007).

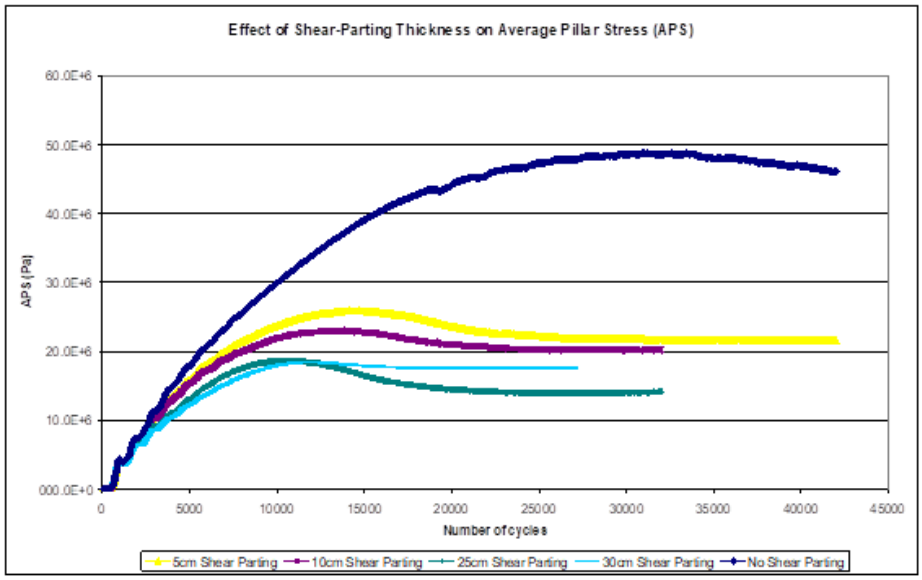

Figure 3-36. Plot of shear parting thickness versus APS (after Dlokweni and Leach, 2007).

Table 3-5. Summary of pillar strength versus shear parting thickness (Dlokweni and Leach, 2007).

	No shear parting	**5 cm shear parting**	**10 cm shear parting**	**25 cm shear parting**	**30 cm shear parting**
Peak Strength	48 MPa	26 MPa	23 MPa	18 MPa	18 MPa
% Strength Reduction	0	46 %	52 %	62 %	62 %

This section briefly described some of the numerical models used to simulate the pillar behaviour at Everest Mine. It mostly focussed on finite difference modelling using FLAC and an inelastic constitutive model to simulate failure in the pillars. These types of codes are not suited to simulate large scale geometries that contain a large number of irregular pillars. To investigate the applicability of a novel numerical models proposed later in this dissertation, additional data was required from Everest Platinum Mine. Underground visits were therefore conducted by the author and the additional data collected is described in the next chapter.

4 DATA COLLECTION AT EVEREST PLATINUM MINE

4.1 Introduction

The author conducted two underground visits at Everest Platinum Mine to investigate the large-scale pillar collapse. The objective was to obtain a better understanding of the mechanism of failure, obtain photographs of the pillars and verify the regional extent of failure. The first visit was conducted on 10 September 2019 and the second visit was on 5 March 2020. Figure 4-1 and Figure 4-2 illustrate plan views of Everest Platinum Mine as well as the route taken during both visits. Limited access during the visits to “high risk” areas prevented the collection of data closer to the crown pillar. The Decline pillars could be visited and information from that area was also collected.

As some parts of the collapsed area was unsafe to enter, the author had to rely on information published earlier by the consultants and the shaft rock engineer many years earlier. This information is also presented in this chapter for completeness. Note that the final collapse was referred to as the “subsidence event” and not pillar failure in earlier reports.

The inclusion of numerous photographs along the route travelled showcases the pillar failure progress from scaling to complete failure. Numerous photographs are included in this chapter to illustrate the mechanism of pillar failure. Such a record has never been published and these photographs are valuable for persons that want to do additional research on this topic in future.

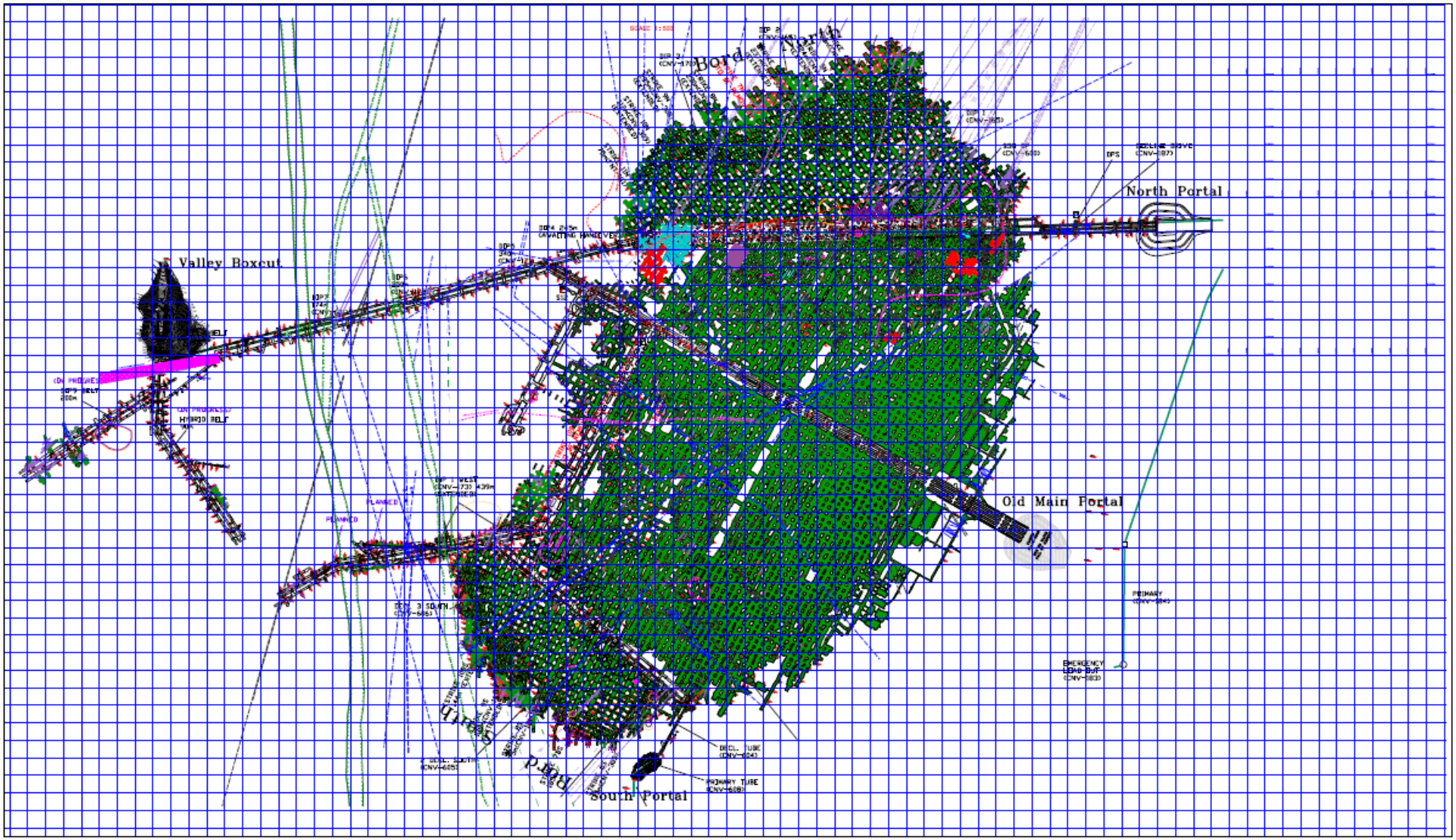

Figure 4-1. Plan view of Everest Platinum Mine showing the extent of the workings at the time when the collapse occurred.

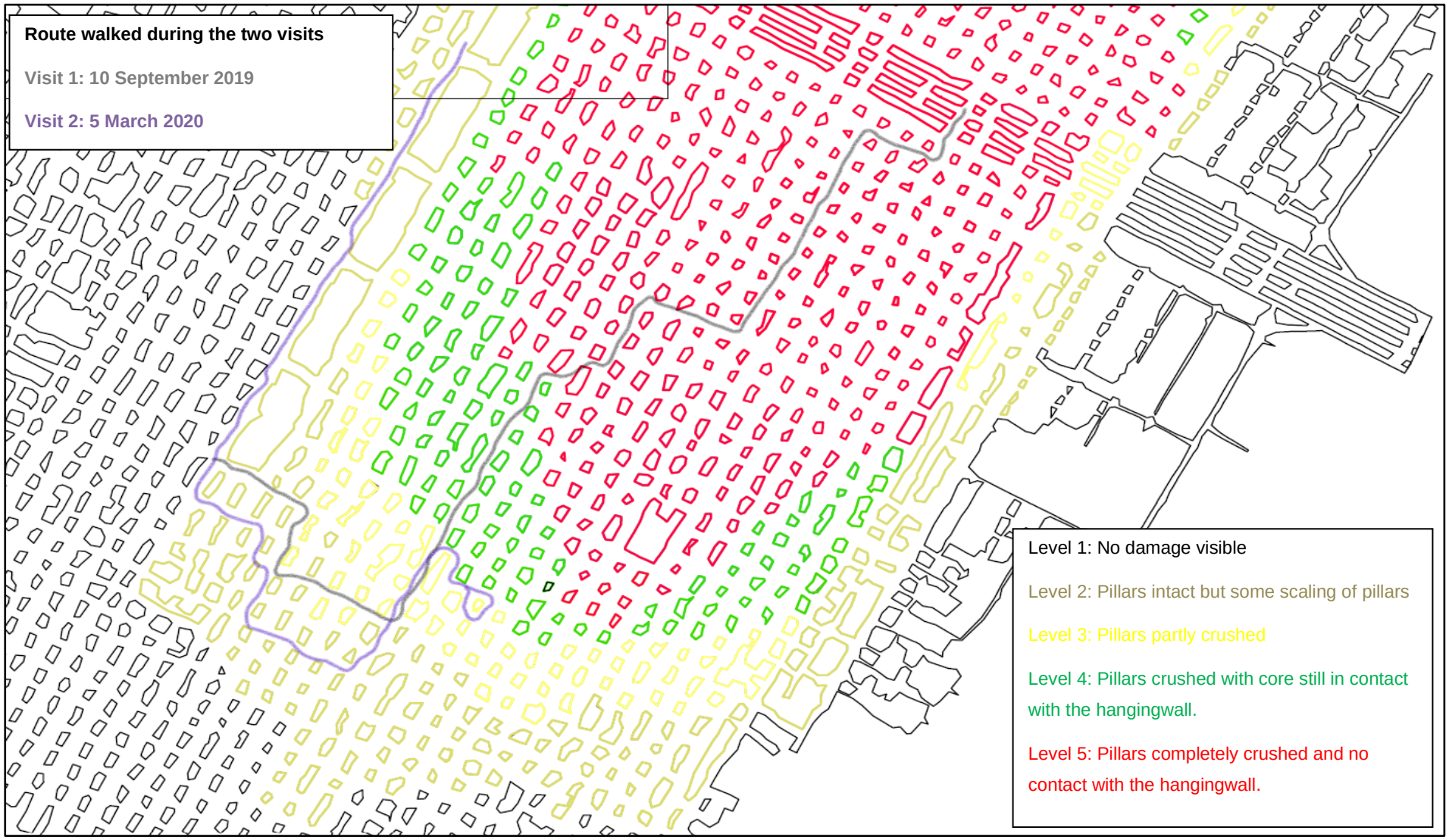

Figure 4-2. Plan view of Everest Platinum Mine showing the two routes travelled during the underground site visits. The extent of the pillar failure and the different failure categories are indicated.

4.2 Underground Observations

Figure 4-3 shows the estimated area of the collapse based on the subsidence observed on surface. These observations were made by the resident rock engineer and a consultant following the collapse on 8 December 2008.

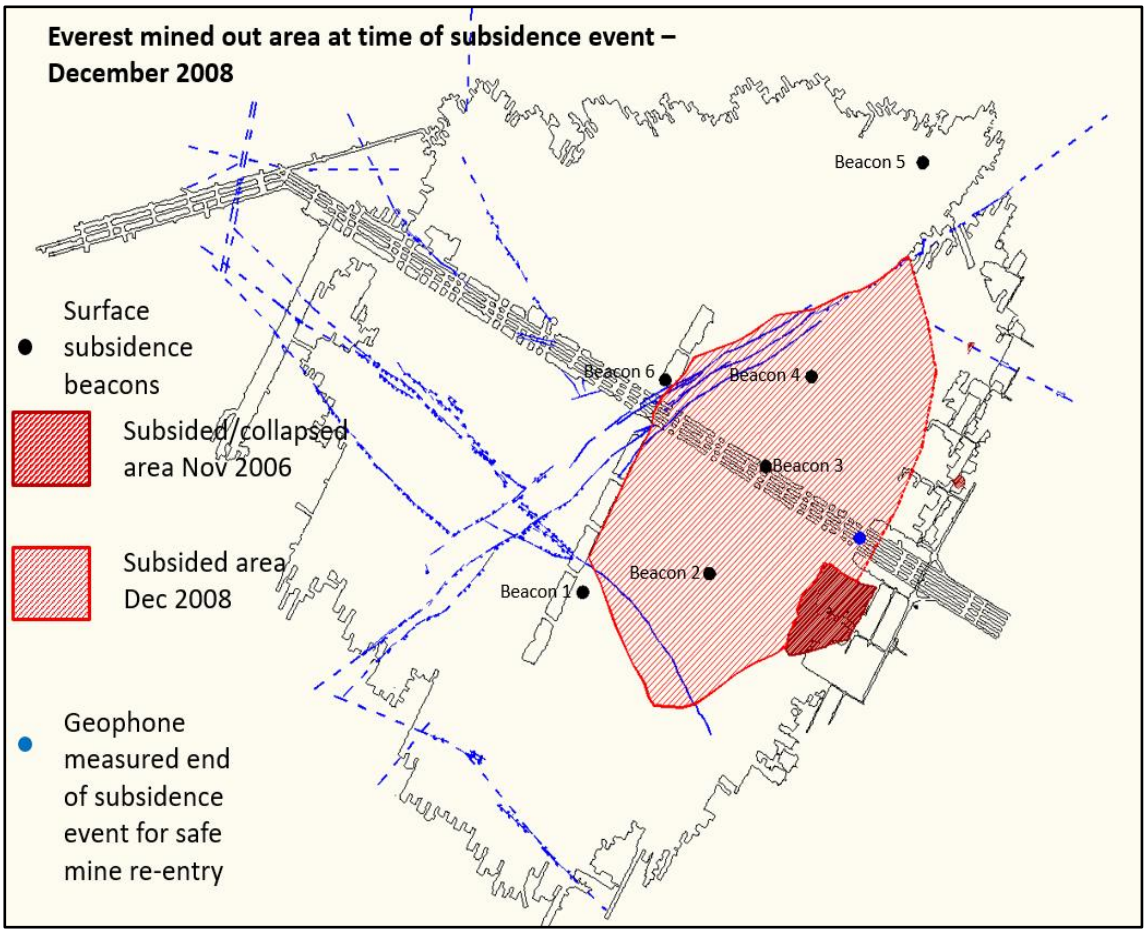

Figure 4-3. Extent of the affected area following the collapse on the 8 December 2008 (after Godden, 2008).

A series of faults striking north-east / south-west created a boundary which delineated the collapsed area. In 2011, the resident rock engineer and a consultant rock engineer conducted a further underground inspection following a proposal to reopen the mine. A new diagram depicting the collapsed area was compiled. The failure was categorised into different levels of failure as shown in Figure 4-4. This was an update of the estimate of the original failure zone. The author of this dissertation wanted to confirm if this extent of the failure zone was still accurate. This was necessary to determine if additional time-dependent

deformation and pillar failure have occurred since the 2011 survey. The visits were also necessary to understand the pillar failure classifications used by the previous workers. From 2008 to 2011, it seems as if the area of collapse has increased when comparing Figure 4-3 and Figure 4-4.

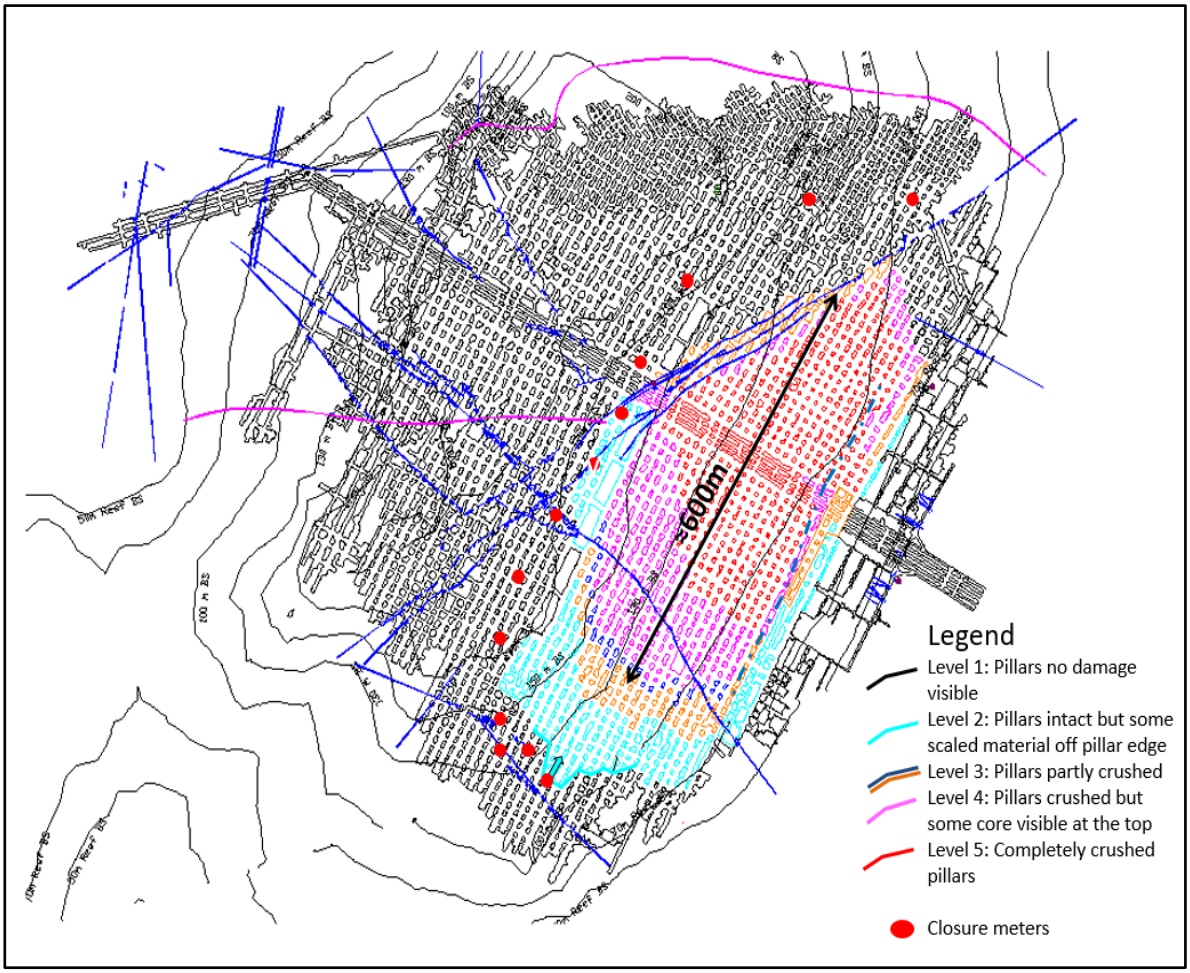

Figure 4-4. The extend of the collapse as of 2011 according to reports by Lombard (2011).

The second visit by the author on the 5 March 2020 was conducted to confirm if Figure 4-4 was still an accurate reflection of the failure zone. The same categories were used to classify the extent of the failure. The initial visit in 2019 enabled the author to better understand the different failure categories. Photographs of the different classifications of failure can be seen below.

Figure 4-5 illustrates the estimated current extent of failure and the different zones based on the observations of the pillars. There has only been a slight increase in the size of the collapsed area. This is an important finding as it seems that only a small amount of additional

time-dependent pillar failure occurred during the last decade. Access into Level 5 was denied due to safety reasons during the second visit, but an inspection of this zone was conducted during the first visit.

No mining has occurred at Everest Platinum Mine for approximately 11 years and only essential services under the care and maintenance strategy have continued. This is limited to the pumping of water and the inspections of escape ways. Unfortunately, the inflow of water was never measured or assessed and the role of water in the ongoing deterioration of the pillars cannot be quantified.

The initial pillar design, in the area where the collapse occurred, specified pillar dimensions ranging from 5 m x 5 m and 6 m x 6 m depending on depth, with a mining height of 2.1 m. It is important to note that many of the pillars that could be measured during the underground visits where smaller than these sizes. The mining plan based on survey offsets done prior to 2008 also indicated that the pillar cutting was done poorly. Many pillars were cut smaller than the design specifications. This is considered an important factor contributing to the failure of the pillars. The pillar scaling could be estimated during the underground visits as the original boundaries of the pillars were still clearly visible on the hangingwall as a result of the shotcrete or whitewash colour signatures.

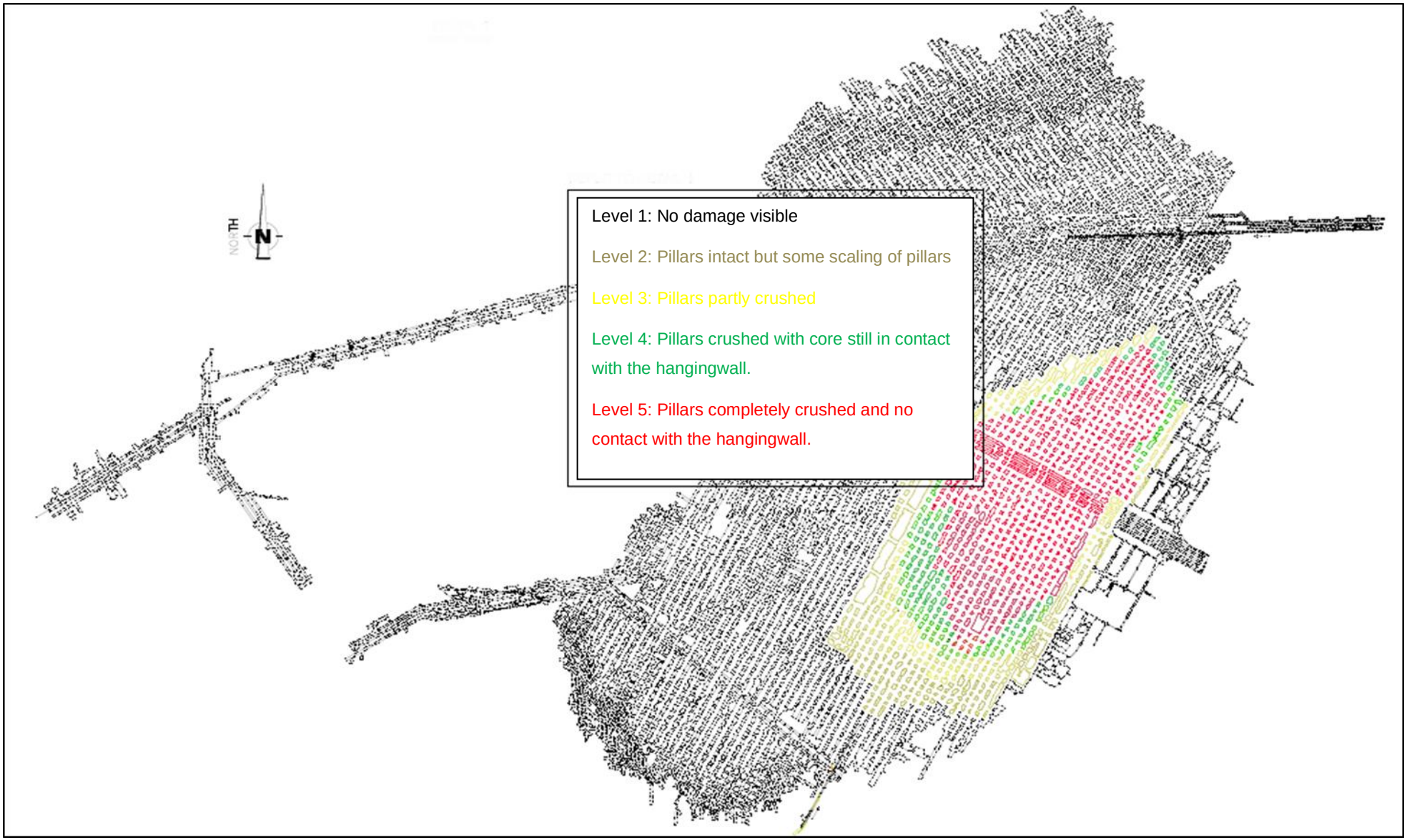

Figure 4-5. Plan view of the extent of pillar failure indicating the estimated collapsed area during 2020.

The stoping width was measured at a number of points along both routes during the visits. Historical records indicate that the mining height varied between 2 m and 2.2 m. Measurements of the stoping height in the zone where no pillar failure was observed had an average value of 2.1 m. Closer to the Declines (Route 1), the stoping width gradually decreased, with a final stoping width of 1.3 m in the Decline area. This implies a total amount of closure of at least 0.7 m occurred in some areas. Tensile cracks close to the Declines were observed and documented. These tensile cracks showed a vertical displacement of approximately 2 cm and in some cases an opening displacement of 1 cm. (Figure 4-6 to Figure 4-21)

During the underground visit, it was found that numerous pillars were shotcreted and therefore the pillar rock mass material and geology could not be recorded. Some pillars were not supported, however, and this provided the opportunity to assess the rock mass conditions.

General observations from the underground conditions illustrated that the geological alteration predominately exists between the TRC and the immediate hangingwall.

The weathering of the alteration zone was evident because of exposure to the atmospheric conditions. The presence of water and high humidity has allowed the alteration to deteriorate into a “muddy” composition that has no cohesive properties and a very low friction angle. Owing to its nature, the alteration zone “squeezed” out between the reef contact and the hangingwall contact in many areas. This has also resulted in slickenside surfaces clearly visible on the up-dip side of the pillars.

Figure 4-6 to Figure 4-21 illustrate photographs taken during the underground visits. The presence of the alteration zone in the pillars is clearly evident in some of these photographs.

Figure 4-6. The typical condition of a pillar in the Level 2 failure zone.

Figure 4-7. Position of the alteration zone in a pillar in the Level 3 failure zone. Note the thick alteration zone at the pillar/hangingwall contact.

Figure 4-8. Another photograph of the nature of the alteration zone at the pillar/hangingwall contact.

Figure 4-9. Thinning of the alteration zone to approximately 10 cm thick at the top reef contact.

Figure 4-10. A pillar in the Level 2 failure zone with joints and fractures visible.

Figure 4-11. Failure of a pillar as a result of the presence of jointing in the Level 2 failure zone.

Figure 4-12. A pillar in the Level 3 failure zone showing extensive scaling and failure. The core of this pillar is still deemed to be intact.

Figure 4-13. Extensive scaling of a pillar in the Level 3 failure zone. Note the hangingwall deterioration due to significant closure occurring.

Figure 4-14. A pillar in the Level 3 failure zone with the alteration zone clearly visible.

Figure 4-15. A pillar in the Level 3 failure zone where the original size of the pillar is clearly visible on the hangingwall owing to the change in colour caused by the white wash.

Figure 4-16. Pillar condition in the Level 4 failure zone. The pillars are crushed, but some contact with the hangingwall is still maintained. The large spans indicate that the pillars were not cut to the planned design.

Figure 4-17. A close-up photograph of the alteration zone in the Level 4 failure zone. It is wet and it has evidence of slickenside surfaces. There is a gap between the pillar material and the hangingwall in this area.

Figure 4-18. A slickenside surface between the crushed pillar material and the hangingwall.

Figure 4-19. Tensile cracks in the hangingwall of the Level 5 failure zone.

Figure 4-20. Relative displacement of a tensile crack in the Level 5 failure zone close to the Decline position.

Figure 4-21. A view illustrating that the pillars adjacent to the Decline have been completely crushed.

Owing to the shallow nature of the operations and large extent of pillar failure, surface subsidence occurred at the mine. Open surface cracks with vertical displacements were recorded by previous workers. Survey measurements also confirmed that surface subsidence did occur. This was recorded on a weekly basis and reported to the Department of Mineral Resources and Energy (DMRE). Figure 4-22 to Figure 4-27 illustrate the vertical subsidence that was recorded during the monitoring period from December 2008 to April 2009. The measurement positions were given in Figure 4-3 and the data agrees with the estimated extent of the collapse at the time. Of interest is that the vertical subsidence increased during this five-month period. Time-dependent deterioration and further collapse of the pillars must have occurred during this time. The horizontal subsidence shows that there was horizontal movement in conjunction with the vertical subsidence (Figure 4-28 to Figure 4-33).

During the site visits, the mine management, who were part of the mining team before and during the event occurred, was interviewed to an obtain a better understanding of the conditions and the sequence of events. Before underground mining was initiated, the outcrop of the UG2 was mined from surface. The underground mining commenced with the sinking of declines on reef, while landfill was used to cover the surface mine (see Figure 4-34). Everest Platinum Mine is situated in a high rainfall area and because of the mountainous terrain, water flows in the area are accentuated. This resulted in large amounts of water flowing into the filled surface mine. The reef, as well as the shear zone above the reef contact is exposed in the deepest section of the surface mine. This resulted in the shear zone being continuously exposed to water and the accelerated weathering of this zone. Following the collapse, measures were implemented to pump out and maintain the water inflow into the old surface mining areas.

In summary, Godden (2009) stated:

> *"Provisional and preliminary analysis suggests that the area down dip and to the north of the dominant, event-limiting fault should, in the long-term, remain in a stable state, but questions remain about the long-term stability of the currently undamaged pillar area to the south of the subsidence zone (the subsidence area could yet grow)."*

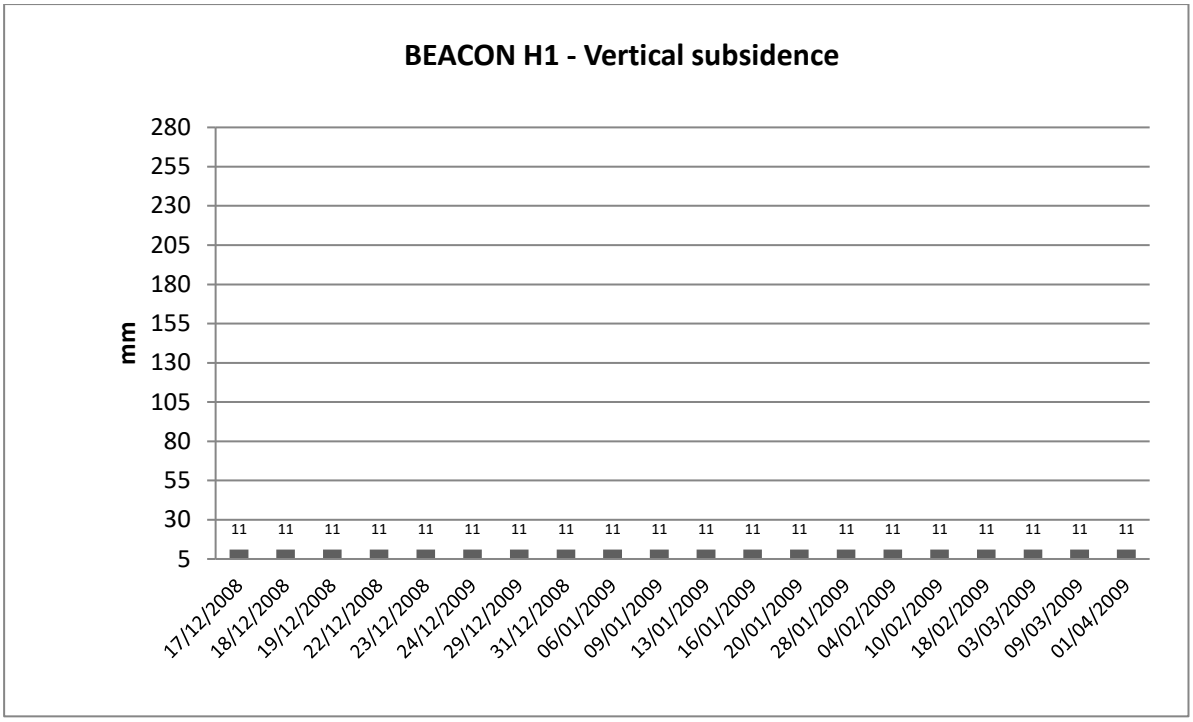

Figure 4-22. Vertical subsidence measured between December 2008 and April 2009 at Beacon H1.

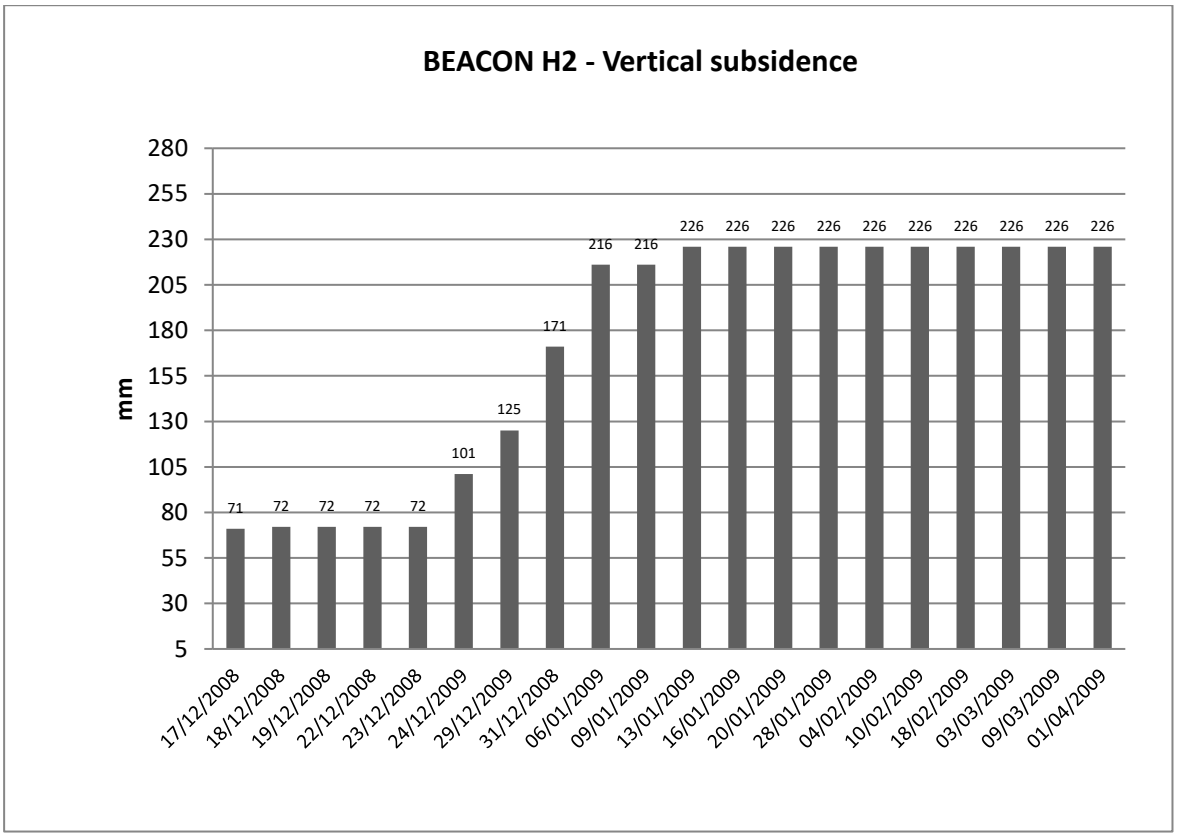

Figure 4-23. Vertical subsidence measured between December 2008 and April 2009 at Beacon H2.

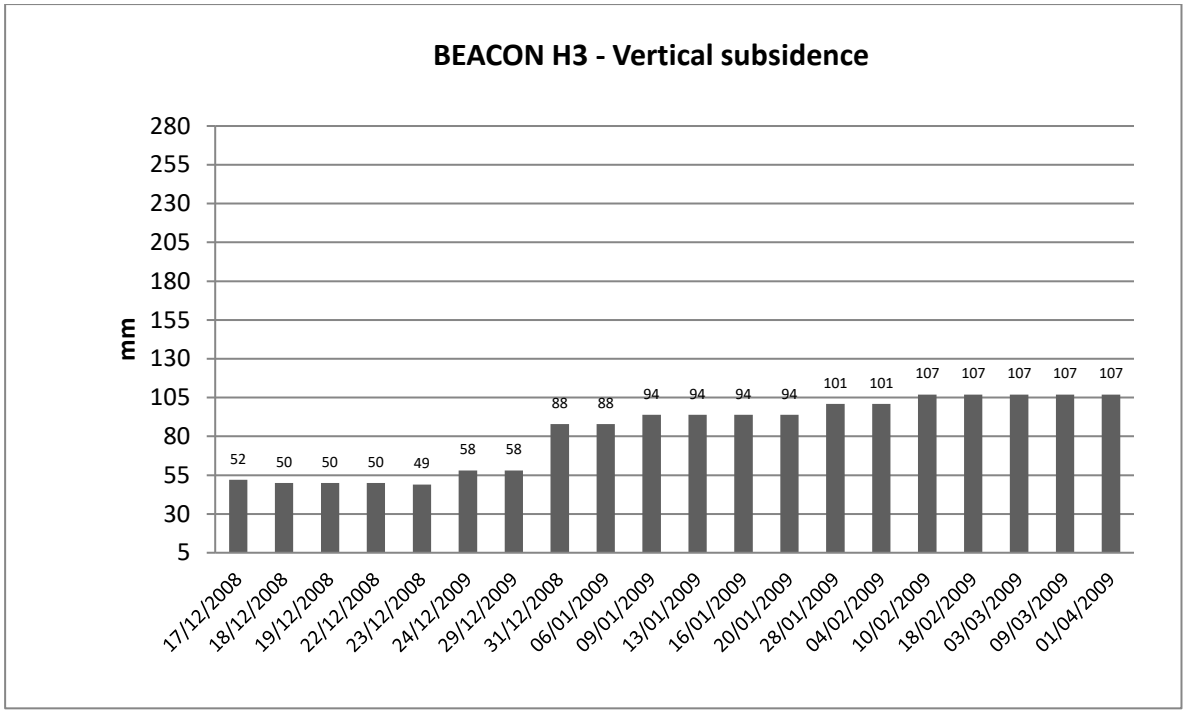

Figure 4-24. Vertical subsidence measured between December 2008 and April 2009 at Beacon H3.

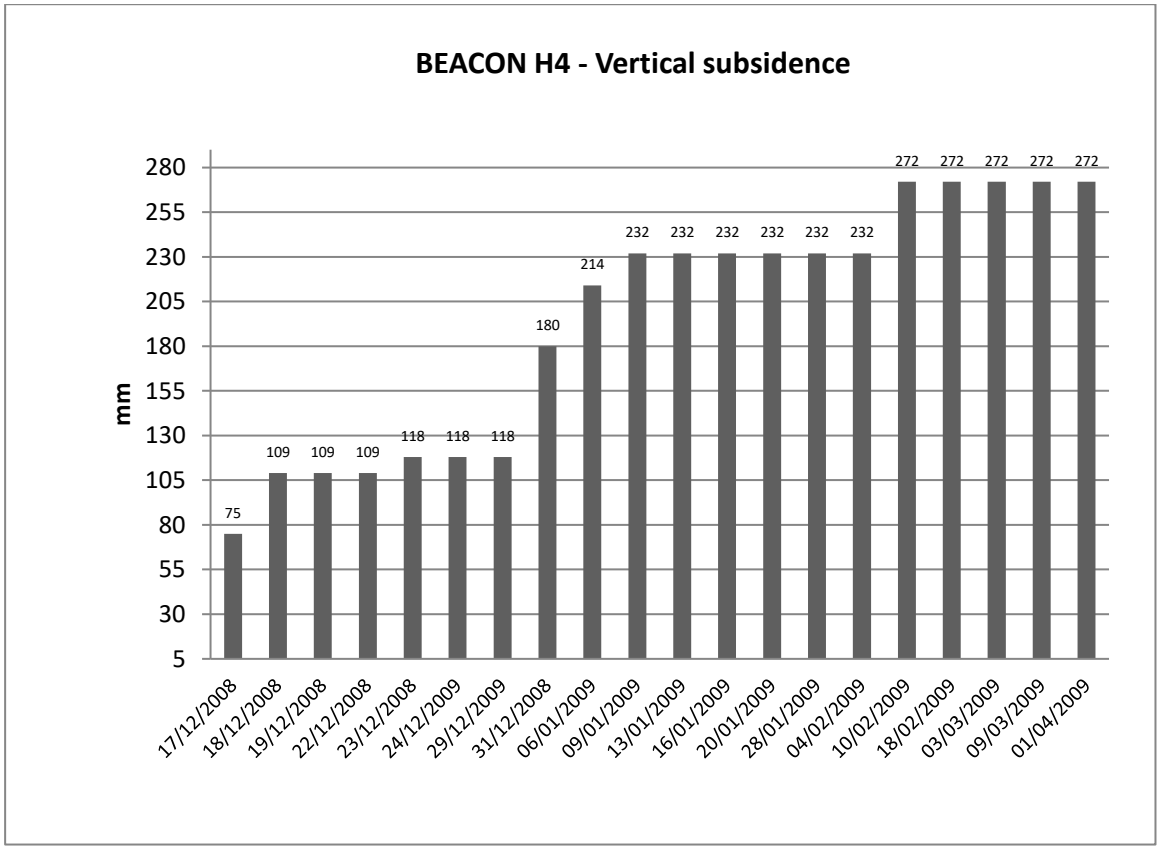

Figure 4-25. Vertical subsidence measured between December 2008 and April 2009 at Beacon H4.

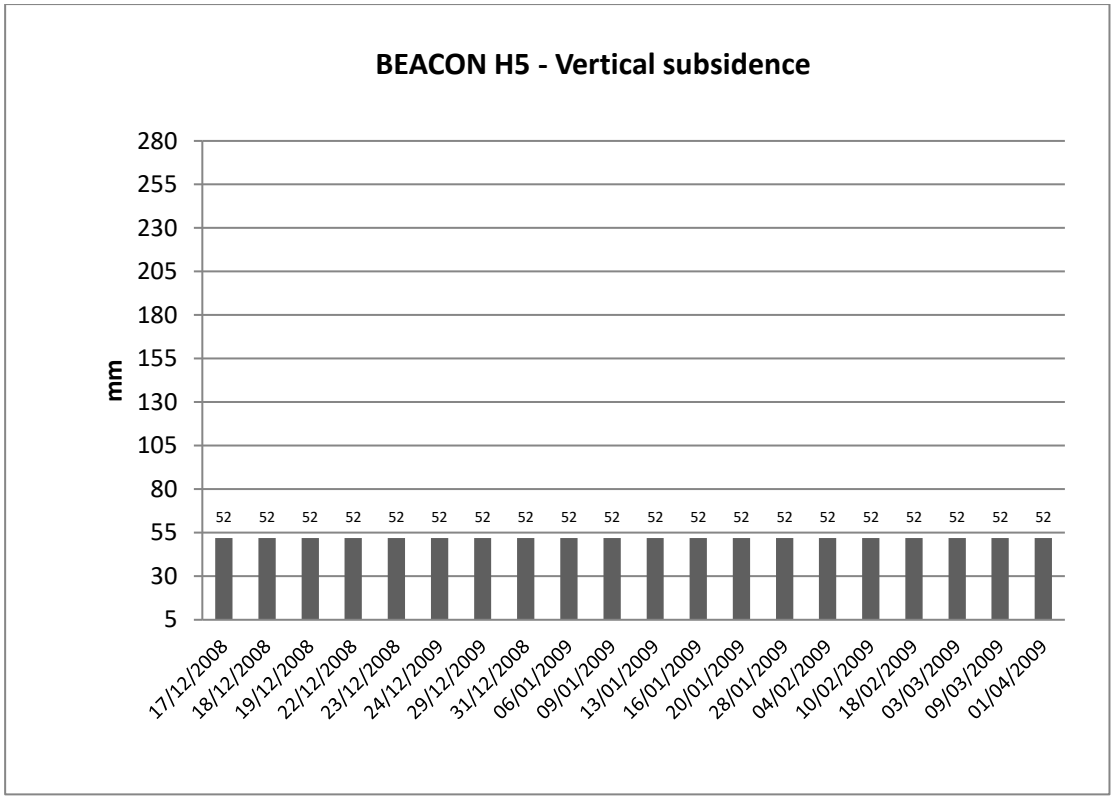

Figure 4-26. Vertical subsidence measured between December 2008 and April 2009 at Beacon H5.

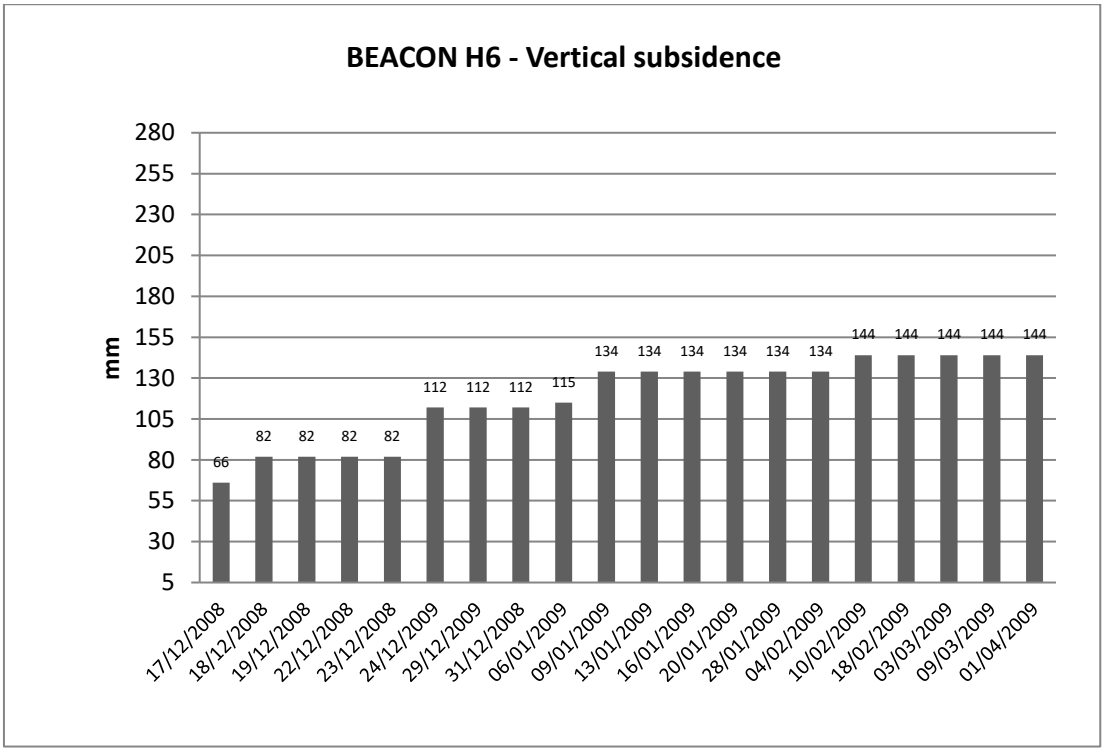

Figure 4-27. Vertical subsidence measured between December 2008 and April 2009 at Beacon H6.

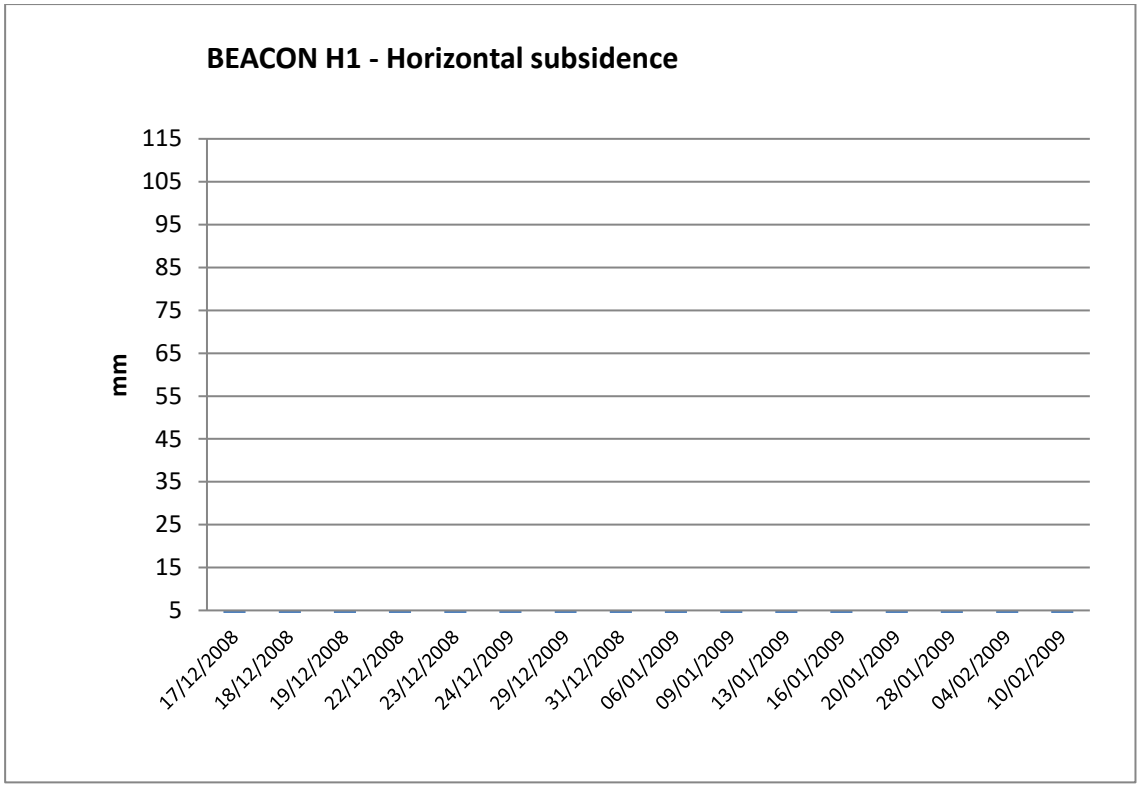

Figure 4-28. Horizontal subsidence measured between December 2008 and April 2009 at Beacon H1.

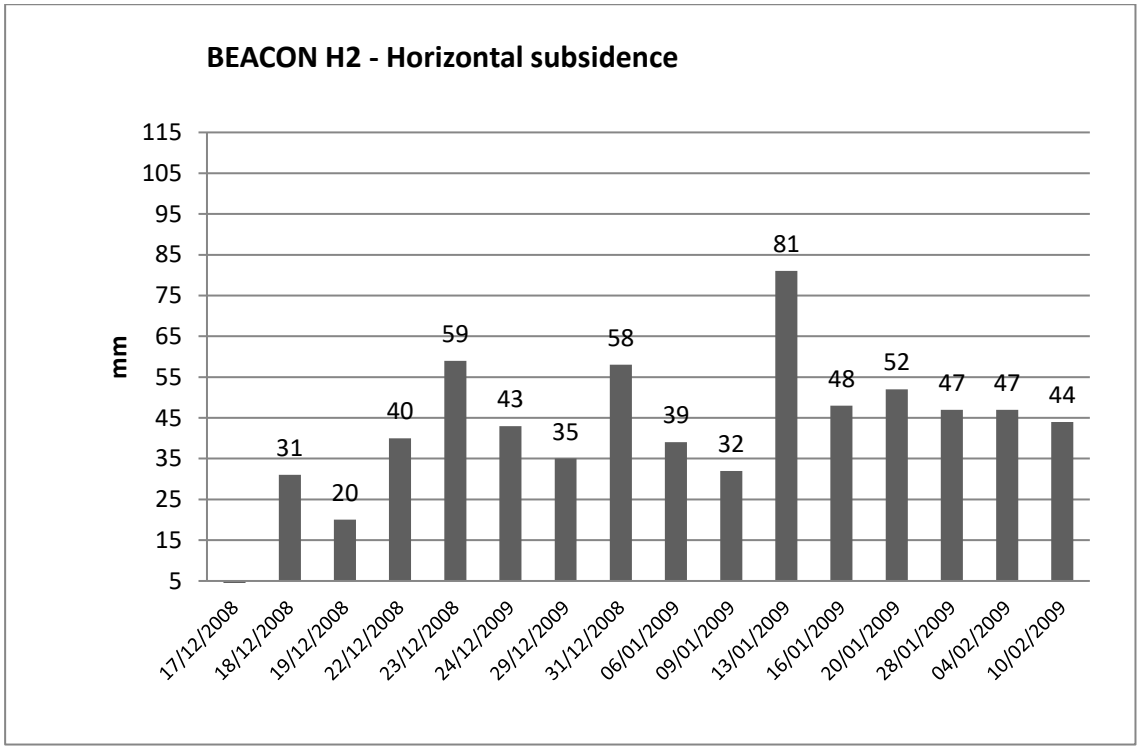

Figure 4-29. Horizontal subsidence measured between December 2008 and April 2009 at Beacon H2.

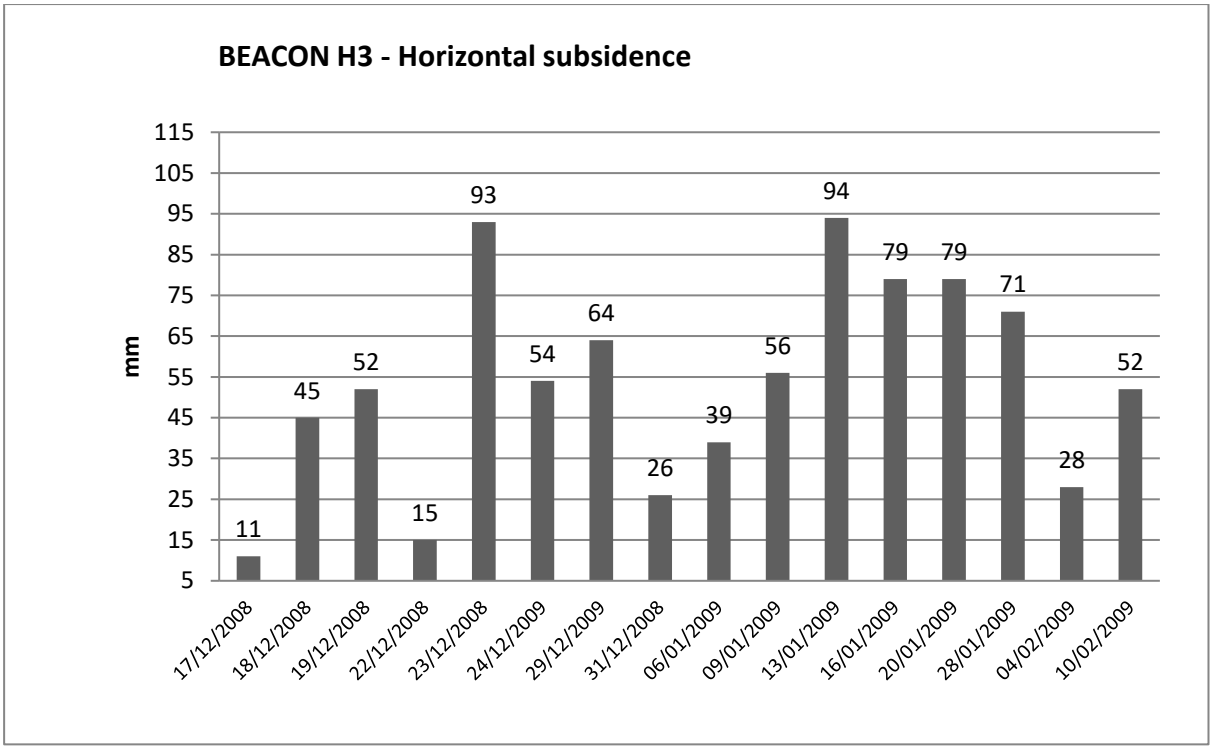

Figure 4-30. Horizontal subsidence measured between December 2008 and April 2009 at Beacon H3.

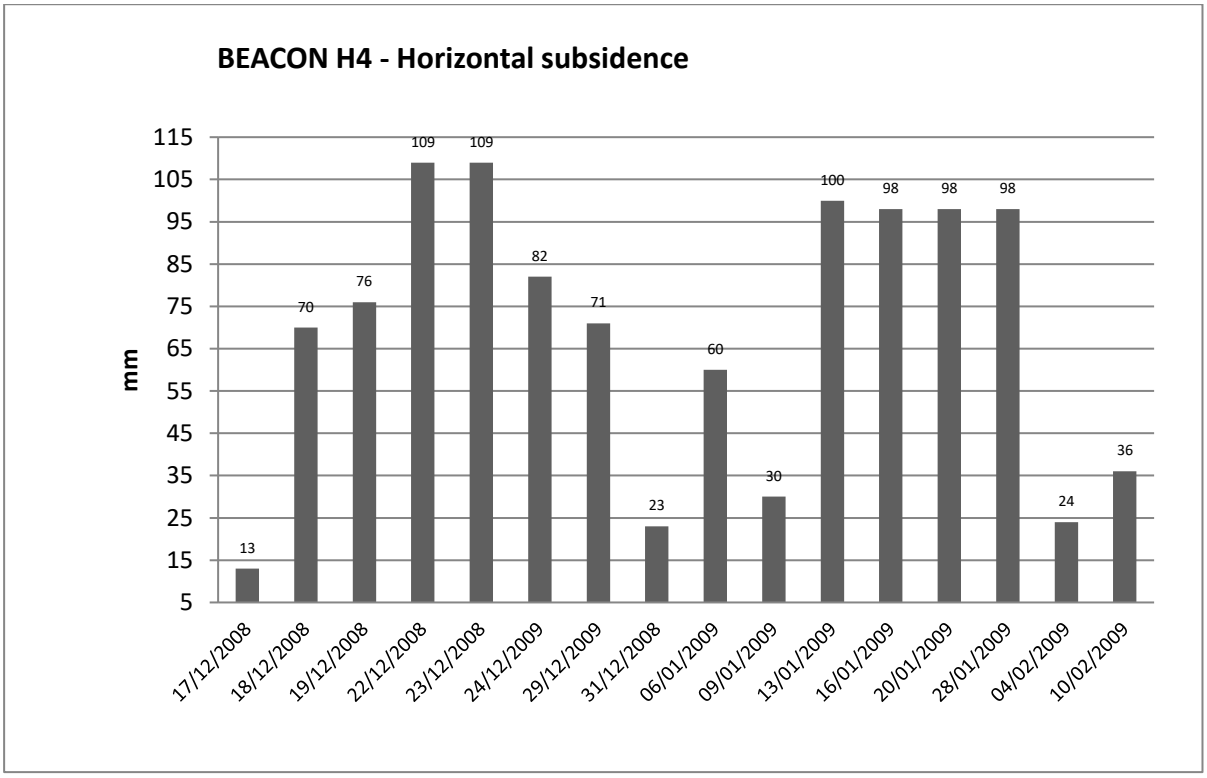

Figure 4-31. Horizontal subsidence measured between December 2008 and April 2009 at Beacon H4.

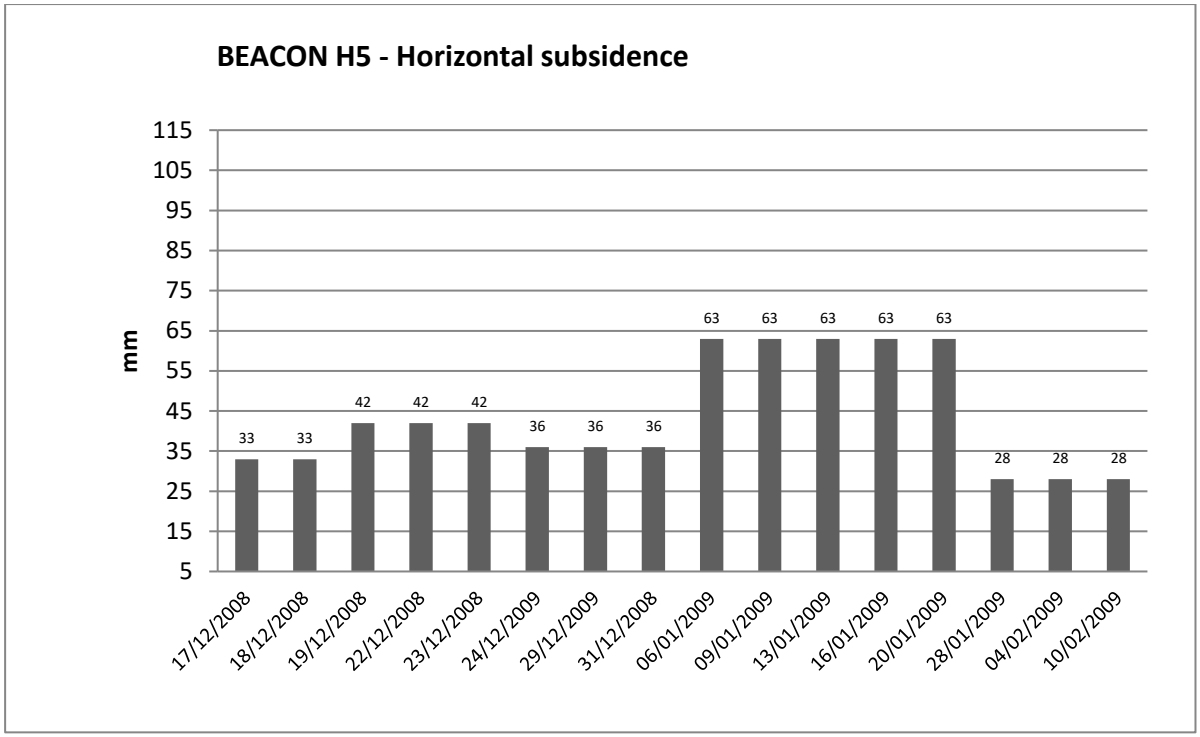

Figure 4-32. Horizontal subsidence measured between December 2008 and April 2009 at Beacon H5.

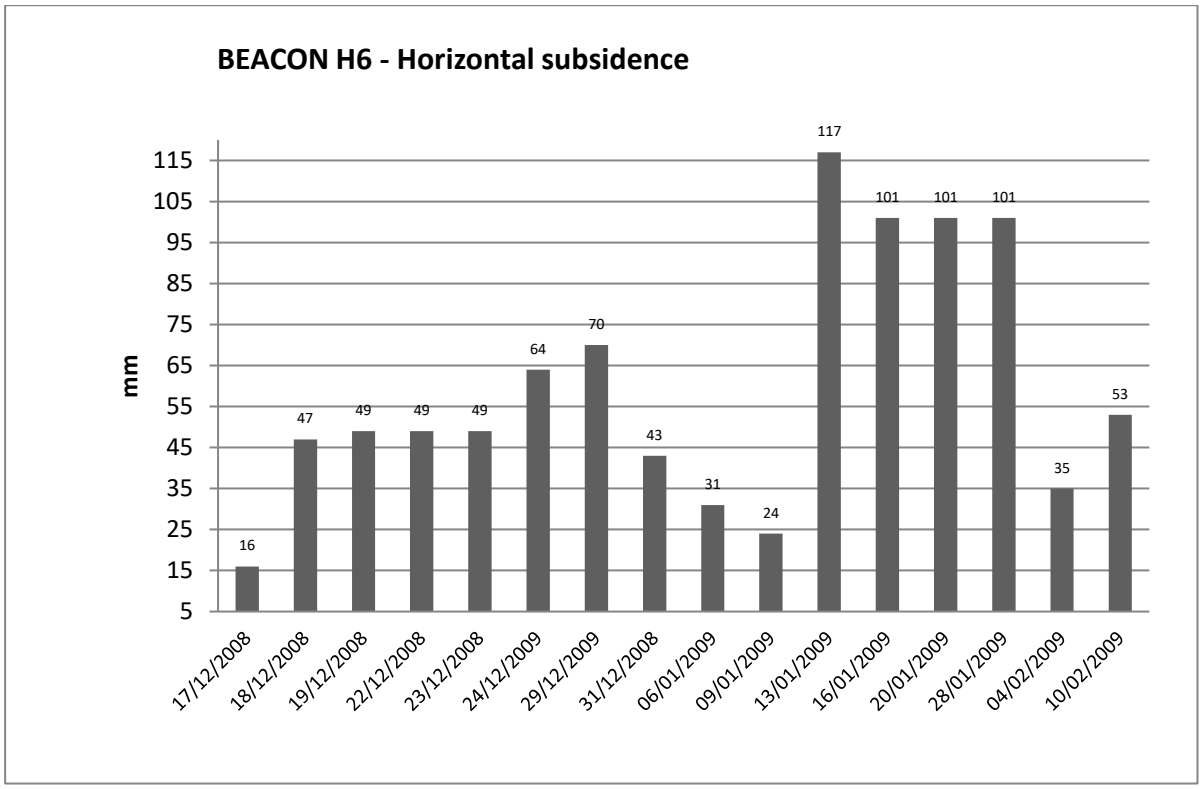

Figure 4-33. Horizontal subsidence measured between December 2008 and April 2009 at Beacon H6.

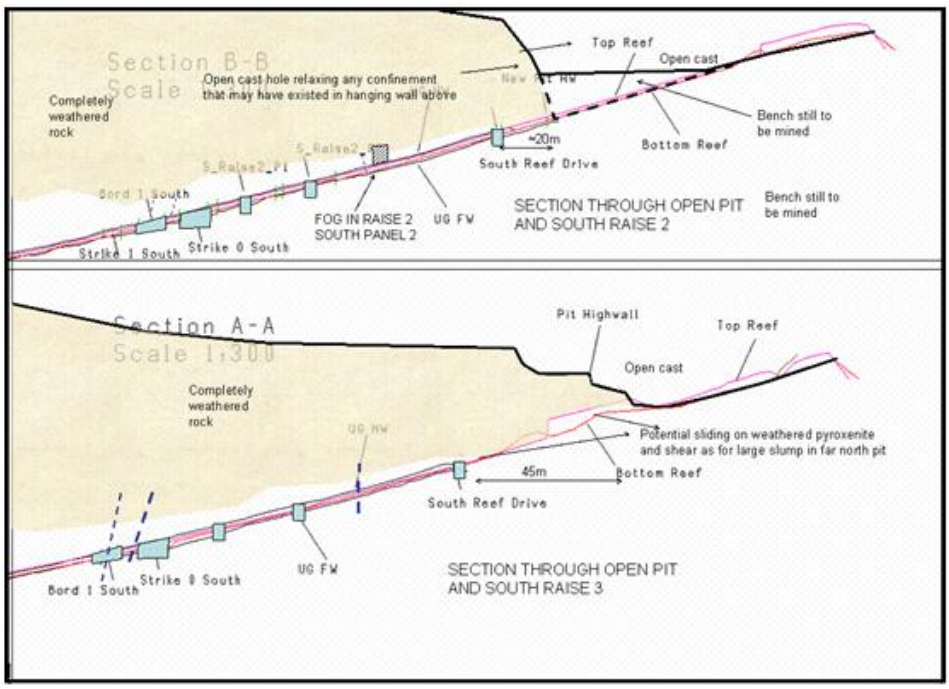

Figure 4-34. Sectional view of the area where the large collapse was experienced in relation to the surface mining (Lombard, 2011).

4.2.1 Additional information regarding the mine stability

The following information is included in this chapter as it gives additional insights into the stability of the mining excavations. This information was obtained from the reports written by mining personnel and consultants and is an extension of the sequence of events given in Table 3-2 in the previous chapter.

During August 2006, local pillar spalling and hangingwall deformation was observed in an initial stoping area close to surface. This area was to the south of the Decline where a conventional breast stoping method was used (Figure 4-35). Rock falls and pillar damage continued in the months that followed and a hangingwall collapse occurred during November 2006. The collapse extended to an approximately north-south trending fault zone located on the down-dip (west) side of the collapse area (Figure 4-35). No surface subsidence was observed or recorded at the time.

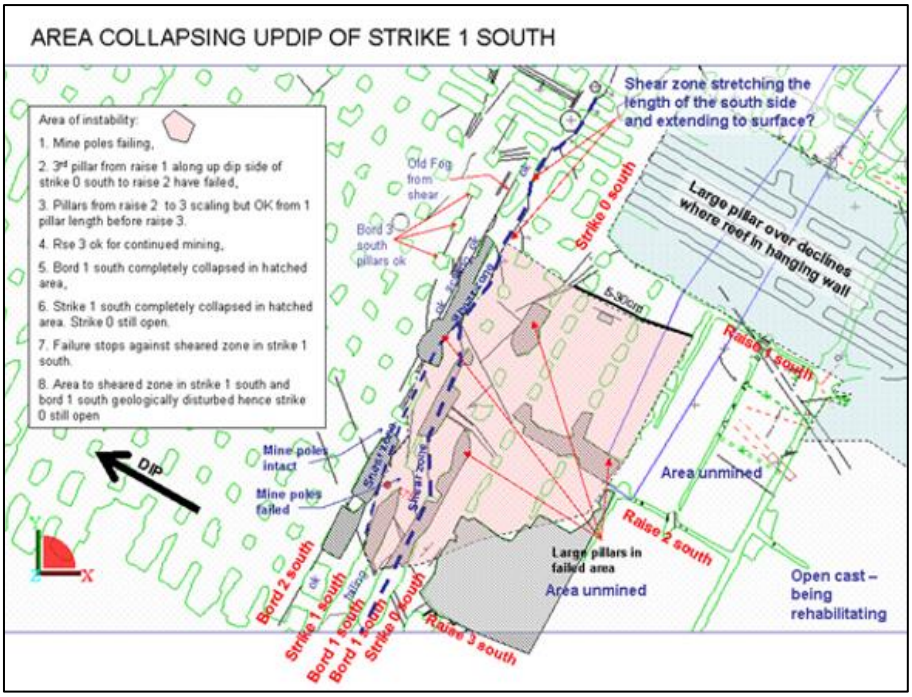

Figure 4-35. Summary of the area that collapsed during conventional breast mining methods, close to the crown pillar and weathering zone. (Lombard, 2011).

Following the November 2006 collapse, various remedial actions were implemented to prevent or reduce the amount of pillar spalling. In-stope closure monitoring stations were installed following the recommendations from consultants. Only a small amount of closure was recorded up to mid-March 2007. Thereafter, no further movement was recorded. At the time, the available data indicated that the pillar spalling and the related hangingwall instability issues had been ameliorated by the implemented remedial actions.

Pillar spalling was again observed during March 2008 in an area in the south side of the mine. Additional closure stations were installed, but these recorded little or no displacement up to November 2008.

Advice from external consultants was requested during September and October 2008. In summary, backfilling was suggested as a means of protecting the declines, but the long lead time, high capital cost and technical constraints (for example, the dip of the reef plane and its impact on backfill efficiencies) rendered this an impractical solution. Consideration was therefore given to support the decline pillars with anchors and straps. It was estimated that this work would take six months to complete. The deterioration of the pillars nevertheless continued.

Following exceptionally heavy rainfall during late November 2008, increasing panel closure was recorded, the failure of the pillars accelerated, and the final subsidence event occurred on 8 December 2008. An interview with the Mine Manager also provided additional information (Pretorius, 2020, pers. comm.):

- Approximately a month before the collapse, an increase in closure was recorded by the closure meters installed underground. This raised concerns regarding the stability of the mine. This was also the start of the rainy season, with relatively high rainfall already been recorded.
- An overtime crew was working during the weekend when the collapse occurred. On the Saturday shift, the crew came out of the mine with no noticeable change in the stability of the mining excavations.
- On Sunday, at the start of the shift, the Mine Manager received a call from the Mine Overseer. It was reported that the pillars in the Decline were scaling “badly”, and an excessive amount of material was lying in the roadways. The Mine Manager instructed the Mine Overseer to remove all mining personnel from underground.
- The Mine Manager, the Mine Overseer and members of the management team proceeded underground. The team stated that audible sounds of rock crushing could be heard underground.
- On Monday morning, it was confirmed that the Decline pillars had been completely crushed, and the Decline was blocked by a large collapse.

Based on the information given above, it is clear that a new mine design methodology is required for areas where weak alteration zones are present in the pillars. Numerical modelling is expected to play a role in the development of such a methodology. A first step would be to back-analyse the Everest Mine collapse using a suitable model. Numerical simulation of mine-wide collapses, caused by pillars weakened by slippery layers, is a very difficult problem, however. This study investigated the use of a limit equilibrium model to simulate the mechanism of pillar failure and mine collapse. The following chapter describes the TEXAN code and the limit equilibrium model that was used for this study.

5 THE LIMIT EQUILIBRUM MODEL IN THE TEXAN CODE

5.1 Introduction

In the displacement discontinuity boundary element method (DDM), mining layouts are estimated as irregular shaped planar cracks (or slits) where the 'width' of the crack, corresponding to the excavation height, is assumed to be negligible compared to the lateral dimensions. This approach has been very successful to simulate the tabular layouts of the deep gold mines in South Africa and early codes using this approach were MINSIM and BESOL. The TEXAN (Tabular EXcavation ANalyser) code (Napier and Malan, 2007) is an enhanced approach in which triangular or quadrilateral element shapes are introduced in conjunction with higher order variations of the displacement discontinuity shape functions. This facilitates a more accurate evaluation of detailed stress and displacement components close to excavation surfaces and allows for the assessment of tabular layouts which includes many irregular-shaped pillars.

A major challenge in the design of pillar layouts is to integrate an appropriate representation of the pillar failure behaviour with the overall analysis of the interactive tabular mining stress distribution. The detailed inelastic analysis of seam or reef crushing behaviour is mostly conducted by means of non-linear finite element or finite difference models whereas the tabular excavation layout stress interactions in three dimensions can be efficiently represented using a boundary element model based on classical displacement discontinuity elements. Some simplification to the problem is possible if the fractured material is confined to the plane of the reef and does not extend into the hangingwall or footwall regions. This will typically be the case for crush pillars in shallow pillar mining layouts. In the present study, a limit equilibrium model implemented in the TEXAN code (Napier and Malan, 2007) is used to represent the behaviour of the failed reef material in the pillars.

Accurate simulations of stress acting on pillars in bord and pillar layouts typically require the simulation of large areas (see Napier and Malan, 2011). Simulated average pillar stress is not always accurate if the element size is not small enough. The poor pillar cutting in underground environments also makes the building of an accurate geometry of the layout very difficult depending on the type of code used. Three-dimensional finite element or finite difference models are therefore seldom used

to simulate bord and pillar layouts on a large scale. These codes are nevertheless very useful to simulate the detailed failure mechanism of a single pillar in a small model. Displacement discontinuities boundary element (DD) programs, using triangular element shapes, overcome the problem of building a large-scale model with many irregular shaped pillars. As a drawback, it is typically impossible for most of these DD codes to simulate the failure of the pillars. As an example, for a platinum mine, Leach (2007) used a DD code to simulate two scenarios namely a “worst-case” scenario where the in-panel crush pillars were not included and a second approach where it was attempted to simulate the effect of the small pillars using a backfill “soup”. Calibration of this backfill material is problematic, and it is questionable if it is a realistic representation of the effect of the crush pillars. The limit equilibrium model as described below is an improved method to introduce pillar failure in these DD codes.

The TEXAN code can currently solve 2D and 3D problems with multiple interacting tabular reef planes and planar fault planes. These planes are tessellated with displacement discontinuity elements to represent stope ride and elastic convergence movements or to model slip movements on fault planes. Elements can be in an “infinite” space or in a “semi-infinite” space with a flat, stress-free surface to simulate excavations close to surface. The rock is assumed to be elastic and isotropic.

Elements can be 2D line segments, 3D triangles or 3D convex quadrilaterals. Square elements can be used if required. The triangular elements are most suitable to simulate bord and pillar geometries with irregular pillar shapes. In comparison, very small elements need to be used in DD codes that only allow the use of square elements.

As described by Napier (unpublished notes, 2021), each element can have one or more internal collocation points giving constant or higher order variation discontinuity densities. Triangular elements can be defined to have 1, 10 or 15 internal collocation points giving constant, cubic (third order) or quartic (fourth order) discontinuity variations respectively. Quadrilateral elements can be defined with 1 or 9 internal collocation points. A quadrilateral element with 9 internal collocation points is assigned a bi-quadratic shape function (fourth order). Stress and displacement field values (so-called “benchmark” values) close to excavation surfaces are accurately computed with higher order elements. Stress singularities can nevertheless arise close (within 0.1 of the element “diameter”) to element boundaries. Field values cannot be computed

accurately within a distance of approximately two to three element “diameters” from the surface when using constant elements.

An undulating reef plane is a difficult aspect to model and typically the reef planes are assumed to be planar to simplify the geometries in TEXAN.

5.2 Description of the limit equilibrium model

Details of the use of this particular model can be found in Du Plessis et al (2011), Napier and Malan (2012), Napier and Malan (2014), Malan and Napier (2018) and Napier and Malan (2021). The derivation of the model is given below for completeness and to illustrate the basic behaviour of the model.

Consider the force equilibrium of a slice of rock in the pillar shown in Figure 5-1. This diagram illustrates the mined bord on the left and part of the pillar on the right. An important aspect of the model is that there is an interface at the pillar contact for both the hangingwall and footwall. Typically, the edge of the pillar will fail where the stress exceeds the specified strength and the remainder of the pillar will remain intact. For weak material properties and high stress, the entire pillar can fail.

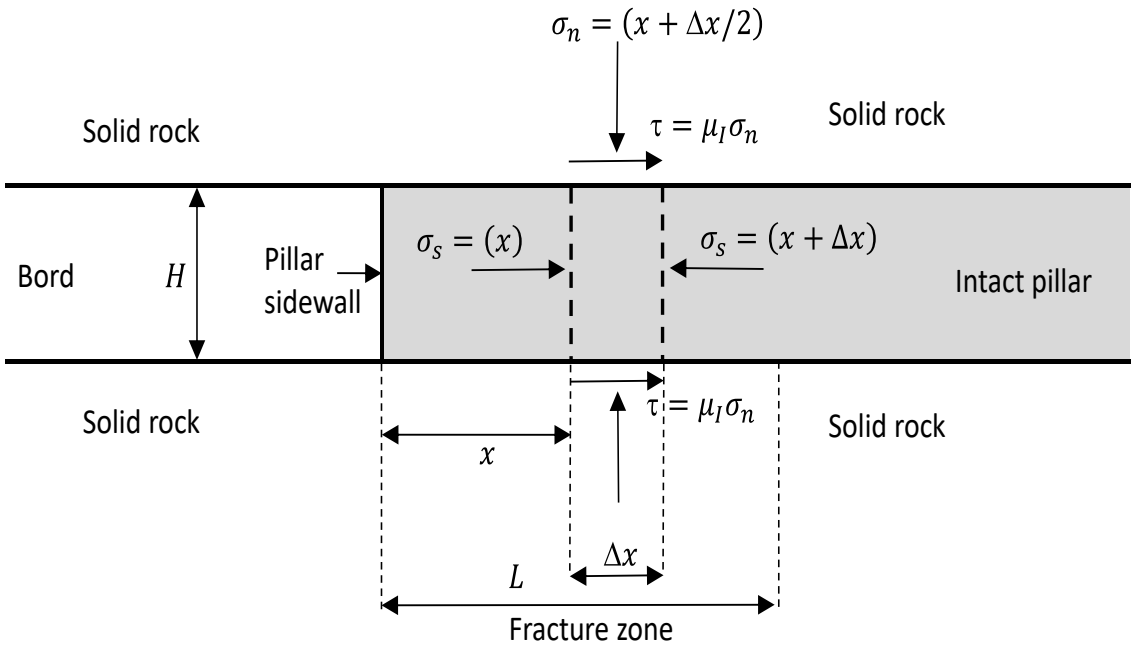

Figure 5-1. Force equilibrium of a slice of rock in a pillar (after Malan, 2019).

It is assumed that at $x = 0$, the edge of the pillar, the material is unconfined and that the seam-parallel stress component σ_s increases as x increases. The slice of rock indicated by the dotted lines in Figure 5-1 is assumed to be in equilibrium. For this to be true, it is required that:

$$H\sigma_s(x) + 2\tau\Delta x = H\sigma_s(x + \Delta x) \quad (5.1)$$

Note that the second term on the left of this equation reflects the effect of the interfaces at the hangingwall and footwall contacts. Equation (5.1) can be rearranged to give:

$$\frac{\sigma_s(x+\Delta x)-\sigma_s(x)}{\Delta x} = \frac{2\tau}{H} \quad (5.2)$$

The left-hand side of equation (5.2) is the definition of a derivative if $\Delta x \to 0$ and therefore equation (5.2) can be written in the form of a differential equation if the width of the slice tends to zero:

$$\lim_{\Delta x \to 0} \frac{\sigma_s(x+\Delta x)-\sigma_s(x)}{\Delta x} = \frac{2\tau}{H} \quad (5.3)$$

or

$$\frac{d\sigma_s}{dx} = \frac{2\tau}{H} \quad (5.4)$$

Equation (5.4) can only be solved if there is a relationship between τ and σ_s. This is achieved by making the following two assumptions:

(1) Assume that there is friction on the interfaces between the pillar, hangingwall and footwall, therefore τ is related to the pillar-normal stress σ_n by the following frictional slip condition:

$$\tau = \mu_I \sigma_n \quad (5.5)$$

where μ_I is the coefficient of friction coefficient at the interface of the pillar contacts. Equation (5.5) can therefore also be written as:

$$\tau = tan\varphi(\sigma_n) \quad (5.6)$$

where φ is the friction angle on the interface.

(2) Assume that σ_n is related to the seam-parallel stress component σ_s by a failure relationship of the form:

$$\sigma_n = m\sigma_s + \sigma_c \quad (5.7)$$

where σ_c and *m* are specified constants. Once failure occur, σ_c can be considered as the strength of the failed pillar material and *m* is a slope parameter. This slope parameter simulates the confinement effect of the failed material on the edges of the pillar. A higher normal stress can therefore be found further away from the edge of the pillar.

Substituting equations (5.6) and (5.7) into equation (5.4) gives the following differential equation:

$$\frac{d\sigma_s}{dx} = \frac{2tan\varphi}{H}(m\sigma_s + \sigma_c) \quad (5.8)$$

Equation (5.8) can be integrated if the variables are separated as follows:

$$\int \frac{d\sigma_s}{m\sigma_s+\sigma_c} = \int \frac{2tan\varphi}{H} dx \quad (5.9)$$

The indefinite integral of the left-hand side of equation (5.9) can be solved as

$$\int \frac{d\sigma_s}{m\sigma_s+\sigma_c} = \frac{ln(m\sigma_s+\sigma_c)}{m} \quad (5.10)$$

This solution can be inserted into equation (5.9) and by solving the simple integral on the right side of equation (5.9), the following solution can be obtained. The solution depends on integration constant A.

$$\frac{ln(m\sigma_s+\sigma_c)}{m} = \frac{2tan\varphi x}{H} + A \quad (5.11)$$

The constant A is derived by applying the boundary condition $\sigma_s = 0$ when $x = 0$. This gives the value of A as

$$A = \frac{ln(\sigma_c)}{m} \quad (5.12)$$

Equation (5.12) can be inserted into (5.11) to give

$$\frac{ln(m\sigma_s+\sigma_c)}{m} = \frac{2tan\varphi x}{H} + \frac{ln(\sigma_c)}{m} \quad (5.13)$$

and by combining the logarithmic expressions

$$\frac{1}{m} ln\left(\frac{m\sigma_s+\sigma_c}{\sigma_c}\right) = \frac{2tan\varphi x}{H} \quad (5.14)$$

This can be written as

$$\frac{m\sigma_s+\sigma_c}{\sigma_c} = e^{2tan\varphi mx/H} \quad (5.15)$$

and from this the solution of the seam-parallel stress follows as

$$\sigma_s = \frac{\sigma_c}{m}\left(e^{2tan\varphi mx/H} - 1\right) \quad (5.16)$$

Equation (5.16) is written in a simpler form by assuming

$$\alpha = \frac{2tan\varphi m}{H} \quad (5.17)$$

This gives

$$\sigma_s = \frac{\sigma_c}{m}(e^{\alpha x} - 1) \quad (5.18)$$

Substituting equation (5.18) into equation (5.7) gives an expression for σ_n :

$$\sigma_n = \sigma_c e^{\alpha x} \quad (5.19)$$

Equation (5.19) implies that the normal stress in the failed pillar edge increases exponentially towards the boundary between the failed and intact rock. This exponential increase in stress is characteristic of the model and it is not clear if this is a good representation of the stress in a failed pillar. Also, important to consider is that it is a requirement that $\sigma_c > 0$, even after failure, otherwise the normal stress will be zero in all the failed parts of the pillar.

With regards to the weak interface at Everest Platinum Mine, from equations (5.17) and (5.19), it is clear that the friction angle on the partings with the hangingwall and footwall play a prominent role in the subsequent distribution of stress in the pillar once failure initiates. Figure 5.2 illustrates the increase in stress from the edge of a failed pillar for different friction angles when assuming the parameters $m = 4$, $\sigma_c = 1\ MPa$ and $H = 2\ m$. Figure 5-3 illustrate the same trends for a value of $m = 2$. The model is clearly sensitive to the selection of friction angle and the residual strength of the failed pillar rapidly decreases for low friction angles. Also clear from the diagram is the very high stresses predicted in the centre of the pillar for large values of friction angles and higher values of m. These sharp peaks of stress in the centre of a failed pillar for high friction angles and slope parameter values are not considered realistic and is one of the drawbacks of the model.

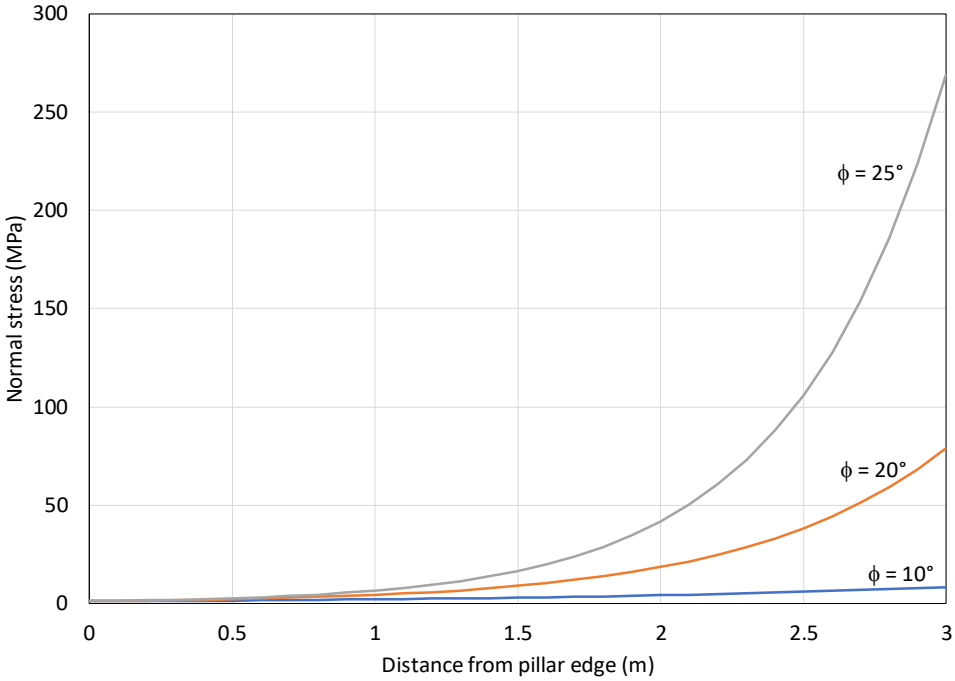

Figure 5-2. Increase in normal stress acting on a completely failed pillar when assuming a limit equilibrium model. The centre of the pillar is at 3 m. The graph is plotted using parameters $m = 4$, $\sigma_c = 1\ MPa$ and $H = 2\ m$.

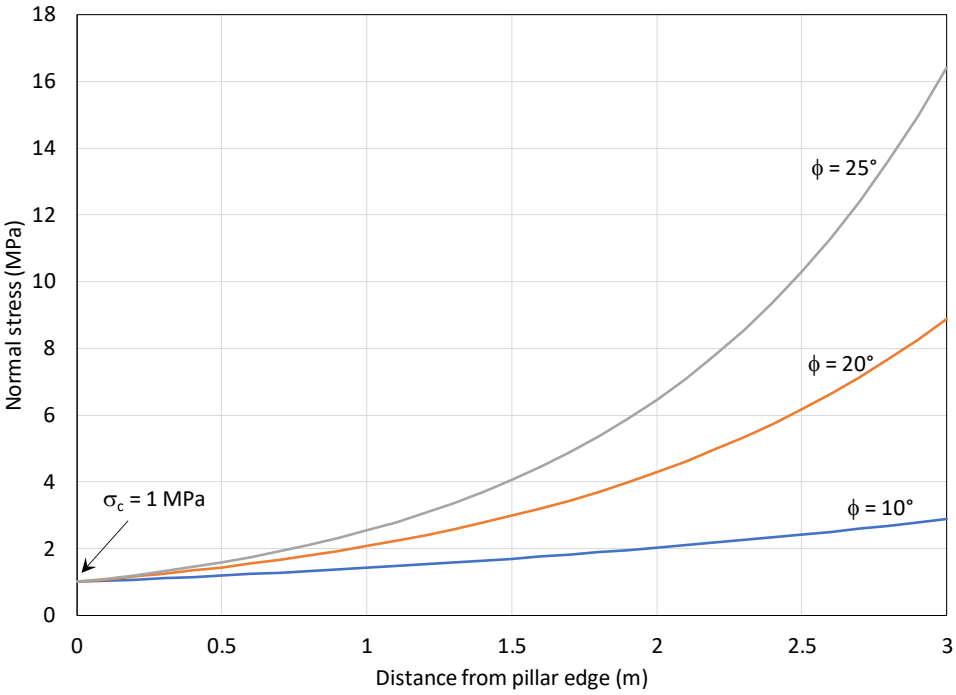

Figure 5-3. Increase in normal stress acting on a completely failed pillar when assuming a limit equilibrium model. The centre of the pillar is at 3 m. The graph is plotted using parameters $m = 2$, $\sigma_c = 1\ MPa$ and $H = 2\ m$. The equations above are a simple derivation

to illustrate the behaviour of the model. In the TEXAN code, a slightly more complex model is implemented where there is a failure relationship between σ_n and σ_s for the intact pillar material given by

$$\sigma_n = m^i \sigma_s + \sigma_c^i \quad (5.20)$$

as well as for the failed pillar material

$$\sigma_n = m^f \sigma_s + \sigma_c^f \quad (5.21)$$

When specifying these parameters, the requirements of $m^i \geq m^f$ and $\sigma_c^i \geq \sigma_c^f$ must be met.

Also, important to note is that the TEXAN code assumes that the intact region of a pillar behaves according to a “spring” model that allows deformation in the normal direction. A “seam stiffness” value therefore also needs to be specified as an input parameter. Typically, this stiffness parameter is selected to match the deformation modulus of the host rock. The code solves the normal stress acting on the pillar and tests if failure of any of the elements will occur according to equation (5.20). If no failure occurs for a particular element, a small amount of strain will occur in the normal direction according to the stiffness parameter specified. If the particular element fails, new strength parameters are adopted according to equation (5.21) and the excess stress for this element gets redistributed to neighbouring elements. Very weak parameters and large numbers of failed pillars can result in a large number of iterations , and increased solution times.

It should be noted that the limit equilibrium model in TEXAN has the ability to simulate time-dependent pillar failure. This is achieved by reducing the intact strength parameters in equation (5.20) after failure in a time-dependent fashion to the failed parameters in equation (5.21). This option was not explored in this study, however, as no data on the rate of pillar scaling was available to the author. As noted in Chapter 4, only a small increase in the size of the failed zone was detected over the last 10 years and it seems that in this quasi-equilibrium state, the rate of time-dependent pillar failure is very slow.

5.3 Behaviour of the limit equilibrium model for a simplified geometry

5.3.1 Effect of element size

A basic pillar geometry (Figure 5-4) was simulated to further explore the behaviour of the limit equilibrium model. It consisted of a single 10 m x 10 m pillar in a square mined area of 50 m x 50 m. The normal stress along Section AA' is plotted in the graphs below. Square elements were used for this model. The input parameters are given in Table 5-1. These are arbitrary parameters to illustrate the behaviour of the model. Calibration of these parameters is described in Chapter 6.

Table 5-1. Input parameters for the test geometry of a single pillar in a mined stope.

Parameter	Value
Intact Strength, σ_c^i	25 MPa
Intact rock slope, m^i	4.0
Crushed Rock Strength σ_c^f	4 MPa
Crushed rock slope, m^f	4.0
Interface Friction Angle, ϕ	10°
Seam Height, H	2.0 m
Seam Stiffness Modulus	35 000 MPa/m

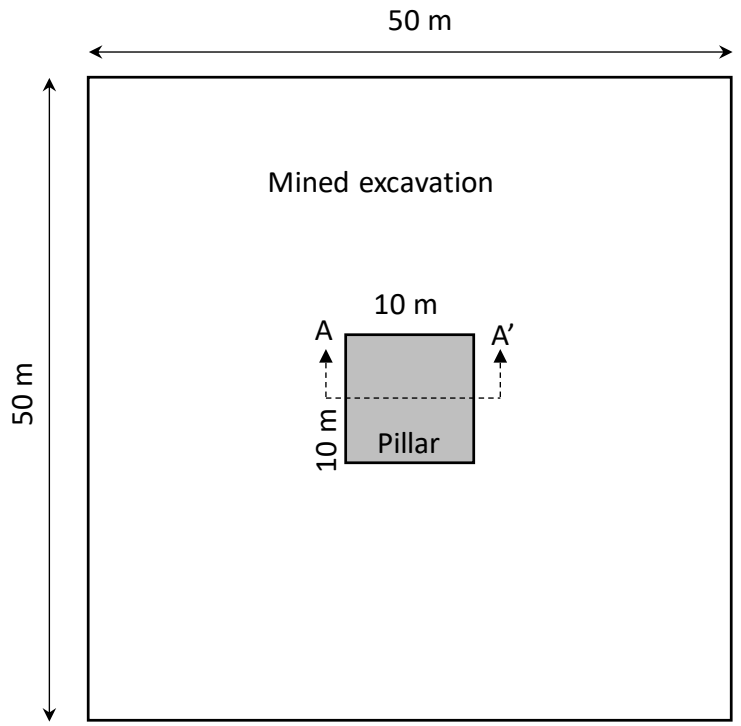

Figure 5-4. Single pillar simulated to investigate the behavior of the limit equilibrium model.

The simulations were conducted with a range of element sizes to investigate the effect of this parameter. Sizes of 2 m, 1 m and 0.5 m were used. The results are given in Figure 5-5 to Figure 5-10. These figures illustrate the failure of the limit equilibrium elements and the normal stress acting on the pillar along Section AA' for each element size. Note that so-called constant-strength DD elements were used in these runs and the elements therefore only contain a single collocation point per element. The plots of failure use different colour dots to indicate whether each collocation point failed or not. The yellow dots are intact elements and brown colour are the failed elements.

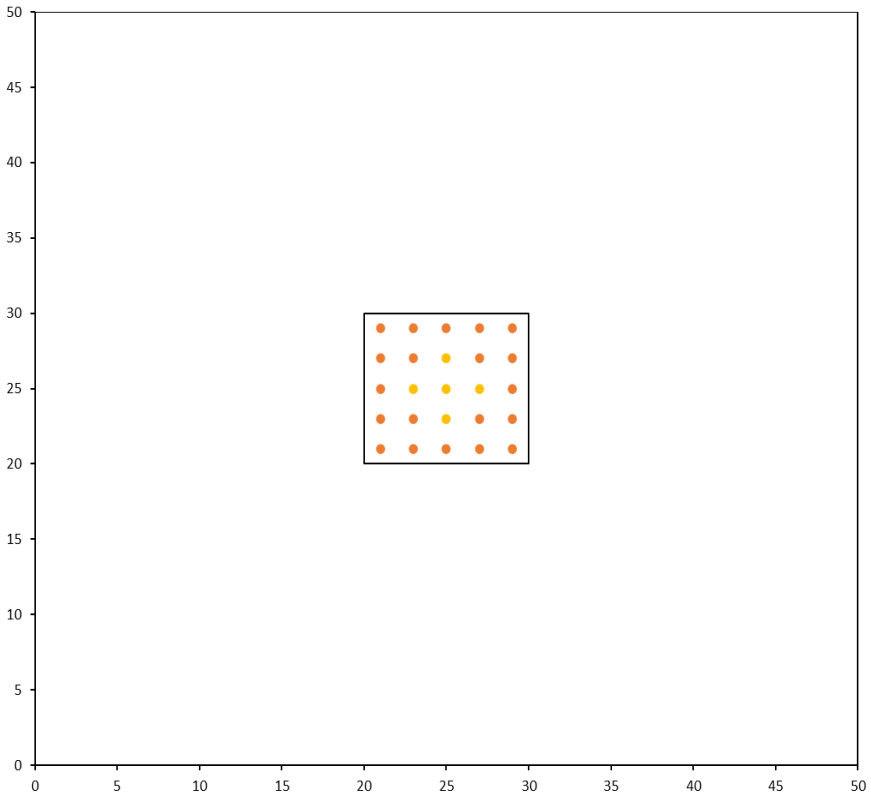

Figure 5-5. Plot of the failed elements when using a 2 m element size. This large element size only required only 25 elements to represent the pillar area. This explains why the dots are so widely spaced. The yellow dots represent intact elements and the brown dots represent failed elements. There are only 4 intact elements in the centre of the pillar.

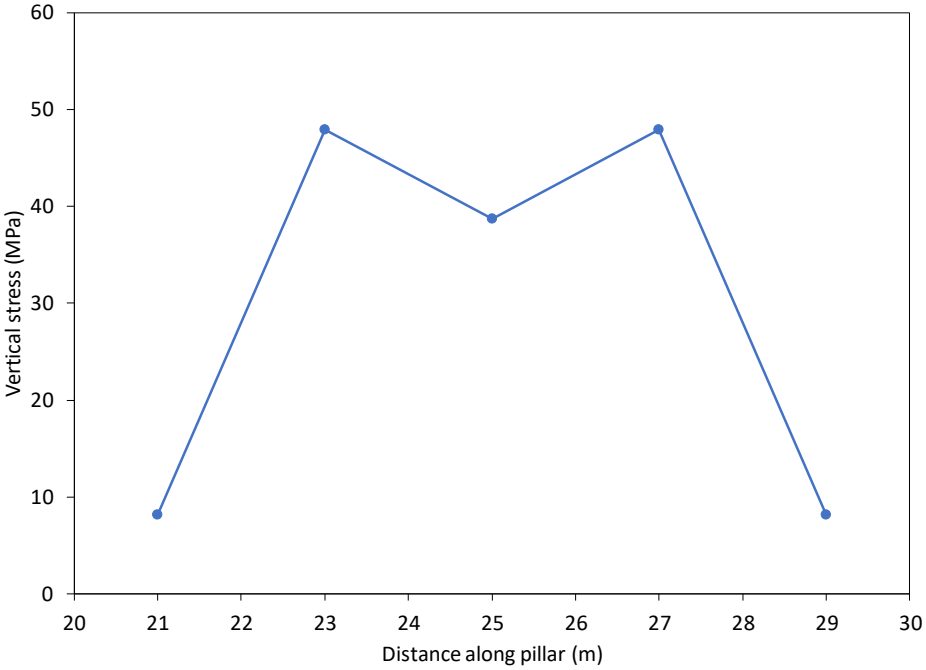

Figure 5-6. Vertical stress along section AA' when using 2 m element sizes.

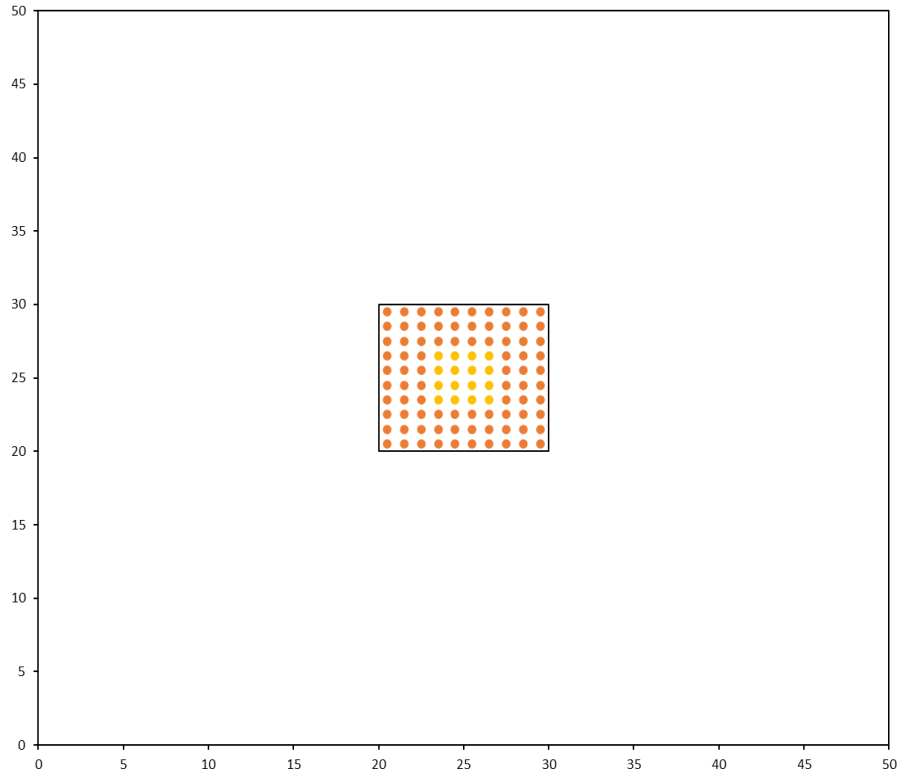

Figure 5-7. Plot of the failed elements for a 1 m element size. The yellow dots represent intact elements and the brown dots represent failed elements.

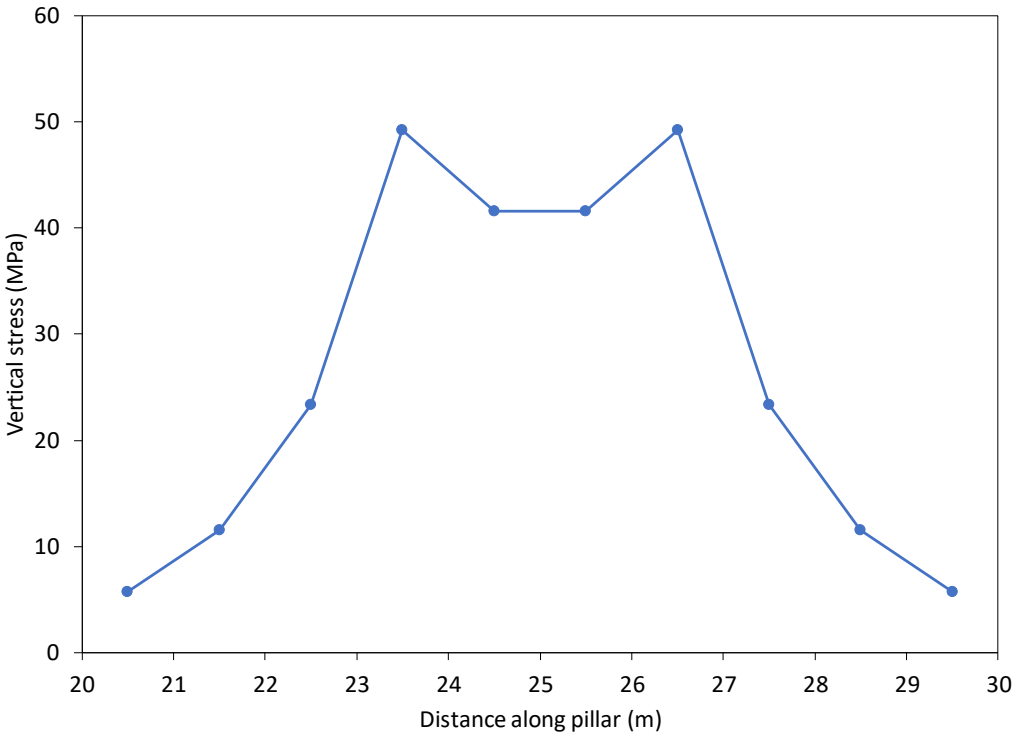

Figure 5-8. Vertical stress along section AA' when using 1 m element sizes.

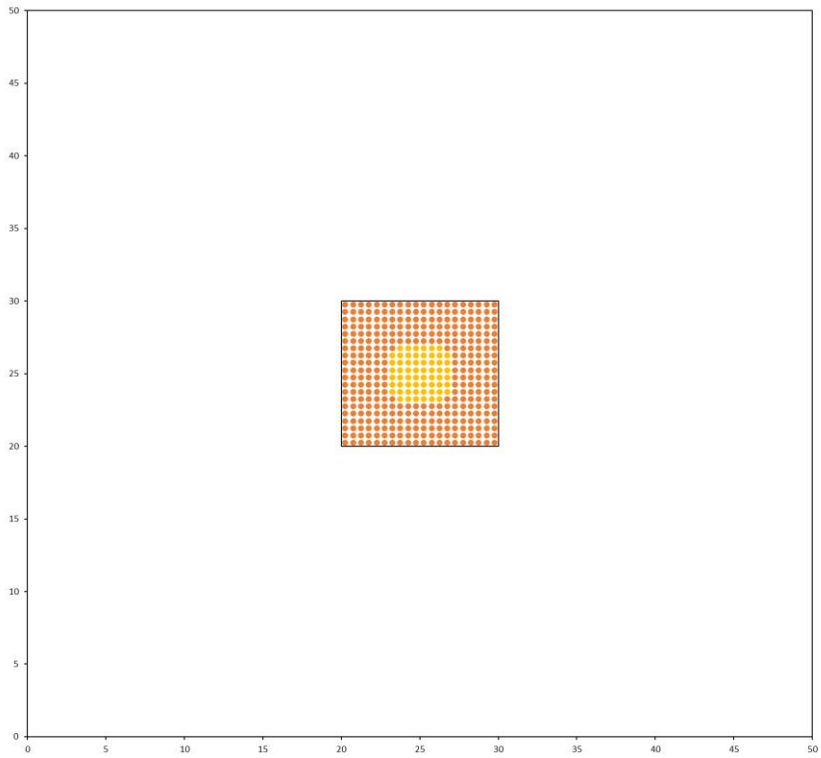

Figure 5-9. Plot of the failed elements when using a 0.5 m element size. The yellow colour represents intact elements and the brown colour represents failed elements.

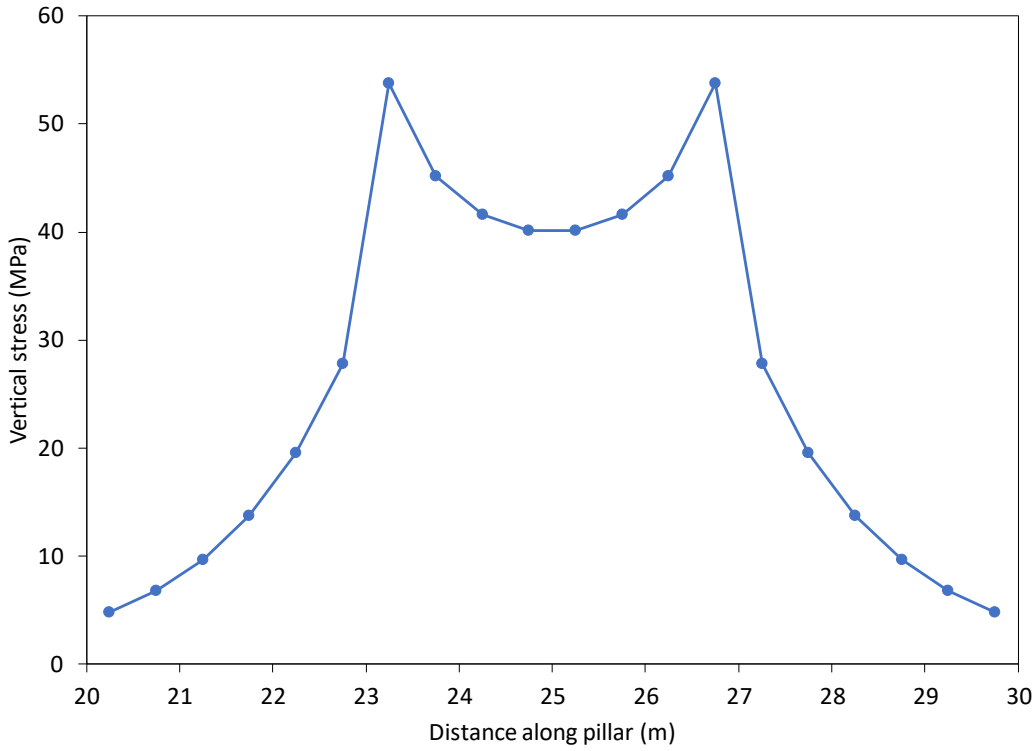

Figure 5-10. Vertical stress along section AA' when using 0.5 m element sizes. Note the clearly defined failed pillar wedges and the intact core of the pillar in the centre.

Figures 5-6, 5-8 and 5-10 illustrate the importance of using small element sizes relative to the size of the pillar to ensure the failure and stress distribution in the pillar can be accurately represented. Figure 5-10 clearly illustrates the intact core and the exponential increases in stress in the failed edges of the pillar.

5.3.2 Effect of intact material strength

The effect of the intact material strength was investigated, and a number of simulations were conducted. An element size of 0.5 m was used for all the simulations illustrated in this section. The results below illustrate the effect of the reducing the intact strength, σ_c^i, from 55 MPa to 10 MPa. For a value of 10 MPa, the pillar was completely crushed. The failure of the pillar is shown in Figure 5-11 and the stress distribution across the pillar is shown in Figure 5-12. Note how the intact core of the pillar becomes progressively smaller until the pillar is completely crushed and the stress increases exponentially towards the centre similar to what the analytical model indicated in the previous section in Figure 5-2 and Figure **5-3**.

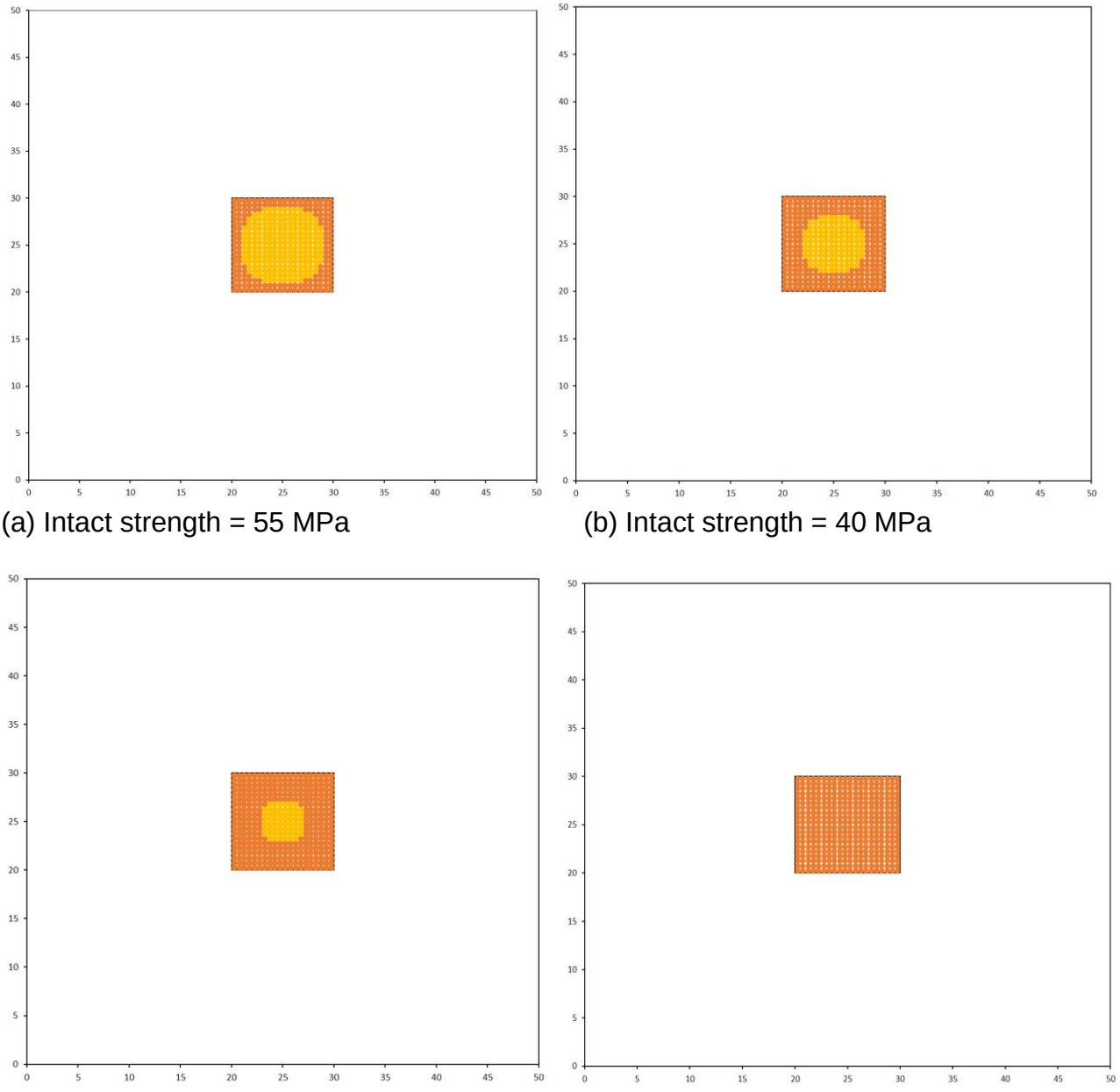

(a) Intact strength = 55 MPa (b) Intact strength = 40 MPa

(c) Intact strength = 25 MPa (d) Intact strength = 10 MPa

Figure 5-11. Simulated pillar failure for various values of intact strength. The other parameters used were intact slope = 4.0; crush strength = 5 MPa; failed slope = 4.0; interface friction angle = 10; seam height = 2.0 m; seam stiffness modulus = 35000 MPa / m). The yellow colour represents intact elements and the brown colour represents failed elements.

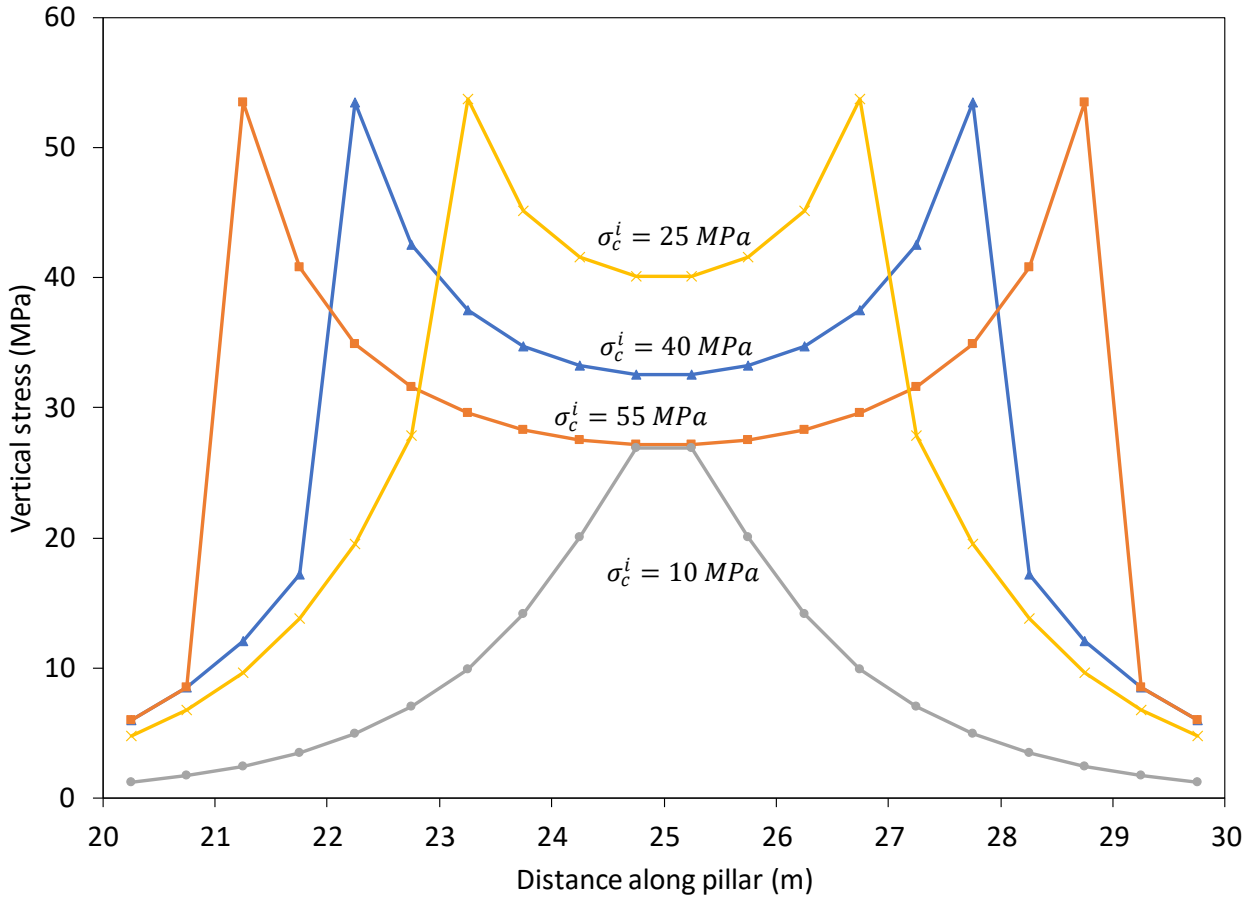

Figure 5-12. Vertical stress along section AA' using 0.5 m sized elements for the variation in intact strength illustrated in Figure 5-11.

5.3.3 Effect of element shape

The simulations above were conducted with square elements. Triangular elements are more suitable to simulate irregular geometries and, as a test, the geometry illustrated above was also simulated with triangular elements. The size of the triangular elements to simulated the pillar area are shown in Figure 5-13. These element sizes were slightly larger than the square element sizes. For the triangular mesh, 284 elements were used to represent the pillar, giving an average element size of 0.35 m^2. For the square element sizes, the element size was smaller at 0.25 m^2.

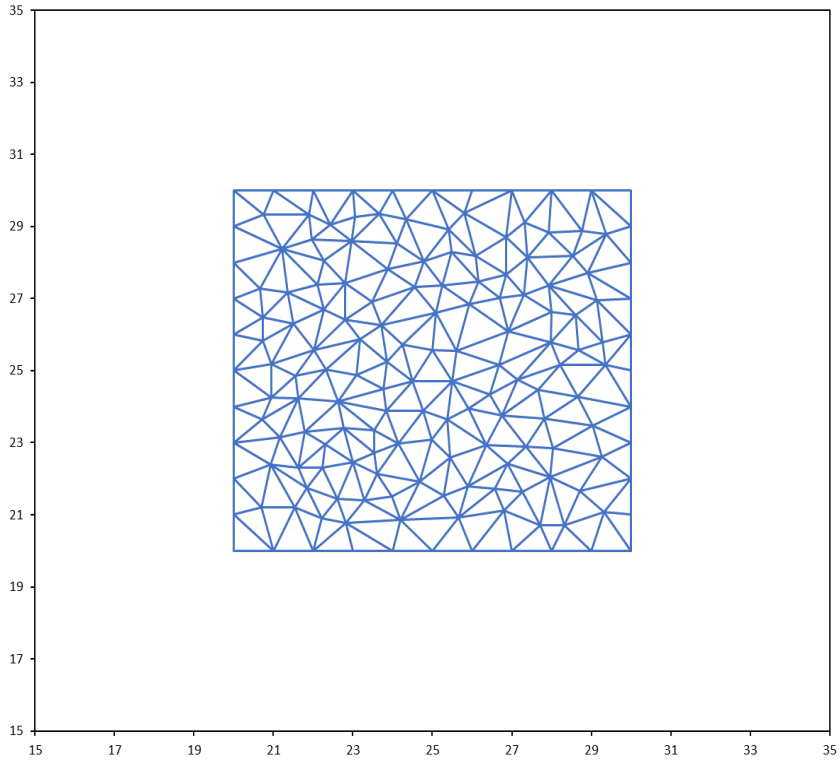

Figure 5-13. Triangular elements used to simulate the pillar. The mined stope was also simulated using triangular elements of a similar size, but it is not shown in this diagram.

Similar properties were used to simulate the pillar and an intact strength of 25 MPa was used. The resulting failure of the pillar is shown in Figure 5-14. Note that the triangular elements are not neatly aligned in rows as the square elements and therefore the collocation points are more randomly positioned depending on the size and shape of the elements. It is tempting to state that this may be a more realistic representation of the irregular failure patterns observed underground, smaller triangular element sizes will also give a more regular intact core shape.

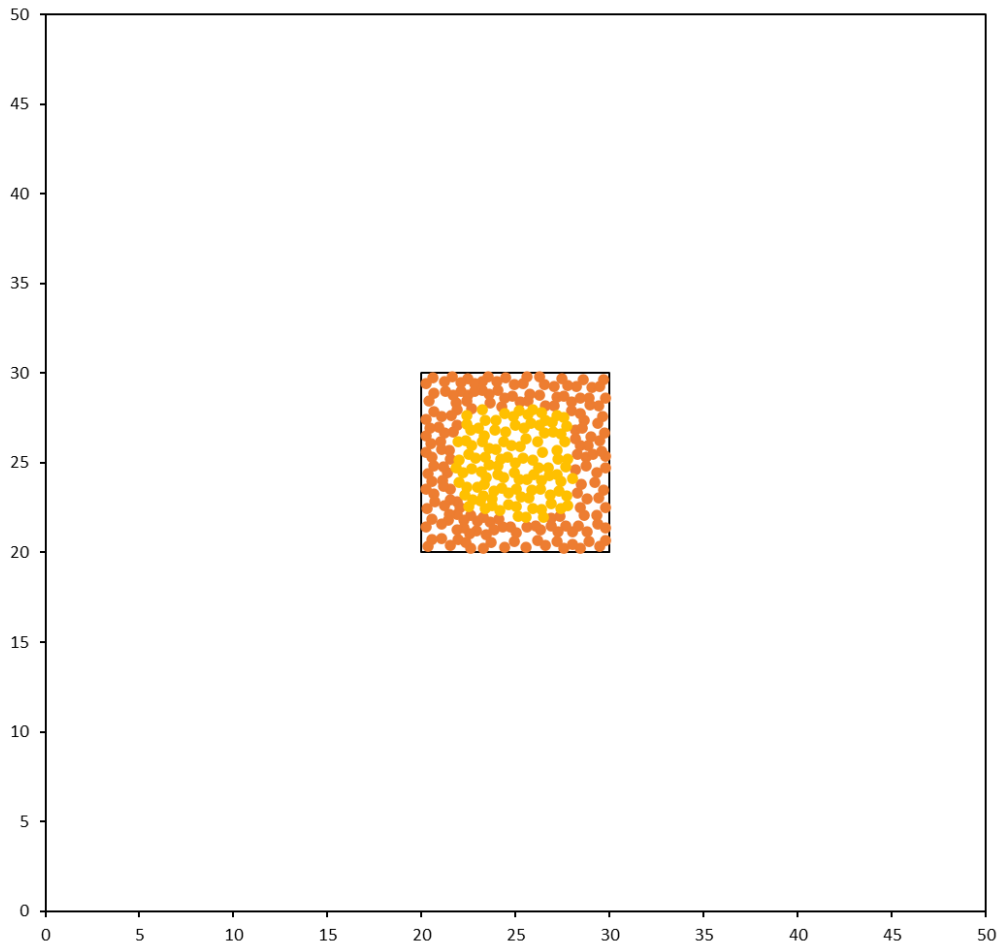

Figure 5-14. The resulting failure pattern when using triangular elements. This was for an intact strength of 25 MPa. The other material properties were similar to those given in the caption of Figure 5-11.

Figure 5-15 illustrates the vertical stress along section AA' for the two different element shapes. Note that the curve for the square elements is more symmetrical, but the triangular one will also be more symmetrical for smaller element sizes. An important aspect to note is that the intact core of the pillar is larger for the triangular elements. This is caused by the element size that is larger for the triangular elements. Small elements, within practical limits, should be used for these simulations and an important finding therefore is that calibration of the model parameters using actual data, such as borehole observations of fracture depth, may be affected by the element sizes used in the model.

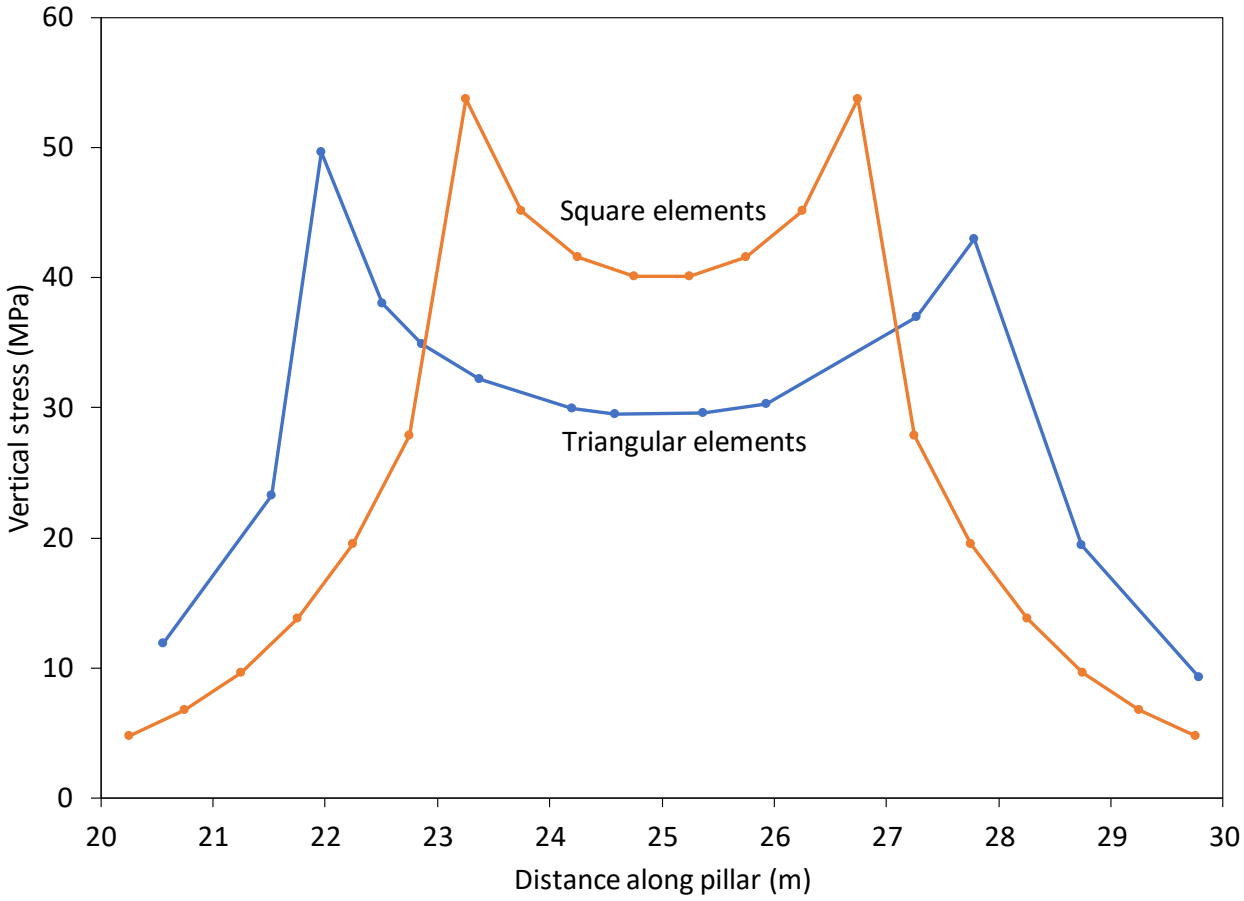

Figure 5-15. Vertical stress along section AA' for square and triangular element shapes.

5.4 Modelling a regular bord and pillar layout

A more complex layout was also simulated. This consisted of a regular bord and pillar layout with a total of 100 pillars. The dimensions of the pillars simulated were 8 m x 8 m with 8 m bord spans. The layout is shown in Figure 5-16 below. These pillar sizes are similar to those typically found in the platinum industry. The following assumptions were made for this model:

- The geometry was simulated as a horizontal excavation with no dip. This simplified the model and the data interpretation.
- All the pillars are assumed to be perfect squares. This is not the case for underground layouts.

- As the limit equilibrium model discussed above was used, it assumed that the weak parting was present in both the hangingwall and the footwall. This is not the case for the actual pillars at Everest Mine where it is only found at the hangingwall contact.
- Square element sizes of 1 m x 1 m were used for this initial simulation.
- The size of the area simulated was 168 m x 168 m. This is approximately the same size as the actual areas simulated at Everest Platinum Mine in the next chapter.
- A total of 28 224 displacement discontinuity elements were generated to simulate this layout.
- No geological faults or other large structures were considered, and the abutments were assumed as solid and not able to fail.

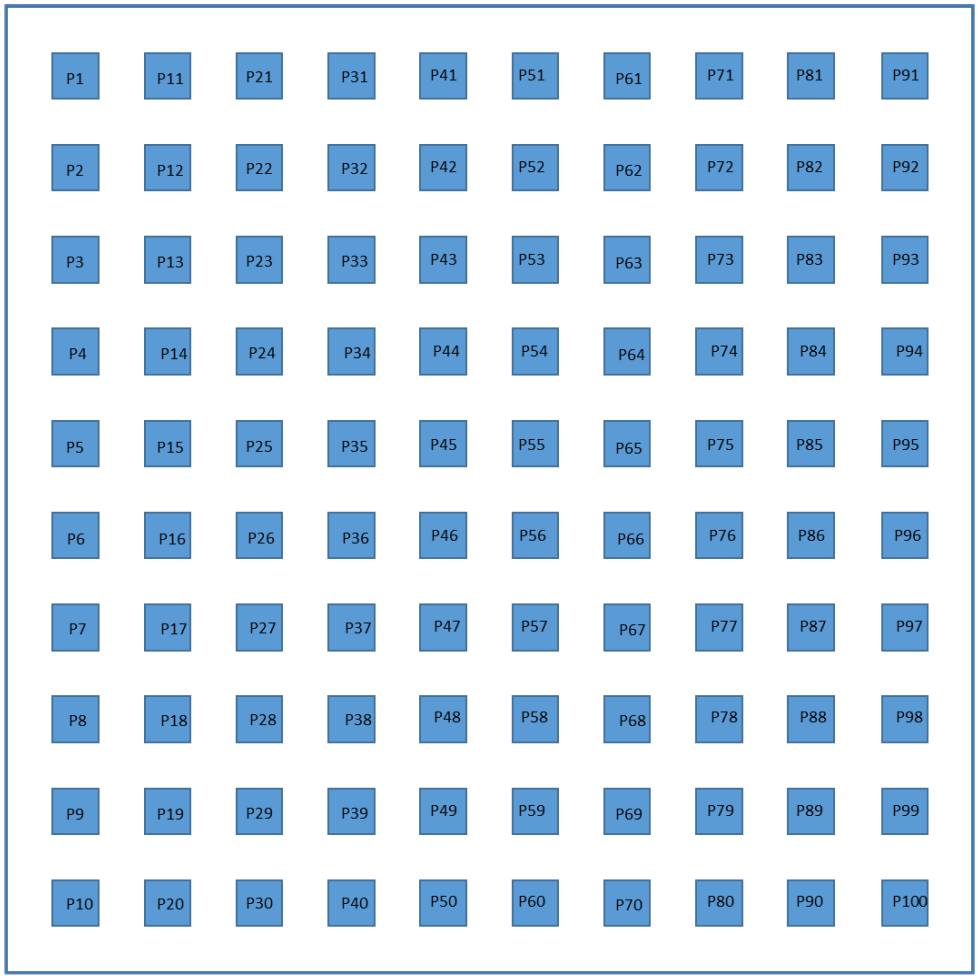

Figure 5-16. Simulated mine layout using the TEXAN code. This simulation served as a useful comparison for the back analysis of Everest Platinum Mine discussed in the next chapter.

A difficulty with the limit equilibrium model is that a large number of parameters need to be calibrated. This has already been illustrated in Table 5-1. Some consideration had to be given to these input parameters and additional work was done in Chapter 6. Napier and Malan (2021) conducted a calibration of these parameters for UG2 pillars at a mine close to Everest, but the geological alteration was not present in these pillars. The parameters below (Table 5-2) are arbitrary values to test the behaviour of the model.

The interface friction angle is an important parameter for the pillar behaviour at Everest Mine. As a complicating factor, the presence of water results in a reduced interface friction angle. As discussed in Chapter 5, the heavy rains during the time of the Everest collapse contributed to the disaster as the water affected the geological alteration in the levels close to surface.

Table 5-2. Input parameters for the TEXAN model of a bord and pillar layout.

Parameter	**Value**
Depth below surface, *h*	200 m
Overburden density, ρ	3 200 kg/m³
Intact Strength, σ_c^i	20 MPa
Intact rock slope, m^i	4.0
Initial Crush Strength, σ_c^i	1 MPa
Interface Friction Angle, ϕ	20°
Seam Height, H	2.0 m
Seam Stiffness Modulus	35 000 MPa
Residual Strength, σ_c^f	2.5 MPa
Crushed rock slope, m^f	2.0

As mentioned above, the friction angle of the pillar/hangingwall interface caused by the geological alteration is an important parameter. No test results were available on the properties of this material. Some insights can be gained by examining friction angles discussed in the field of soil mechanics due to the soft texture and crumbling nature of the alteration zone (Table 5-3). Typically, material is classified as either granular or cohesive. The difference between cohesive and granular material is described below.

"Granular material" means gravel, sand, or silt (coarse-grained soil) with little or no clay content. Granular soil has no cohesive strength. Some moist granular soils exhibit apparent cohesion. Granular soil cannot be moulded when moist and crumbles easily when dry.

"Cohesive material" means clay (fine-grained soil), or soil with a high clay content, which has cohesive strength. Cohesive soil does not crumble, can be excavated with vertical side slopes, and is plastic when moist. Cohesive soil is hard to break up when dry and exhibits significant cohesion when submerged. Cohesive soils include clayey silt, sandy clay, silty clay, clay and organic clay.

Table 5-3. Soil friction angle for numerous weak geotechnical materials.

Description	Soil friction angle [°]		
	Min	Max	Specific value
Well graded gravel, sandy gravel, with little or no fines	33	40	
Poorly graded gravel, sandy gravel, with little or no fines	32	44	
Sandy gravels - Loose			35
Sandy gravels - Dense			50
Silty gravels, silty sandy gravels	30	40	
Clayey gravels, clayey sandy gravels	28	35	
Well graded sands, gravelly sands, with little or no fines	33	43	
Well-graded clean sand, gravelly sands - Compacted	-	-	38
Well-graded sand, angular grains - Loose			33
Well-graded sand, angular grains - Dense			45
Poorly graded sands, gravelly sands, with little or no fines	30	39	
Poorly-graded clean sand - Compacted	-	-	37
Uniform sand, round grains - Loose			27
Uniform sand, round grains - Dense			34
Sand	37	38	
Loose sand	29	30	
Medium sand	30	36	
Dense sand	36	41	
Silty sands	32	35	
Silty clays, sand-silt mix - Compacted	-	-	34
Silty sand - Loose	27	33	
Silty sand - Dense	30	34	
Clayey sands	30	40	
Clayey sands, sandy-clay mix - compacted			31
Loamy sand, sandy clay Loam	31	34	
Inorganic silts, silty or clayey fine sands, with slight plasticity	27	41	
Inorganic silt - Loose	27	30	
Inorganic silt - Dense	30	35	
Inorganic clays, silty clays, sandy clays of low plasticity	27	35	

Clays of low plasticity - compacted			28
Organic silts and organic silty clays of low plasticity	22	32	
Inorganic silts of high plasticity	23	33	
Clayey silts - compacted			25
Silts and clayey silts - compacted			32
Inorganic clays of high plasticity	17	31	
Clays of high plasticity - compacted			19
Organic clays of high plasticity	17	35	
Loam	28	32	
Silt Loam	25	32	
Clay Loam, Silty Clay Loam	18	32	
Silty clay	18	32	
Clay	18	28	
Peat and other highly organic soils	0	10	

Of interest from the table is that some of the inorganic clays of high plasticity can have a friction angle as low as 17°. This motivated an initial adoption of a friction angle of 20° for the TEXAN run as given in Table 5-2.

The result of the preliminary TEXAN model is shown in Figure 5-17. Of interest, is that for the weak parameters selected, even the pillars adjacent to the solid abutment are failed.

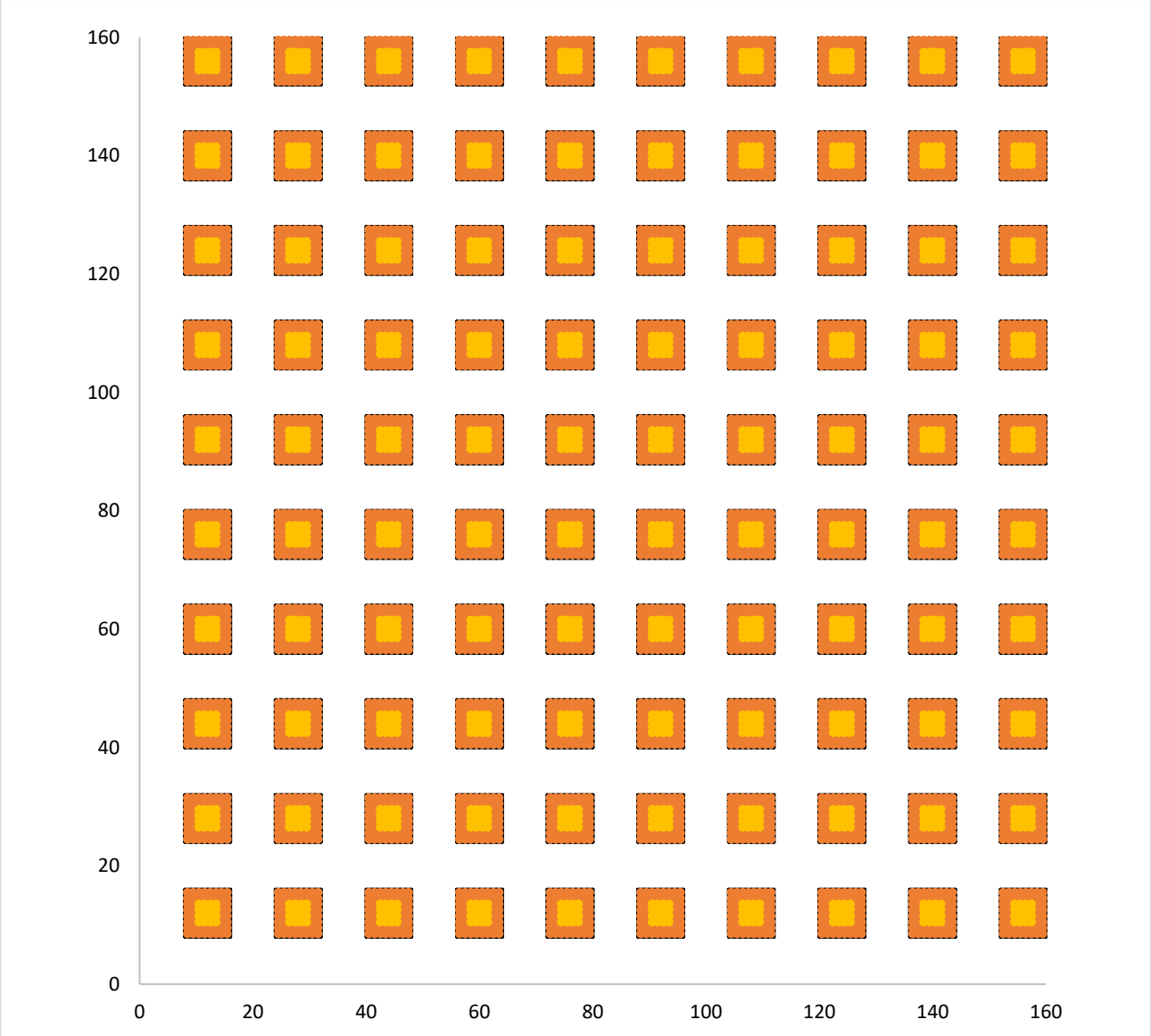

Figure 5-17. Illustration of the pillar failure as simulated by the TEXAN code for the parameters given in Table 5-2. Similar to the previous figures, the yellow colour represents intact elements and the brown colour represents failed elements.

5.5 Summary

This chapter introduced a limit equilibrium model to simulate the pillar failure at Everest Mine. It appears to be useful model to represent pillar failure in displacement discontinuity codes as it can simulate the progressive pillar scaling and the intact cores of the pillars. The results indicate that the residual strength of the pillar will be negatively or positively affected by the selection of friction angle of the parting planes at the hangingwall and footwall contacts.

A drawback of the model is that it is a symmetrical model and it assumes that partings, with the same friction angle, exist at both the contacts of the pillar with the hangingwall and footwall. This is not the case for the pillar failure mechanism at Everest Mine. A further difficulty is that the model introduces a large number of parameters that needs to be calibrated. This is explored in more detail in the next chapter.

6 SIMULATING THE FAILED PILLARS AT EVEREST PLATINUM MINE

6.1 Introduction

The modelling results presented in Chapter 5 indicated that the limit equilibrium model will be a useful tool to simulate the pillar failure at Everest Platinum Mine. This chapter describes the attempts to calibrate the model whilst utilising parameters from the calibration conducted in chapter 5. Numerous Texan Code models were run in an attempt to determine these parameters.

Small element sizes had to be used to ensure that the limit equilibrium model simulates realistic pillar failure depths. Owing to the limitation of the number of elements that can be used in TEXAN, the entire mine and all the mines pillars could not be simulated and therefore the rockmass beyond the boundaries are assumed as solid. The approach followed in this study was therefore to simulate two areas of the mine as previously described in chapter 5.

These two areas are described as “Collapsed” and “Intact” in this chapter. The simulated areas were 160 m x 160 m in size and were selected following the underground visits to the mine. The selection of the two areas was guided by the key objective calibration of the model. If the same set of parameters indeed predict pillar failure in the collapsed area and in the intact area, these parameters can be used with some degree of confidence for future mining areas with similar ground conditions.

6.2 Input parameters for the TEXAN model

6.2.1 Areas selected for modelling

Figure 6-1 illustrates the two areas selected for modelling. The areas were selected based on the underground site visit documented and explained in Chapter 4. The sizes of the pillars in the two blocks indicated clearly show the difference in the pillar sizes. The depth below surface for both areas does vary, however both areas were modelled at the same depth below surface to ensure that an accurate comparison between the areas was simulated.

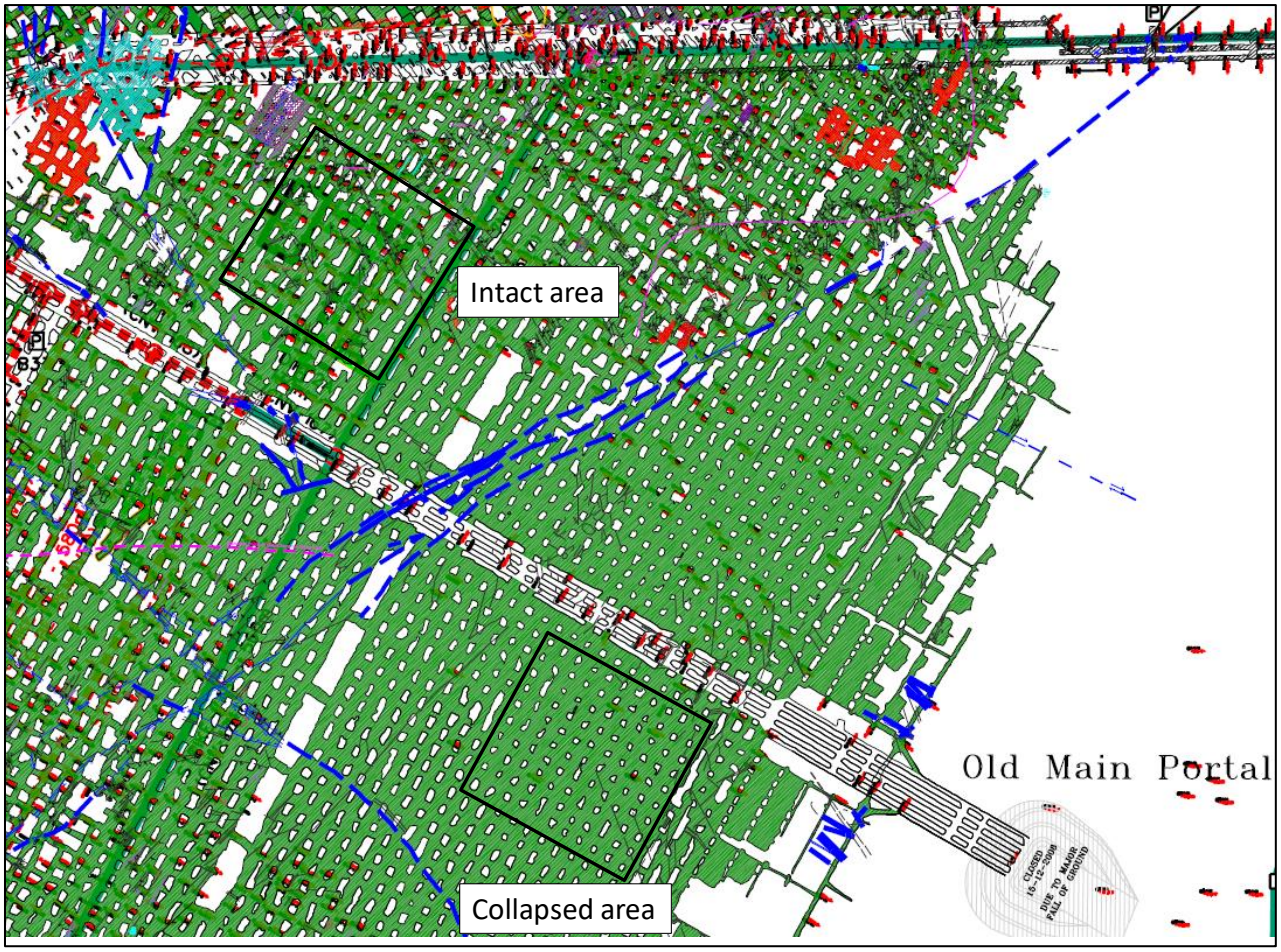

Figure 6-1. The two areas selected for detailed modelling (the two black squares) are shown in this figure. Note that the pillar sizes are larger in the intact area.

Figure 6-2 and Figure 6-3 illustrate enlarged views of the two areas. As the areas were simulated with no dip, they were also rotated to simplify the digitising and meshing process for the models.

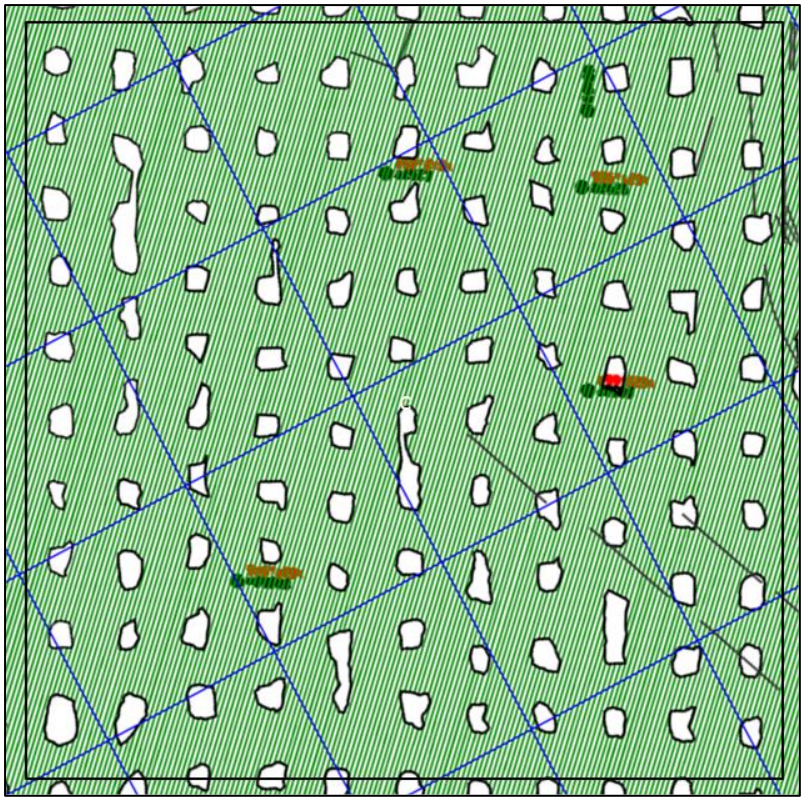

Figure 6-2. Pillar shapes in the collapsed area.

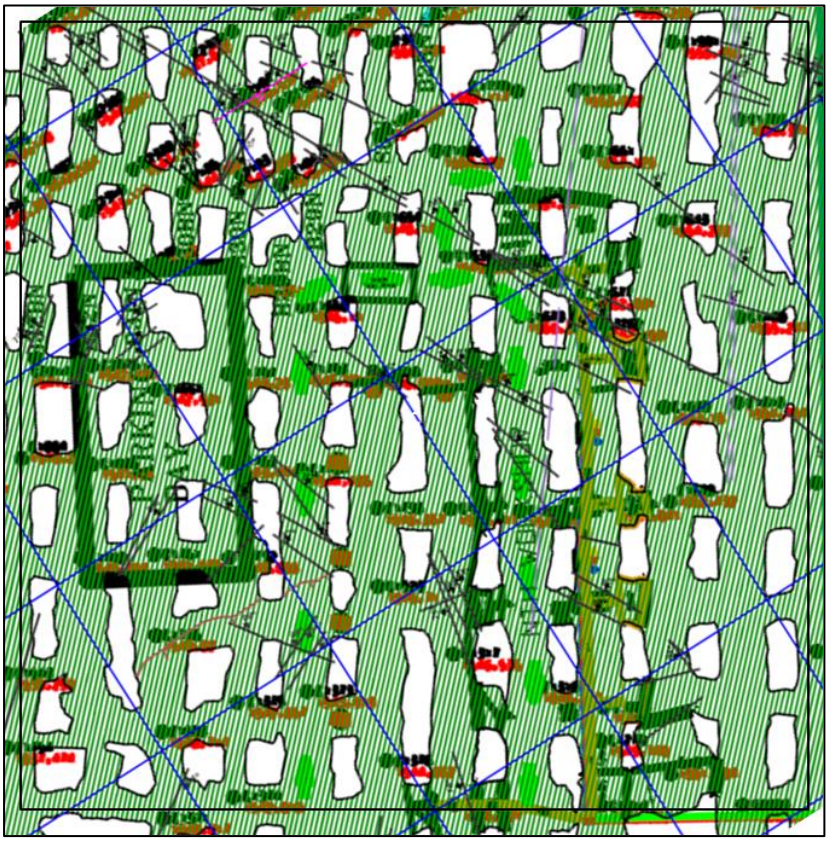

Figure 6-3. Pillar shapes in the intact area.

The pillar shapes shown in Figures 6-2 and 6-3 were approximated using straight line polygons. This simplified the digitising and meshing process. The simplified geometries are shown in Figures 6-4 and 6-5. These simplified geometries where then digitised and numbered for the input into TEXAN Code whereby the numerical analysis could commence.

The layouts shown in Figures 6-4 and 6-5 were meshed using triangular elements. Examples of the meshes used are shown in Figures 6-6 and 6-7. The mined-out area and all the pillars had to be meshed to allow pillar failure using the limit equilibrium model.

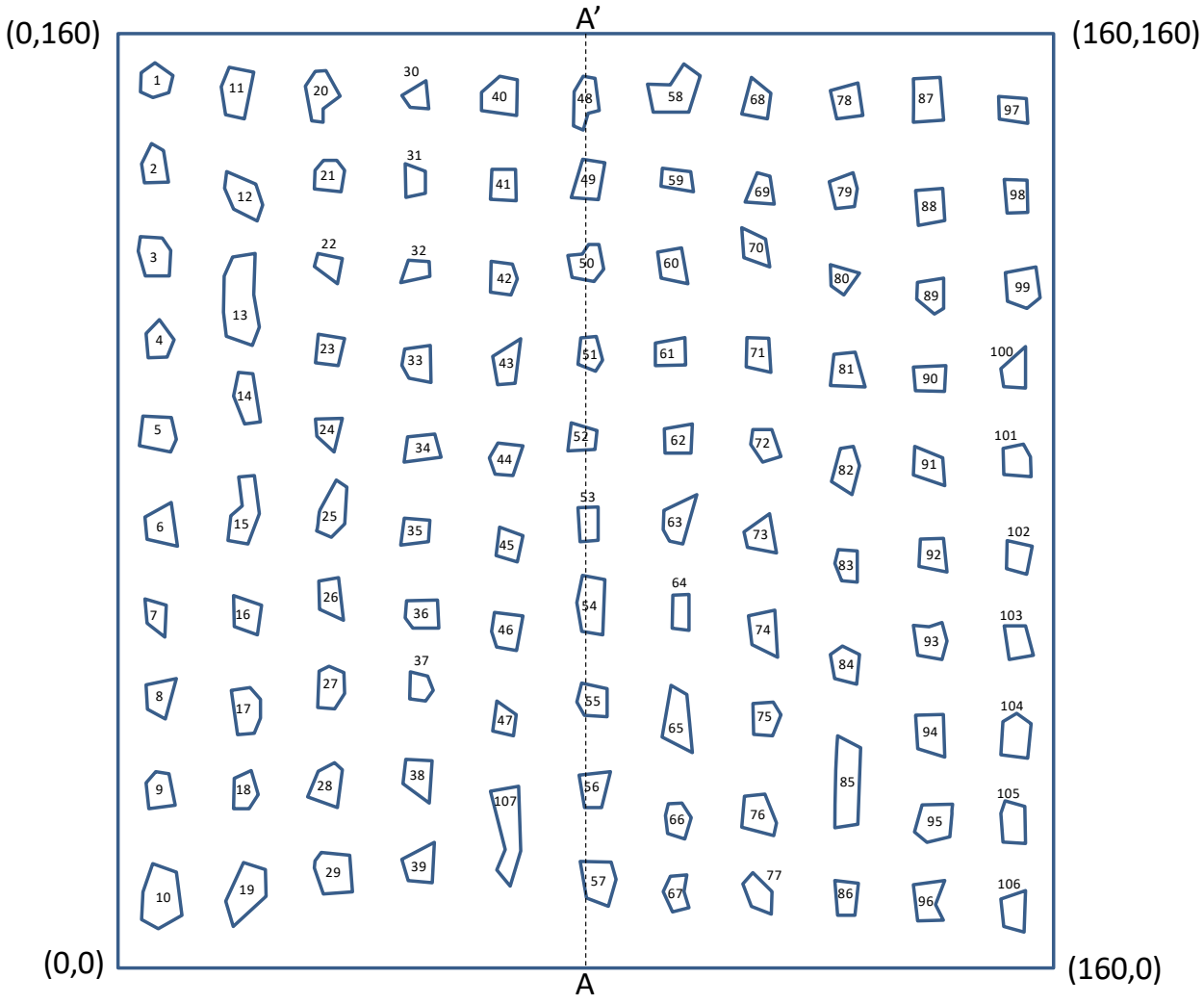

Figure 6-4. Simplified geometry of the pillars in the collapsed area.

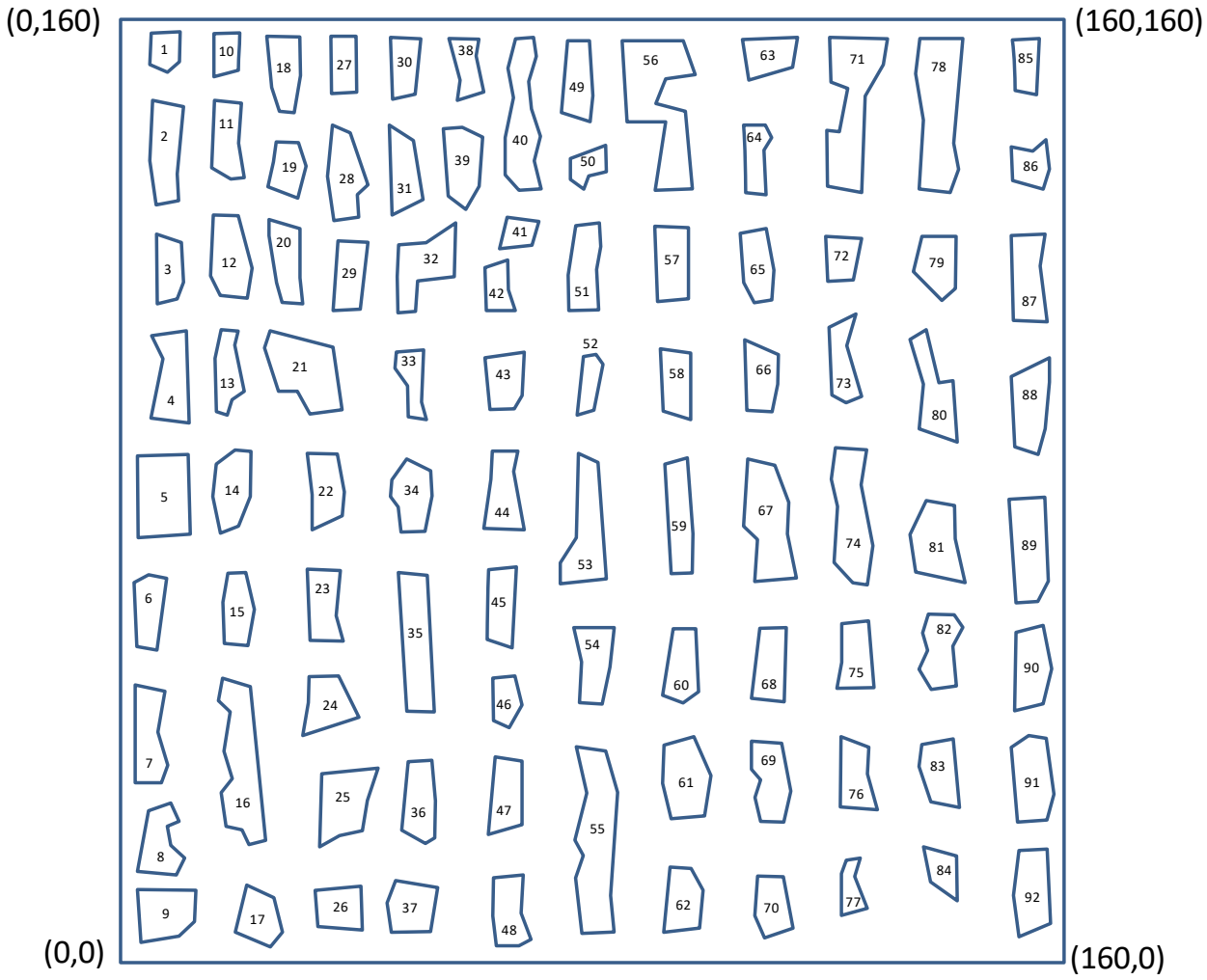

Figure 6-5. Simplified geometry of the pillars in the intact area.

A brief discussion on the size of the areas selected is necessary. Ideally, larger areas than those illustrated in Figure 6-1 should be modelled. The version of TEXAN available to the student was limited to 60 000 elements. The total number of elements used to simulate the layout shown in Figure 6-4 was 52 366 and for the layout in Figure 6-5 was 55 679. Currently, a new TEXAN code that allows up to almost 270 000 elements is available and larger runs should be considered as future work. The size of the models used for this study nevertheless gave good insights into the applicability of the limit equilibrium model and first estimates of calibrated parameters could be obtained.

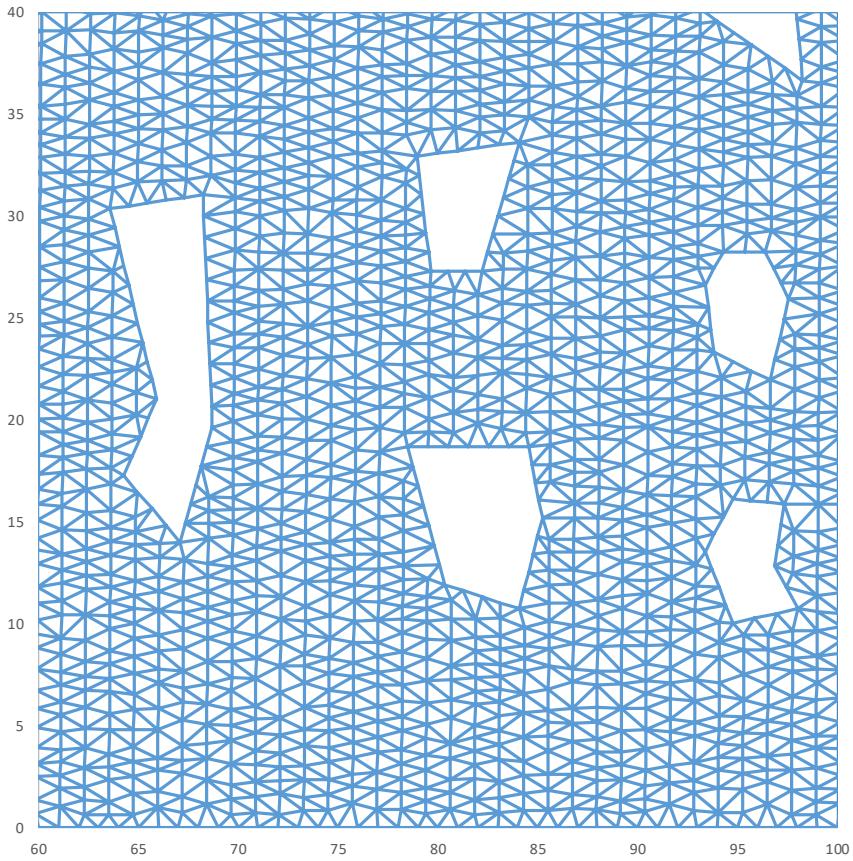

Figure 6-6. Part of the mesh used to simulate the collapsed area.

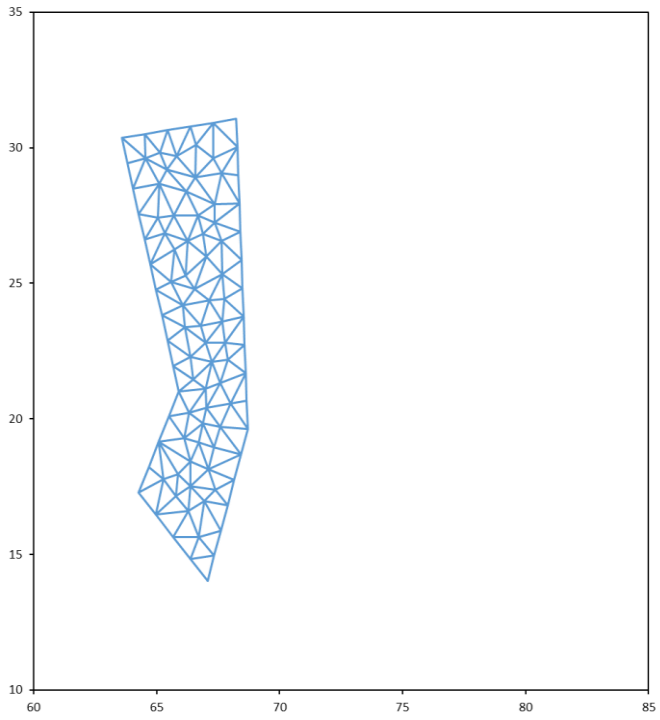

Figure 6-7. Mesh used to simulate pillar P107 the collapsed area (pillar in the left of Figure 6-6). The pillar numbers are also given in Figure 6-4.

The building of the model geometries highlighted an important difference between the two areas. The difference in extraction ratio between the areas was evident and this is illustrated in Table 6-1. The planned extraction ratios are based on data collected and discussed in Chapter 4. The actual extraction ratios were calculated from the digitised meshes. Note that the extraction ratio in the collapsed area was high and exceeded the original design.

Table 6-1. Extraction ratio of the two simulated areas.

Area	Planned extraction ratio	Actual extraction ratio
Intact area	83.45%	67.11%
Collapsed area	83.45%	87.84%

A graphical representation of the designed versus actual pillar size, as surveyed by the mine and represented on the mine plans, is shown in Figure 6-8 and Figure 6-9.

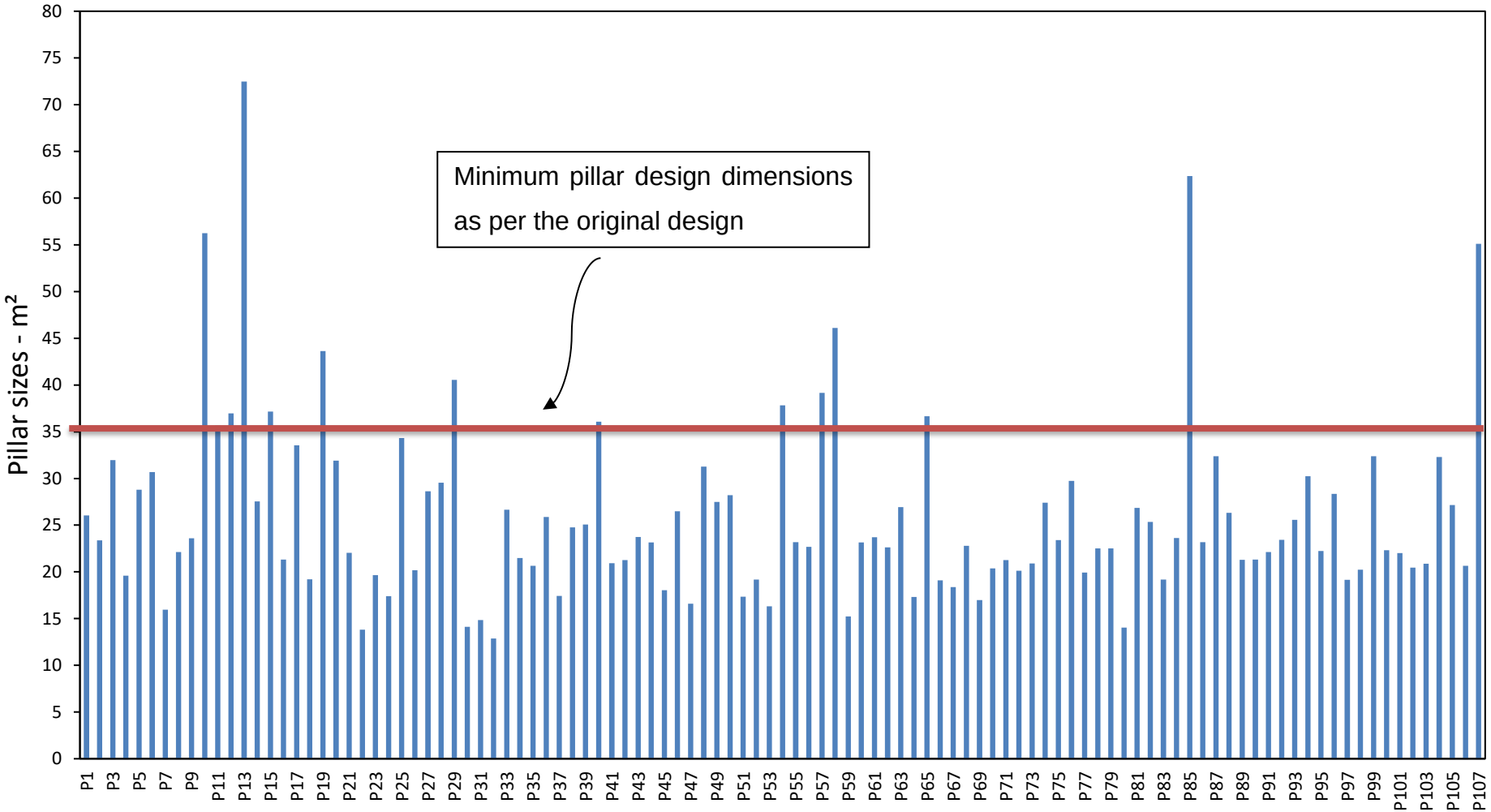

Figure 6-8. Illustration of the actual pillar sizes in m² for the **collapsed area** compared to the design pillar size.

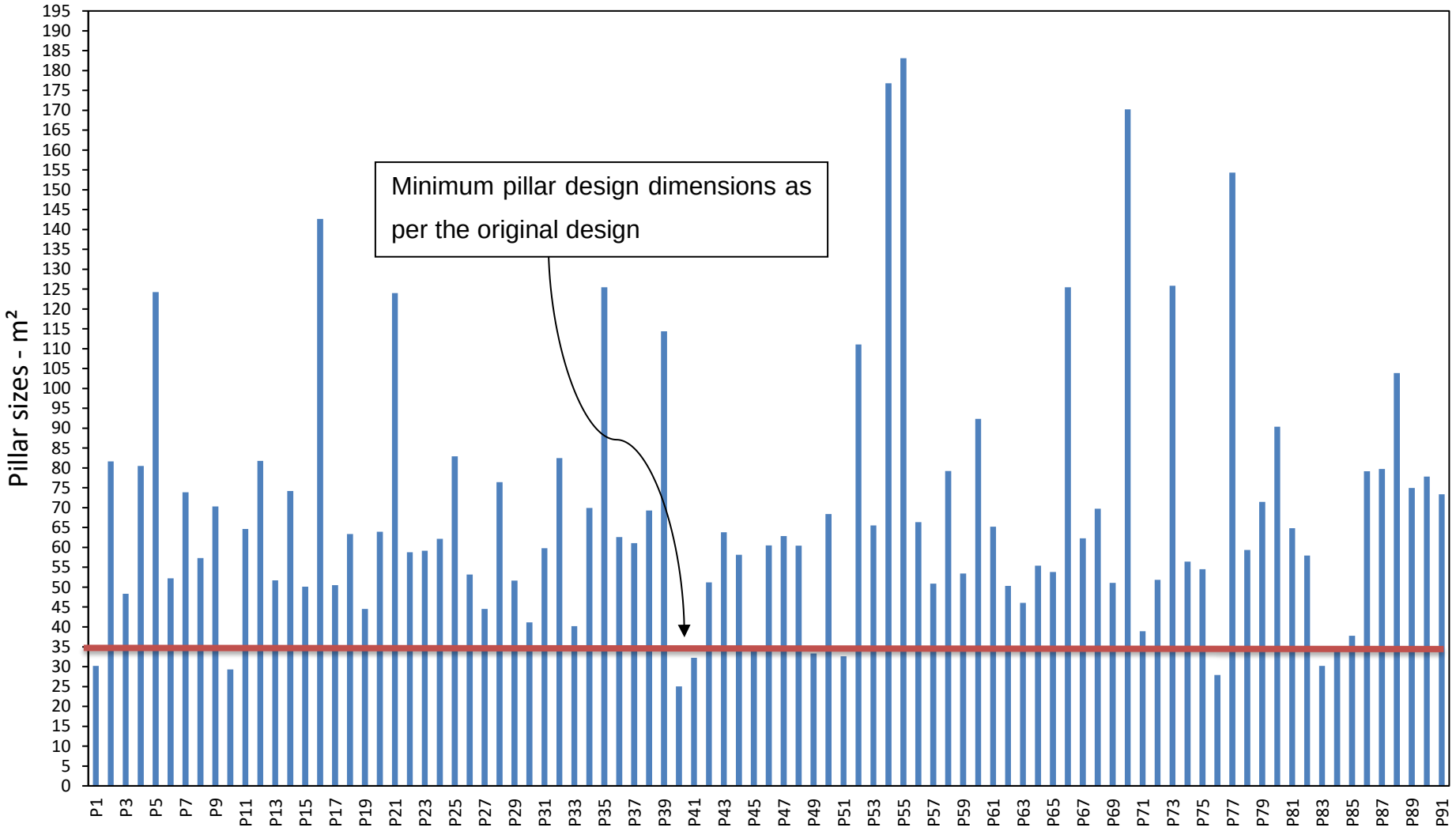

Figure 6-9. Illustration of the pillar sizes in m² for the **intact area** compared to the design pillar size.

6.2.2 Model parameters

For the initial simulations, the parameters in Table 6-2 were used. These were selected to represent a very weak rock mass material to test the model geometries and failure of the pillars. In contrast, when using parameters $\sigma_c^i = 60\ MPa$, $m^i = 7$ and $\phi = 30°$, all the pillars remained intact and this is not the behaviour that was seen underground. Similar properties were used for the initial models of both areas even though the interface friction angle was lower in the collapsed area owing to the presence of water and the resulting weathering of the alteration layer. In Chapter 5, it was noted that friction angle values as low as 17° was recorded for some clays. Further calibration of the model was conducted in the following section.

Table 6-2. Input parameters for the initial TEXAN modelling.

Parameter	Value
Depth below surface, *h*	113 m (collapsed) and 217 m (intact)
Overburden density, ρ	3 000 kg/m³
Intact Strength, σ_c^i	25 MPa
Intact rock slope, m^i	4.6
Crushed Rock Strength σ_c^f	4 MPa
Crushed rock slope, m^f	4.6
Interface Friction Angle, ϕ	10°
Seam Height, H	2.0 m
Seam Stiffness Modulus	45 000 MPa/m

6.2.3 Modelling results

As described above, the initial simulations were conducted using the parameters given in Table 6-2. Figure 6-10 illustrates the failed pillars for the collapsed area as simulated by the code. The orange colour is the failed portions of the pillars and the yellow portions are still intact. For these parameters, most of the pillars have failed. A few pillars in the corner of the model, where the stresses are the lowest, were still intact. This is to be expected as only a finite size model could be simulated and the code treats the material outside the model as a solid abutment.

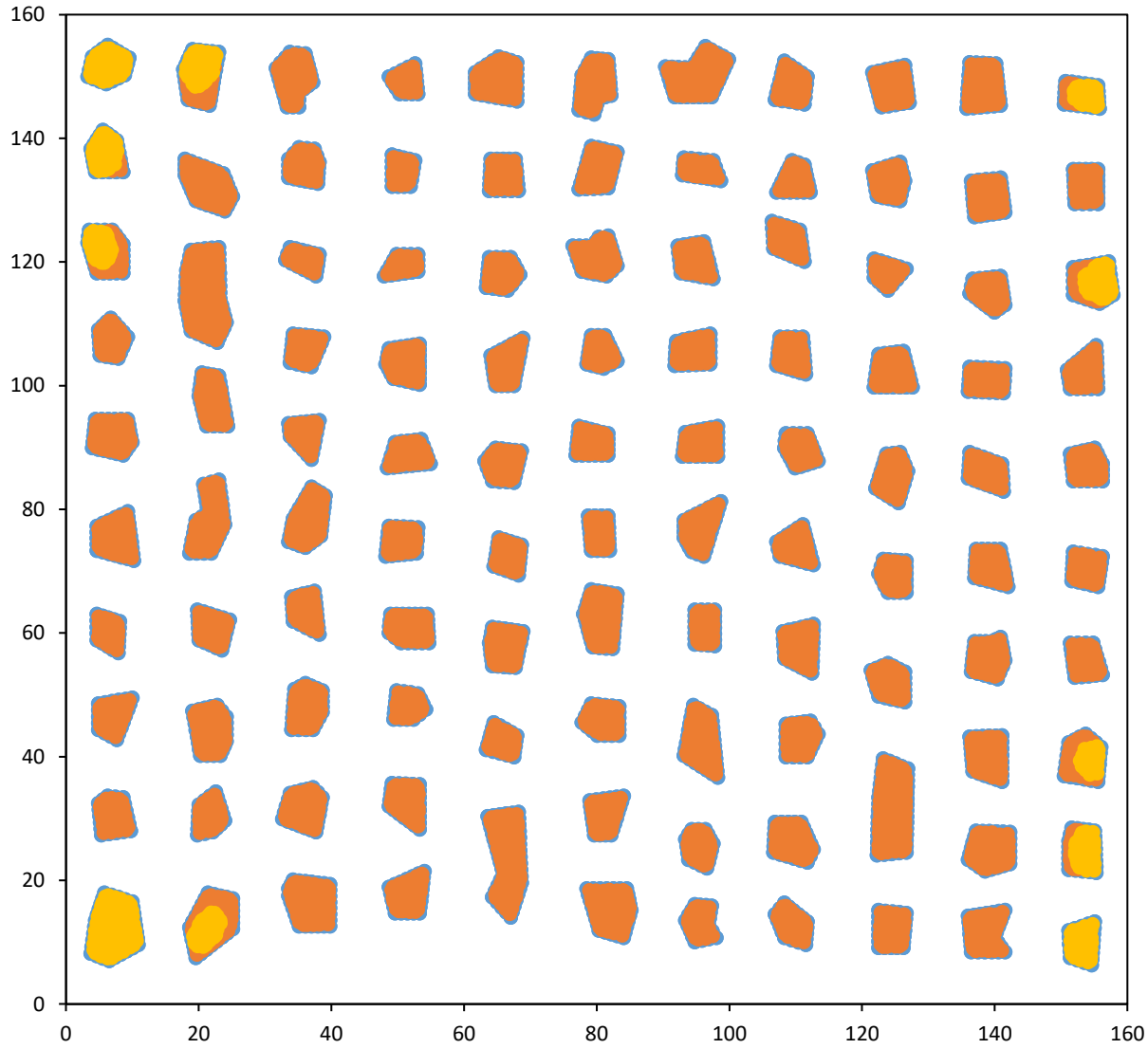

Figure 6-10. Simulation of pillar failure for the **collapsed area**. The orange colour denotes failure and the yellow denotes intact pillars.

Of interest is the amount of closure experienced in the model as a significant amount of closure was recorded in the mine as described in Chapter 4. The closure along line AA' (see Figure 6-4) was plotted. This is illustrated in Figure 6-11. As expected, the closure is very small across the pillars, but it exceeded 1.5 m between some pillars. As discussed in Chapter 4, the closure measured during the underground visit varied between 0.7 m and 0.8 m at the center of the collapse. These were not accurate as the measurements were not done with closure instruments, but with a tape measure and estimating the original stoping width. The height of the opening after the collapse was approximately 1.3 m and the surveyed stoping height during mining was

approximately 2.1 m. The TEXAN code modelling therefore seems to predict a larger amount of closure although it is encouraging that it is of the same order as the measurements. The closure may be larger in the model compared to the actual measurements as it simulated complete failure (with the associated exponential increase in stress towards the centre of the pillar predicted by the limit equilibrium model). In reality the residual strength of the crushed pillars may be large than that predicted by the parameters in

Table **6-4**.

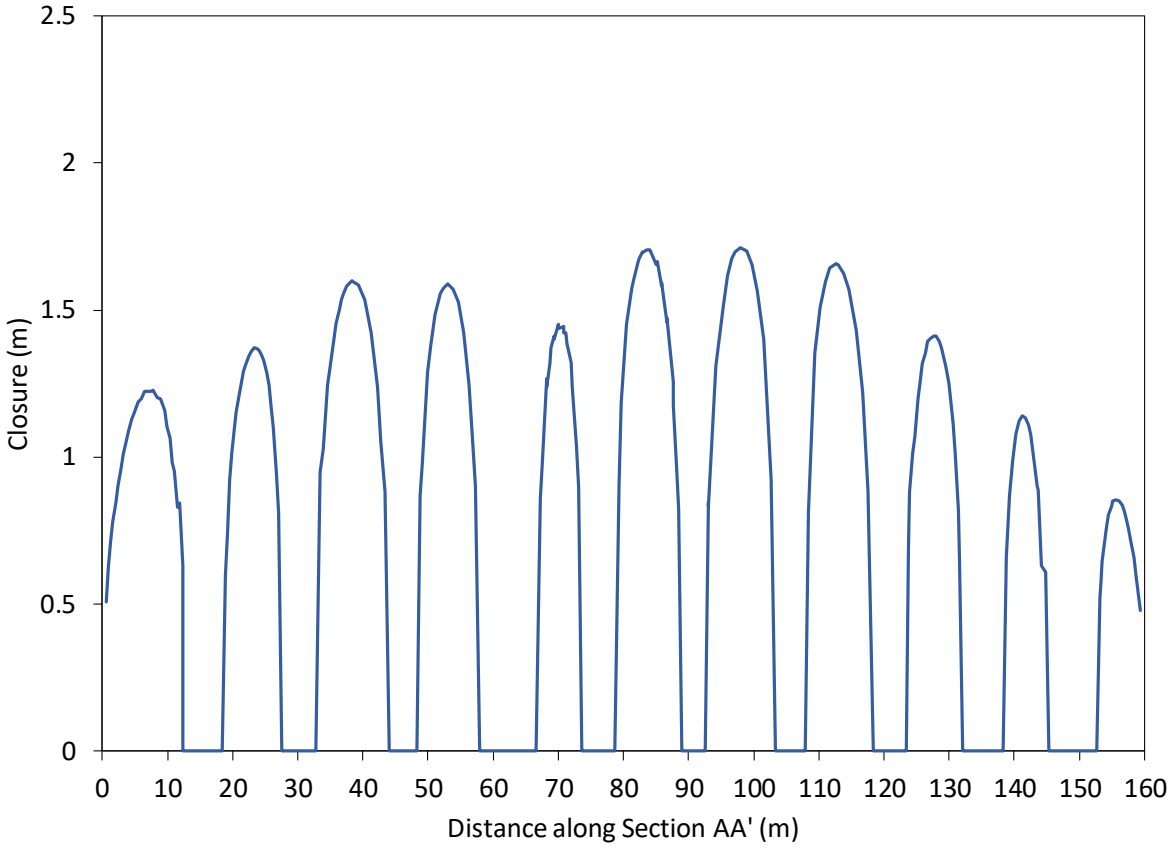

Figure 6-11. Simulated closure along Section AA’ for the collapsed area.

For a three-dimensional illustration of the closure, the data generated from the TEXAN run was converted into a format that could be imported into Minex. This allowed for the representation of the data in a graphical format showing the closure of the area as isopach’s. This is illustrated in Figure 6-12. Note that very high closure exceeding 2.5 m was recorded in some intersections. Note that the seam height of 2 m specified in Table 6-2 is only used in the limit equilibrium model calculations and the displacement discontinuity nature of the TEXAN code allows a higher amount of closure in the solution.

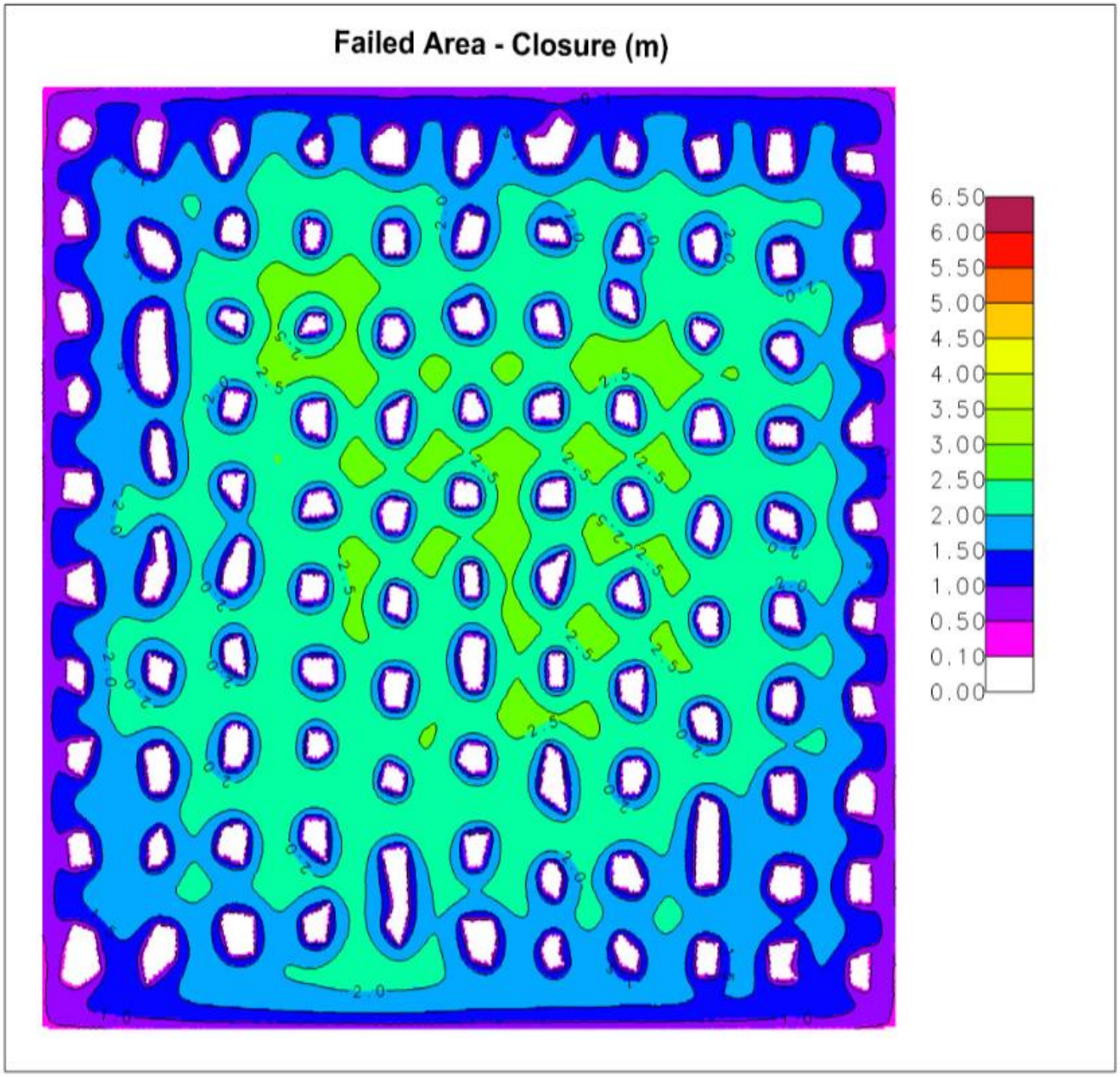

Figure 6-12. Closure data for the simulation of the collapsed area as plotted in Minex.

A simulation was also conducted on the intact area using the same parameters given in Table 6-2. The simulated pillar failure is given in Figure 6-13. Note that more of the pillars now have an intact core compared to the collapsed area shown in Figure 6-10. This is to be expected as the pillars are larger with smaller stress levels. The simulated amount of pillar failure is, however, greater than that observed for this area underground and the model parameters therefore appear not to be appropriate. Section 6.3 discuss the model calibration in more detail.

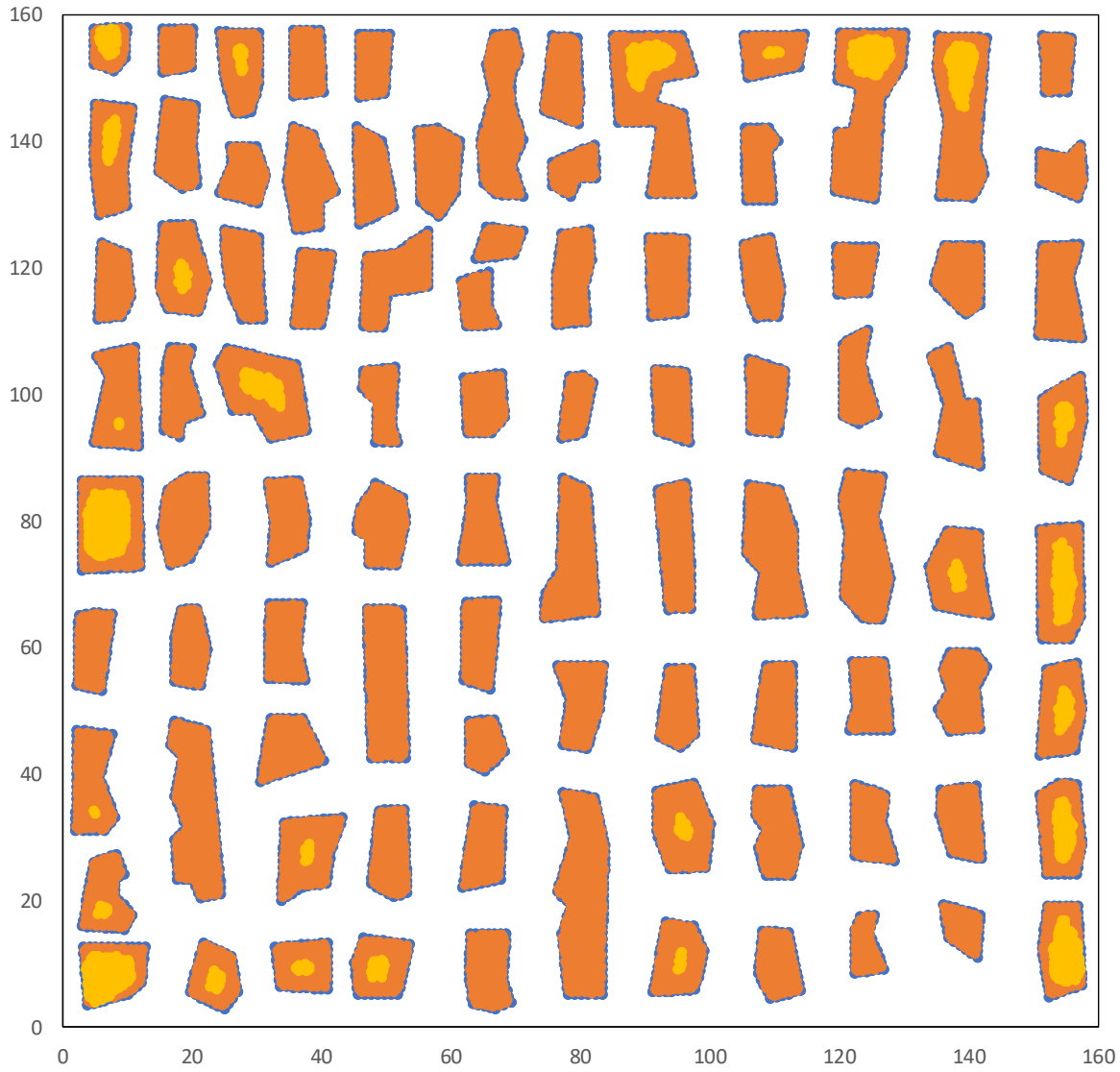

Figure 6-13. Simulation of pillar failure for the **intact area**. The orange colour denotes failure and the yellow denotes intact pillars.

The simulated closure is plotted in Figure 6-14. The maximum closure for this area is smaller than for the collapsed area. This is to be expected as the pillars are larger and the extraction ratio smaller.

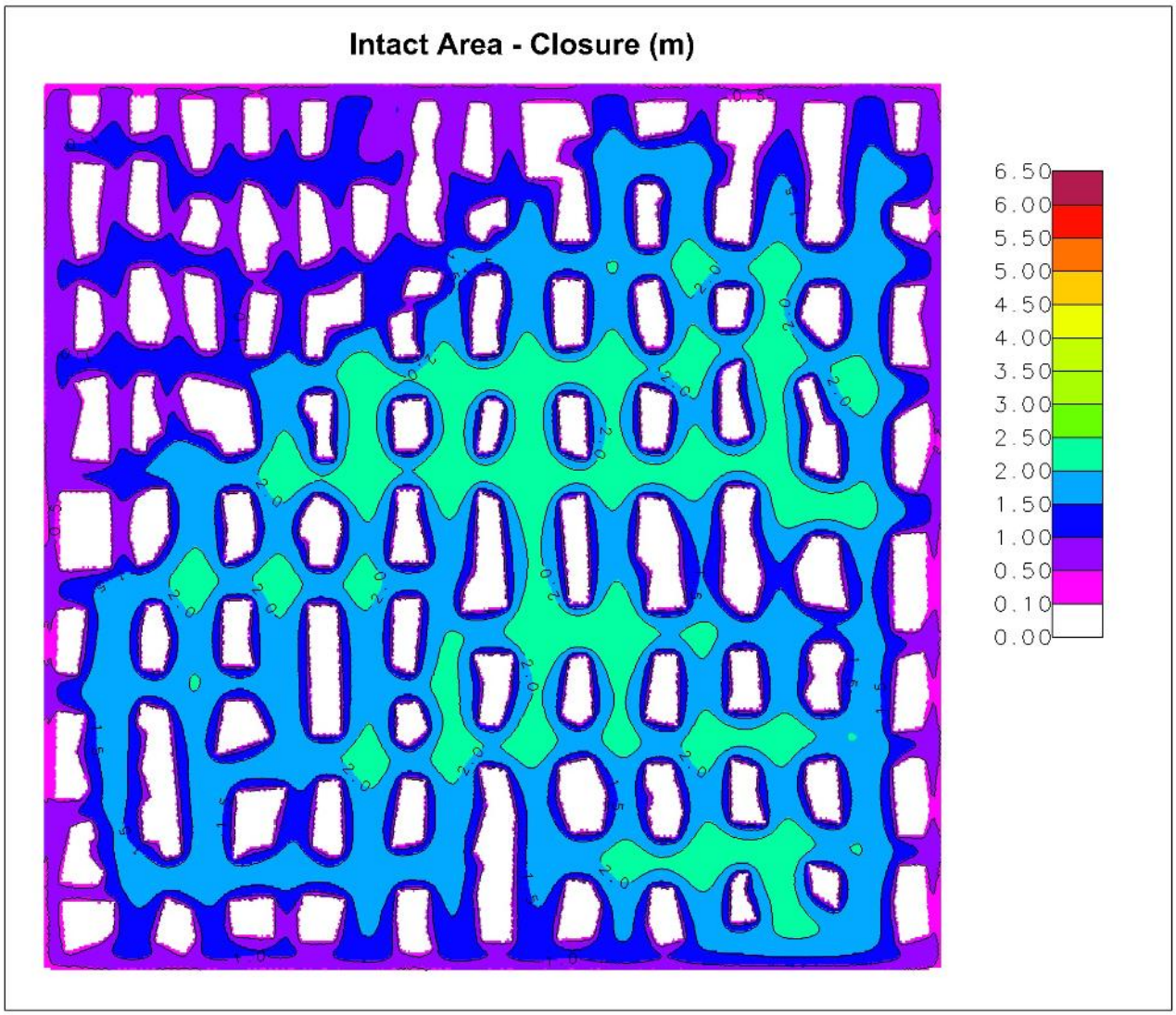

Figure 6-14. Closure plot data from TEXAN using Minex for an output of the intact area.

The average pillar stress (APS) for both areas was also analysed. For each area, two simulations were conducted. In the first simulation, the pillars of the allocated area were not allowed to fail (called rigid pillars) and for the second simulation, the limit equilibrium model was utilised to simulate the pillar failure. The results are illustrated in Figure 6-15 and Figure 6-16. As expected, the APS was highest for the very small pillars when assuming a rigid pillar model. For the weak limit equilibrium model parameters used, the pillars fail extensively and the APS drop to around 10 MPa in both cases. The tributary area stress (TAT) was calculated for both areas for the particular depth below surface. For this calculation, the dimensions of the pillars were based on the initial design of 6 m by 6 m pillars with 8 m bords.

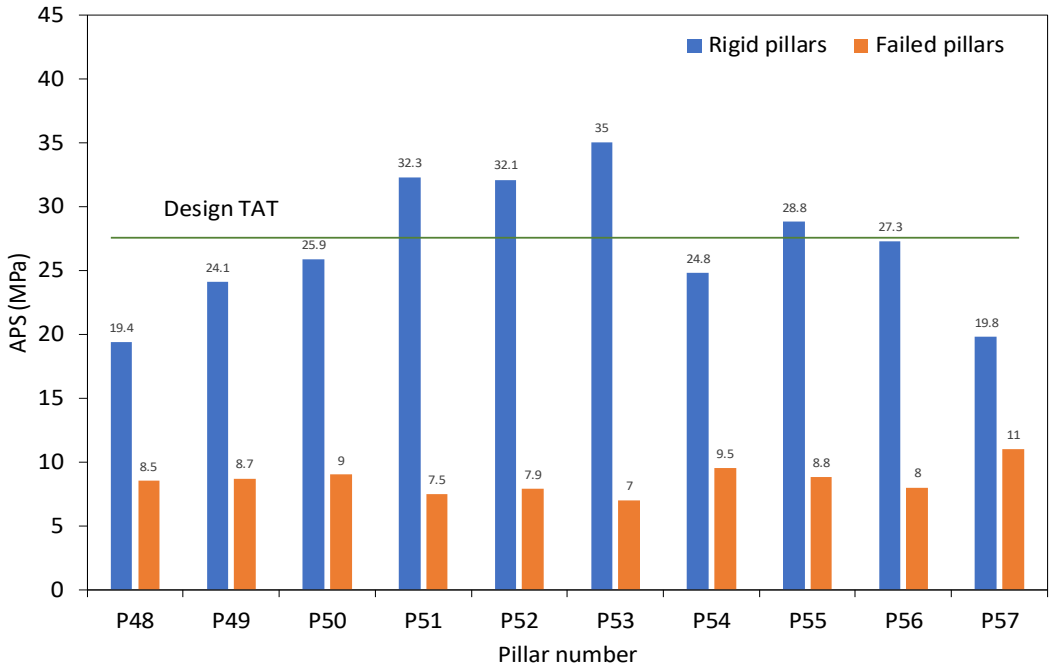

Figure 6-15. Simulated average pillar stress (APS) for some pillars in the **collapsed area**. For the "rigid pillars" simulation, the pillars were not allowed to fail and for the "failed pillars" simulation, the limit equilibrium model constitutive code was used. The design TAT is the stress predicted for a regular layout using tributary area stress.

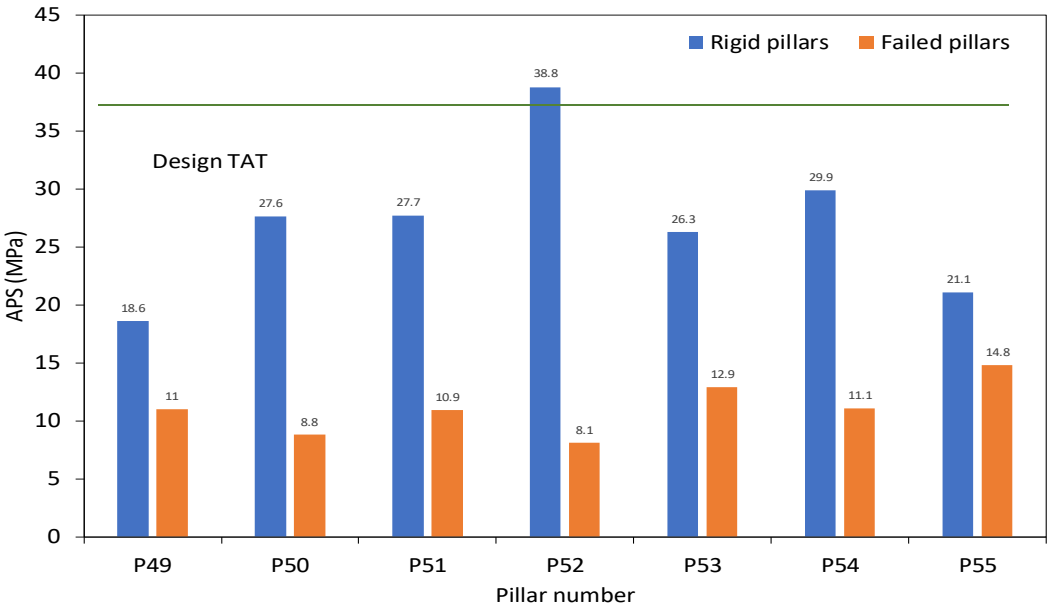

Figure 6-16. Simulated average pillar stress (APS) for some pillars in the **intact area**. For the "rigid pillars" simulation, the pillars were not allowed to fail and for the "failed pillars" simulation, the limit equilibrium model constitutive code was used. The design TAT is the stress predicted for a regular layout using tributary area stress.

6.3 Model calibration

From the observations described in Chapter 4, it is known that the pillars are extensively failed in the “collapsed area”, but they are mostly intact in the so-called “intact area” simulated above. The parameters given in Table 6-2 are therefore not correct for the intact area as the simulation results in extensive pillar failure. Further calibration runs were therefore conducted to obtain a better calibration of the models. The simulations conducted and the parameters used are shown in
Table **6-3** and
Table **6-4**. The pillar failure percentage was simply calculated as the ratio of the total number of failed elements divided by the total number of pillar elements

Table 6-3. Model input parameters and results for the collapsed area.

Area 1 - Collapsed Area													
Parameters	**Set 1**	**Set 2**	**Set 6**	**Set 7**	**Set 8**	**Set 9**	**Set 10**	**Set 11**	**Set 12**	**Set 13**	**Set 14**	**Set 15**	**Set 16**
Intact Strength (MPa)	**60**	25	30	30	30	30	30	30	30	30	30	30	30
Intact rock slope	7	4.6	4.6	4.6	4.6	4.6	4.6	4.6	4.6	4.6	4.6	4.6	4.6
Initial crush strength (MPa)	4	4	4	**5**	**7.5**	**10**	4	4	4	4	**10**	**5**	4
Crushed rock slope	7	4.6	4.6	4.6	4.6	4.6	4.6	4.6	4.6	4.6	4.6	4.6	4.6
Interface friction angle	30	10	**20**	**20**	**20**	**20**	**25**	**15**	**10**	**5**	**15**	**15**	**10**
Seam height (m)	2	2	2	2	2	2	2	2	2	2	2	2	2
Seam stiffness modulus (MPa/m)	45000	45000	45000	45000	45000	45000	45000	45000	45000	45000	45000	45000	45000
Pillar failure percentage	0.0%	72.9%	30.6%	23.2%	10.9%	5.3%	20.9%	50.3%	72.3%	91.1%	11.3%	36.2%	74.1%

Table 6-4. Model input parameters and results for the intact area.

Area 2 - Intact Area																
Parameters	**Set 1**	**Set 2**	**Set 3**	**Set 4**	**Set 5**	**Set 6**	**Set 7**	**Set 8**	**Set 9**	**Set 10**	**Set 11**	**Set 12**	**Set 13**	**Set 14**	**Set 15**	**Set 16**
Intact Strength (MPa)	60	25	30	30	30	30	30	30	30	30	30	30	30	30	30	30
Intact rock slope	7	4.6	4.6	4.6	4.6	4.6	4.6	4.6	4.6	4.6	4.6	4.6	4.6	4.6	4.6	4.6
Initial crush strength (MPa)	4	4	4	4	4	4	5	7.5	10	4	4	4	4	**10**	**5**	4
Crushed rock slope	7	4.6	4.6	4.6	4.6	4.6	4.6	4.6	4.6	4.6	4.6	4.6	4.6	4.6	4.6	4.6
Interface friction angle	30	10	**30**	**40**	**50**	**20**	**20**	**20**	**20**	**25**	**15**	**10**	**5**	**15**	**15**	**10**
Seam height (m)	2	2	2	2	2	2	2	2	2	2	2	2	2	2	2	2
Seam stiffness modulus (MPa/m)	45000	45000	45000	45000	45000	45000	45000	45000	45000	45000	45000	45000	45000	45000	45000	45000
Pillar failure percentage	0.0%	81.9%	13.7%	6.2%	2.2%	26.4%	21.3%	14.0%	8.7%	18.8%	43.8%	80.8%	99.5%	4.8%	34.3%	82.3%

To select the most appropriate parameters, it was considered that the presence of water was a key difference between the intact area and the collapsed area. As a result, the alteration zone was dry and hard in the intact area and wet and slippery in the collapsed area. The effective friction angle of the pillar contact with the hangingwall was therefore substantially lower in the collapsed area compared to the intact area. This needs to be reflected in the calibration study. Unfortunately, no laboratory test results of these friction angles were available during this study and it needs to be investigated in future. The other rock parameters are considered to be identical for both areas. Based on these considerations, and the various simulations, the parameters of “Set 12” for the collapsed area (

Table **6-3**) and the parameters for “Set 10” for the intact area (

Table **6-4**) are considered to be the best calibration. The presence of water likely creates an effective stress condition that results in the 'appearance' that friction has reduced.

The simulated condition of the pillars in the two areas are shown in Figure 6-17 and Figure 6-18. These are encouraging results as the pillars in the centre of the collapsed area are completely failed and there is only minor scaling in the centre of the intact area. This agrees with the underground observations for the two areas. The pillars on the edges of the collapsed area are still intact, but this is only caused by the fact that these pillars are next to the modelled abutment.

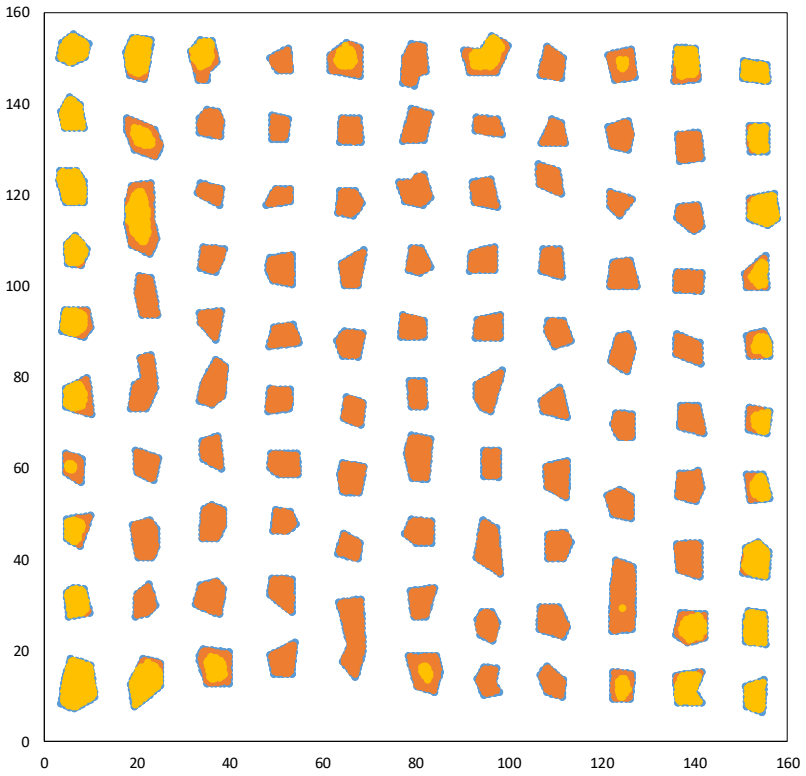

Figure 6-17. Simulation of pillar failure for the **collapsed area** using "Set 12" calibration parameters. The orange colour denotes failure and the yellow denotes intact pillars.

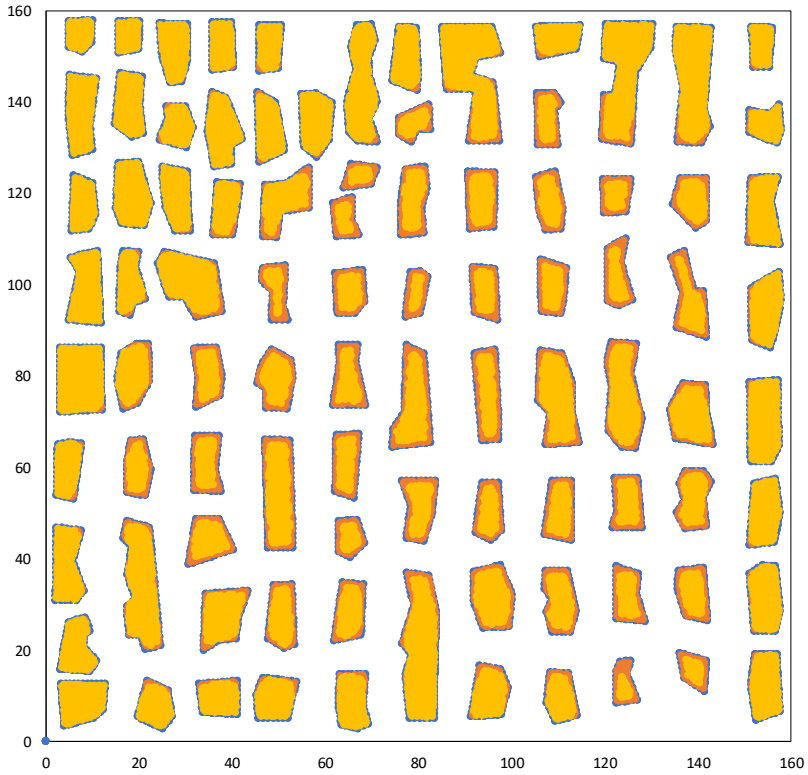

Figure 6-18. Simulation of pillar failure for the **intact area** using "Set 10" calibration parameters. The orange colour denotes failure and the yellow denotes intact pillars.

Of further interest was that the careful simulation of the two areas and the actual pillar shapes allowed for the back calculation of the K-value for the Hedley and Grant pillar formula. For this back calculation, the pillars were simulated as rigid pillars and the APS values calculated for each pillar. For the collapsed area, the pillars failed at these APS values and this was therefore the maximum strength of the pillars. The calculated K-values are shown in the Appendices and an average value of 19 MPa was obtained for the collapsed area. The value for some of the failed pillars were below 10 MPa and K = 10 MPa may therefore be a good approximation to use for the Hedley and Grant formula for these types of pillars. This will result in extremely conservative layouts and highlights the detrimental effect of these alteration layers on pillar strength.

6.4 Summary

This chapter illustrated the practical use of the limit equilibrium model in the TEXAN code to simulate the pillar failure at Everest Mine. Two areas of mine were simulated. These areas were selected as the one area collapsed and the other remained stable. The difference between the areas was that the pillars were smaller in the collapsed area and water was also presented in this area. This resulted in the weathering of the alteration zone and the decrease in friction angle on the contact between the pillars and the hangingwall.

It seems as if the numerical models are able to simulate the observed pillar behaviour. Encouraging was that the same parameters could be used for the two areas except that the friction angle of the interfaces were varied. This resulted in the different behaviour in the two areas.

A challenging aspect highlighted in this chapter is that the calibration of the limit equilibrium model is very difficult. Future work needs to study methods to better calibrate this model. Laboratory testing is required to determine the rock strengths as well as the friction angles of the wet and dry alteration zone material.

As the proposed model seems capable to simulate the behaviour of the pillars where the weak alteration zone is present, this model now needs to be used to investigate an alternative layout that will ensure stable regional mine layouts in future. This is explored in the next chapter.

7 PROPOSED MINE DESIGN FOR PILLARS WITH ALTERATIONS

7.1 Introduction

From the historic case studies of large-scale collapses and the numerical modelling presented in this study, it is clear that an alternative mine layout is required in areas where the alteration layer is present. A modified mine layout is proposed in this chapter. The previous chapter described a preliminary calibration of the limit equilibrium model to simulate the pillar behaviour for these conditions. These calibrated parameters are used to explore an alternative layout design. The proposed mining layout is for a bord and pillar mining method in a tabular, shallow-dipping orebody. These orebodies are typically those encountered in the Bushveld Complex in South African. It is an important problem to solve as there is greater urgency to ensure that mechanised mining can be used in future, even for these “difficult” orebodies that contain the alteration layers. Conventional, labour, intensive mining methods, as encountered in the deep gold mines and some of the intermediate depth platinum mines, are not an option where alterations are present.

This study highlighted three critical factors that influence the overall stability of the pillars when encountering weak alteration layers in the orebody. These factors need to be considered during any design, regardless of the mining layout. These three aspects are listed below:

- The ingress and management of ground water is crucial. The presence of water should be limited as far as practically possible.
- The ongoing monitoring of pillar sizes is critical to ensure that the pillars are cut as per the design specification. The monitoring should also be extended to existing pillars to record any early signs of pillar scaling.
- The use of regional or barrier pillars is critical to compartmentalise the mine. This will prevent mine-wide collapses. To ensure economically viable mining operations, a minimum extraction ratio needs to be obtained. This will require small in-panel pillar sizes, together with regional pillars to ensure regional stability.

With regards to the barrier pillars, during the underground investigations described in Chapter 4, it was noted that the large barrier pillars implemented at Everest Platinum Mine prevented the collapse to propagate beyond these pillars. The barrier pillars did show signs of minor scaling, but is seems as if they were able to contain the pillar failure.

Some of the other important aspects that needs to be considered during the mine design process and subsequent mining operations are the following:

1. The presence of any weak geological alteration layers needs to be identified during the early stages of exploration and mining. It is critical to understand the position of these layers within the orebody before any layout design work is conducted.
2. Conduct laboratory testing on the weak geological layer to understand aspects such the friction angles of these layers and the effect of water.
3. Pillar robbing will increase the extraction ratios. This will increase the stresses acting on the pillars and aggravate the situation when a weak layer is present in the pillar.
4. Reduce the exposure and ingress of water to underground workings.
5. Carefully assess the transition from open pit mining to underground mining and the possible exposure of the crown pillar to a build-up of water.

7.2 Proposed Mine Layout

Numerous alternative mining layouts were considered by the author. Owing to the requirement of a mechanised mining operation and the characteristics of the orebody (narrow seam, tabular, flat-dipping), the only practical option was a modified bord and pillar mining method.

The proposed mining layout was proposed based on the rock engineering study described in this report, practical mining knowledge of the author had the goal of achieving the maximum extraction ratio. When considering these factors, the only suitable option appears to be a compartmentalised bord and pillar layout. An overriding consideration is the stability of the mine. As a next step for each proposed mining site with alteration layers, a comprehensive mining feasibility study needs to be conducted to determine the economic feasibility of using this proposed layout. Such a feasibility study is considered beyond the scope of this specialised rock engineering study.

The proposed mining layout for an orebody that contains a weak geological alteration layer is shown in Figure 7-1. Note that the diagram only shows part of the layout to illustrate the inclusion of barrier pillars. Each “compartment” will contain 144 pillars of size 7 m x 7 m and will be surrounded by large barrier pillars with holings at specified distances. The numerical modelling illustrated in this chapter was used to determine the size of the barrier pillars. The modelling was based on a depth of 200 mbs, for a shallow platinum mine, mining UG2, in wet conditions. The parameters obtained from Chapter 5 and 6 were used for the model deemed as a worst-case scenario.

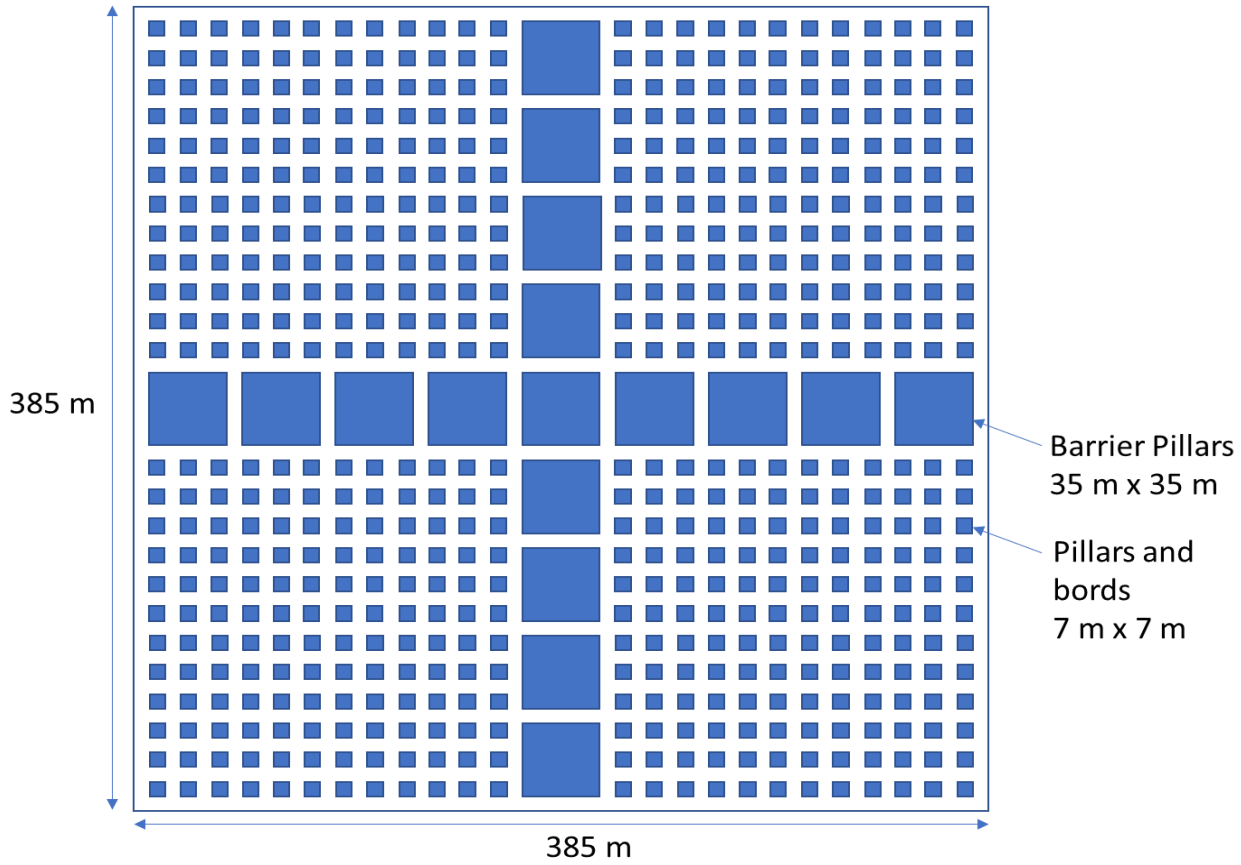

Figure 7-1. Proposed mining layout for the ore bodies that have the presence of weak geological alteration layers.

The proposed mining layout allows for the maximum extraction with the protection of infrastructure, entrances and exits for the LoM. This layout could become problematic with regards to the mining sequencing if not followed as per the mine scheduling. Traditionally

all bord and pillar mining was mined by a stoping crew. Conventional mining methods require a specialised crew allocation based on the either development, ledging or stoping. Bord and pillar mining does not require the specialised crew for on-reef development. The proposed mining layout of a compartmentalisation bord and pillar will, however, require the allocation of specialised crews for both development and stoping to ensure the availability of mining blocks as dictated by the scheduling. The large barrier pillars will require optimised “ventilation layouts” to ensure flow of air and adequate cooling. The installation of infrastructure as close as possible to the mining faces also needs to be considered. This will improve the mining efficiencies and allow for a productive section.

A rock engineering related benefit of compartmentalisation and the pre-development of blocks will be the early identification and interpretation of geological conditions. This will allow for better planning in terms of larger geological structures and aspects such as optimum mining directions relative to joint orientations. This should allow for safer mining conditions and more mining flexibility.

The compartmentalisation will allow for each mining block to achieve an extraction ratio (which includes the barrier pillars) that typically varies from 69% and 74%, while maintaining the overall stability of the mining operation. Table 7-1 shows the difference in extraction ratio for different size barrier pillars. Layout 1 is the traditional Everest Platinum Mine layout, which is used as a baseline to compare with the proposed new extraction ratios. Layout 2 shows the decrease in extraction ratio if pillars are designed with more conservative parameters using a traditional bord and pillar layout. Layout 3 is the proposed new layout for different barrier pillar sizes. This table illustrates the effect of barrier pillar size on extraction ratio.

Table 7-1. Extraction ratios for the different layouts.

Layouts	Total Area	Pillar Area	Mined Area	Extraction %
1	148225	35721	112504	**75.9**
2	148225	59290	88935	**60.0**
3 (15 m barrier)	133225	32049	101176	**75.9**
3 (20 m barrier)	136900	35024	101876	**74.4**

3 (25 m barrier)	140625	38849	101776	**72.4**
3 (30 m barrier)	144400	43524	100876	**69.9**
3 (35 m barrier)	148225	49049	99176	**66.9**
3 (35 m split barrier)	148225	46074	102151	**68.9**

7.3 Numerical modelling of the proposed layouts

Based on the work described in Chapters 5 and 6, the TEXAN code with the limit equilibrium model was used to determine the optimum barrier pillar size for the layout proposed in Figure 7-1. The objective of this modelling was to determine if the barrier pillars will survive during the complete collapse of all the in-panel pillars on a scale similar to the Everest Mine collapse. The parameters shown in Table 6-2 was therefore used to simulate a very weak rock mass. These parameters are similar to the calibrated parameters for the "collapsed area" as shown in Table 6-3 except that the intact strength parameter was slightly smaller at 25 MPa. This was used to simulate a "worst case" scenario and to partially compensate for the limited size of the model. It was important to investigate the behaviour of the barrier pillars if the in-panel pillars fail adjacent to these larger pillars.

The simulated failure of the pillars for the different barrier pillar sizes are shown in Figure 7-2 to Figure 7-7. Note the extensive failure of the in-panel pillars in all cases.

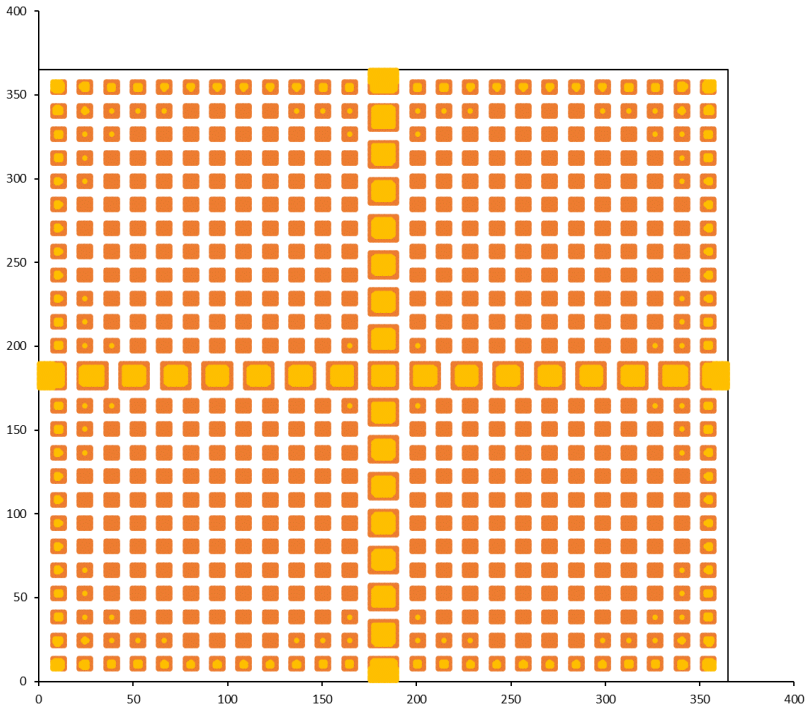

Figure 7-2. Simulated pillar failure if the barrier pillars are of a size 15 m x 15 m. The orange colour denotes failure and the yellow denotes intact rock.

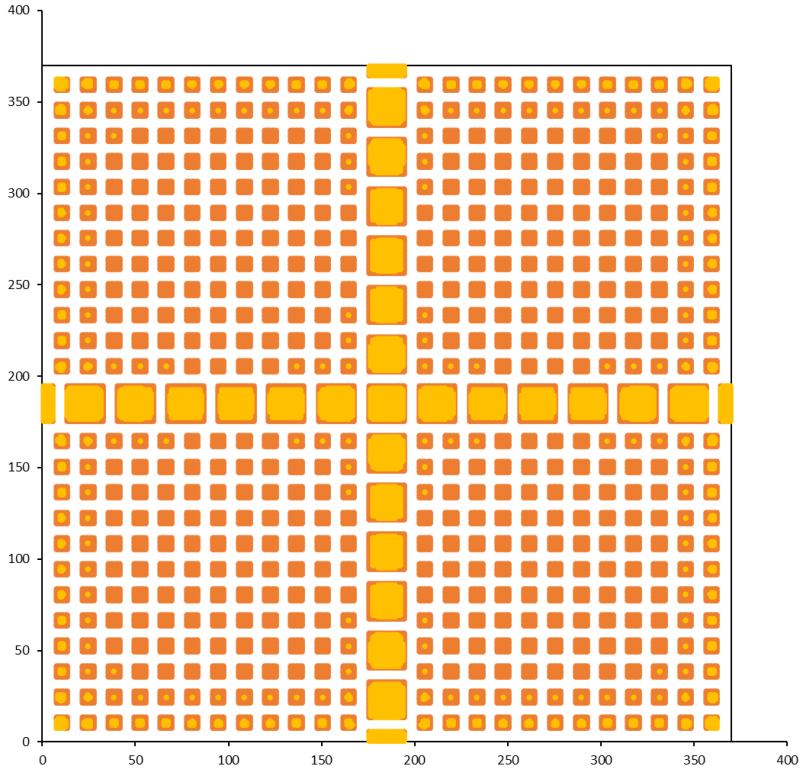

Figure 7-3. Simulated pillar failure if the barrier pillars are of a size 20 m x 20 m. The orange colour denotes failure and the yellow denotes intact rock.

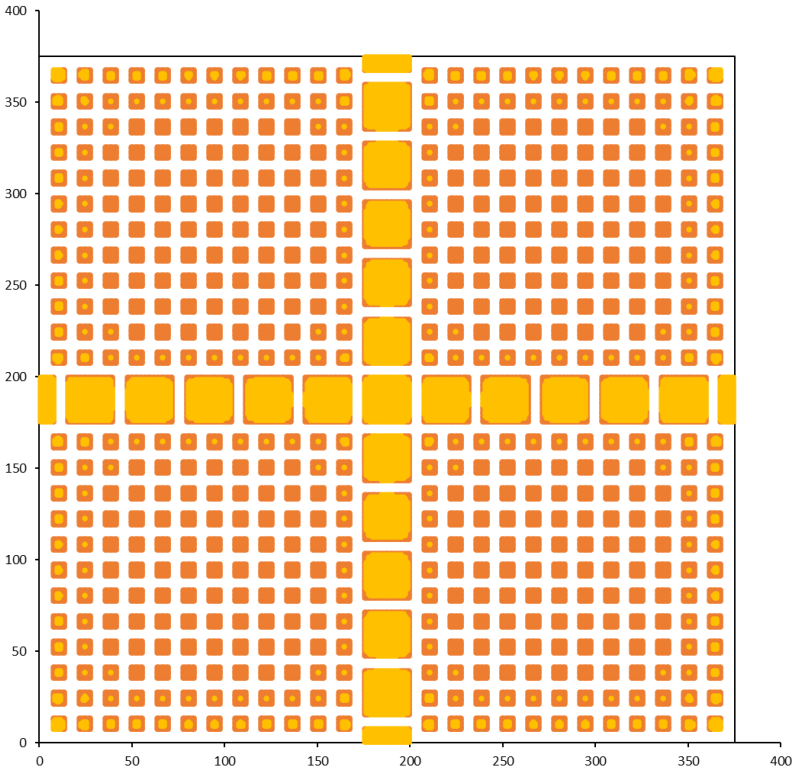

Figure 7-4. Simulated pillar failure if the barrier pillars are of a size 25 m x 25 m. The orange colour denotes failure and the yellow denotes intact rock.

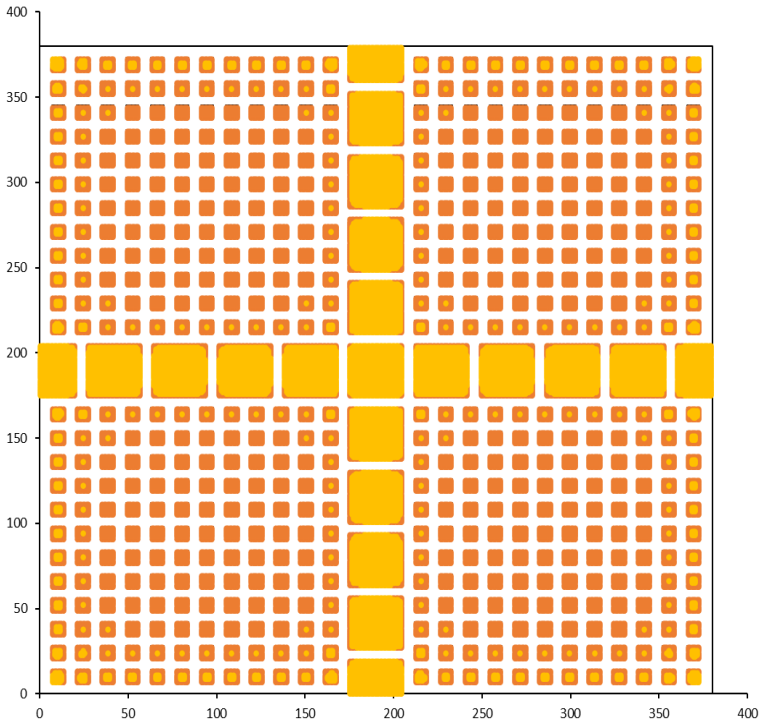

Figure 7-5. Simulated pillar failure if the barrier pillars are of a size 30 m x 30 m. The orange colour denotes failure and the yellow denotes intact rock.

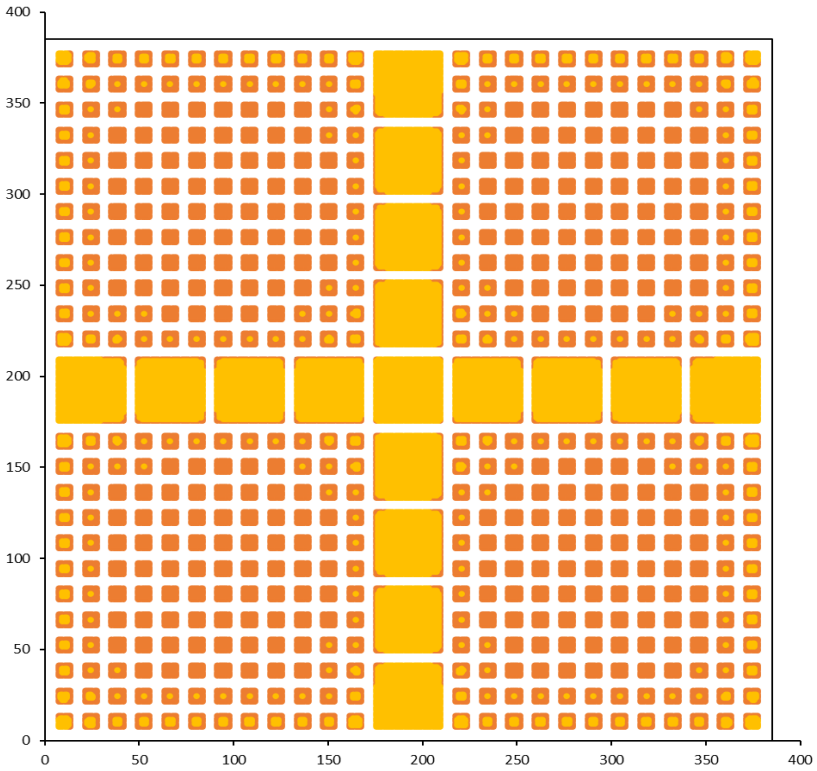

Figure 7-6. Simulated pillar failure if the barrier pillars are of a size 35 m x 35 m. The orange colour denotes failure and the yellow denotes intact rock.

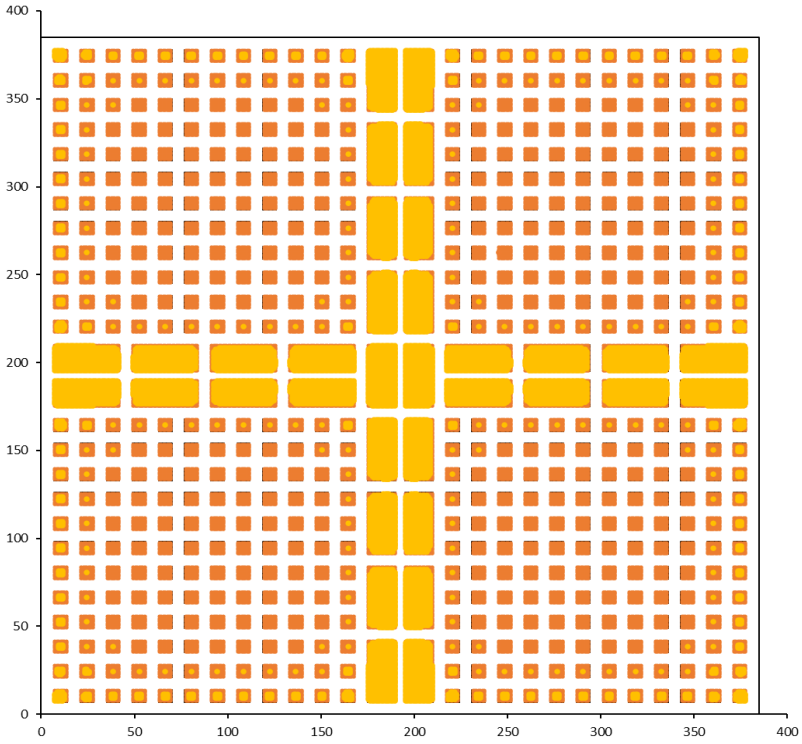

Figure 7-7. Simulated pillar failure for “split” barrier pillars of a size 35 m x 35 m (each portion 15 m x 35 m). The orange colour denotes failure and the yellow denotes intact rock.

For the 15 m and 20 m wide barriers, some scaling is noted after the in-panel pillar collapse. It is therefore recommended to use at least 25 m wide pillars. To ensure safe travelling throughout the mine in case of large collapses, the split barrier option presented in Figure 7-7 may be a good solution. The simulated amount of scaling on the pillars are only minor and are not more extensive than that experienced by the solid 35 m wide pillars. This option gives an extraction ratio of 69%. Although less than the “ideal” 75%, it should be remembered that it is very difficult to maintain excavation stability for these types of conditions and the slightly lower extraction ratio will make safe mining possible.

8 CONCLUSIONS

This study investigated the problem of determining hard rock pillar strength when geological alterations are present in the pillars. These alteration layers are found in the Bushveld Complex where the pyroxenite layers have been exposed to hydrothermal fluid flow, serpentinization and subjected to layer-parallel shearing. The resulting clay-like material and the weak partings is defined as the alteration zone. These alterations substantially weaken the pillars, and a better understanding of pillar strength will allow for improved designs to be implemented in future.

The dissertation includes a literature review and describes three valuable case studies of pillar collapses in Southern Africa. This is an important contribution of this study as this information has never been collated. This includes a Zimbabwean operation in the Great Dyke, the Wonderkop Mine in the Western Bushveld and Everest Platinum Mine in the Eastern Bushveld. Access to the Everest Platinum Mine was still possible and most of the work in this study focusses on the pillar behaviour at this mine. Two underground visits at the mine were conducted by the author to collect additional information. A geological alteration is present at the top reef contact at this location, and this resulted in a mine-wide collapse and closure of the mine.

The literature survey indicated that almost no information is currently available on appropriate design methodologies if weak geological alteration layers are present in the pillars. This is an area where numerical modelling can be used to determine pillar strength and to simulate identified pillar failure mechanisms. The influence of weak partings on pillar strength can be investigated using numerical modelling codes that can simulate these partings and inelastic rock behaviour.

Empirical methods are still popular in the rock engineering fraternity to determine pillar strength. The Hedley and Grant formula, which was derived for Canadian uranium pillars, has been used extensively in South African hard rock pillar designs. Very few collapses of hard rock bord and pillars mines have been reported in the country. This pillar strength formulation therefore seems to be mostly conservative, but its application at the three mines

mentioned above did not prevent the collapses of the underground workings. A back analysis of the collapsed area at Everest Mine indicated that the K-value in the popular Hedley and Grant empirical strength formula is less than 20 MPa and can be as low as 10 MPa. When using this as a design parameter, this will result in designs that are not economically viable and an alternative layout will have to be considered.

This study proposed an alternative numerical modelling approach to determine the stability of bord and pillar layouts where alteration layers are present. The displacement discontinuity code, TEXAN, proved to be useful to simulate the pillar failure. The capability of the code to simulate irregular-shaped pillars on a large scale was useful for this kind of study. Furthermore, the built-in limit equilibrium model allows the pillar scaling and failure to be simulated. The model contains an interface at the hangingwall and footwall contacts and this appears to be able to simulate the effect of the geological alterations. The limit equilibrium model was studied in detail for this project. A mathematical derivation illustrated one of the drawbacks of the model namely that it predicts an exponential increase in stress towards the centre of a completely failed pillar. It is not clear if this is a good approximation of actual pillar failure behaviour. It is nevertheless an effective method to introduce pillar failure in a displacement discontinuity boundary element model.

For the Everest Mine, two areas were simulated, namely part of the collapsed area and a second area, with larger pillars that is still stable. This allowed for a first order calibration of the limit equilibrium model. The effect of friction angle on the weak partings was illustrated during this calibration exercise. The calibrated values for the two areas were identical, except for a 10° friction angle for the collapsed area and 25° friction angle for the stable area. This difference is justified owing to the presence of water in the collapsed area. This resulted in weathering of the alteration layer and a decrease in the friction angle.

The calibrated model was subsequently used to explore alternative layout designs for these ground conditions. Barrier pillars will clearly be necessary to compartmentalise the mine. The numerical modelling predicted that the barrier pillars will remain stable, even for large scale collapses, provided their width exceeds 25 m. Main access routes into the mine can be protected by a double row of pillars, which is at least 15 m wide, to provide for a safe travelling way.

In summary, a key finding of the study is that geological alterations substantially reduce the strength of hard rock pillars and a revised design methodology is required. The traditional South African design methodology of using the empirical Hedley and Grant formula does not work in these cases. A displacement discontinuity numerical model using a limit equilibrium model appears to be useful to simulate this pillar behaviour on a mine-wide scale. After calibration of the model, this can be used to explore appropriate layouts and aspects such as the required width of barrier pillars.

9 RECOMMENDATIONS FOR FUTURE STUDIES

Although significant progress was made in this study to better understand the detrimental effect of weak layers in pillars, further studies are required. These include the following:

1. As described above, the limit equilibrium model is a symmetrical model with partings at both the hangingwall and footwall contacts. It needs to be explored if this can be modified to a single parting plane model for cases where there is a single weak parting at the hangingwall contact.
2. Pillars with a weak layer needs to be simulated with a finite difference or finite element code that can simulate the inelastic rock behaviour. These results need to be compared with the TEXAN code and the limit equilibrium model to gain further insight into the applicability of the model.
3. Further work is required to calibrate the limit equilibrium model. Of particular interest is the friction angles of the alteration zone material for dry and wet material. This material needs to be tested in the laboratory.
4. The time-dependent failure of the pillars was beyond the scope of this study, and this also needs to be explored in future. The limit equilibrium model can be easily extended to simulate time-dependent scaling.
5. Regarding future feasibility studies, better core recovery and the identification of weak geological alteration layers is required.
6. The proposed new layout focussed mostly on rock engineering aspects and did not consider the other mining engineering aspects such as ventilation requirements. This needs to be explored in future to confirm that the new layout is practical and will result in profitable mining operations.

10 REFERENCES

Bieniawski, Z.T. and Hustrulid, W.A. (1976). A review of coal pillar strength formulas. Rock Mechanics and Rock Engineering, Rock Mechanics Chapter 8, 115–145.

Bieniawski, Z.T. and Van Heerden, W.L. (1975). The significance of in situ tests on large rock specimens, International Journal of Rock Mechanics, Mineral Sciences and Geomechanics. Abstract., Volume 12 no.4, pp. 101-113.

Dlokweni, T. and Leach, A. R. (2007). Parametric study to examine the effect of shear parting characteristics on pillar behaviour at Everest mine. Consultancy report by Itasca Africa (Pty) Ltd for Everest Platinum Mine. November.

Du Plessis M., Malan D.F. and Napier J.A.L. (2011) Evaluation of limit equilibrium model to simulate crush pillar behaviour. Journal of the South African Institute of Mining and Metallurgy, Volume 11, no 12, December.

Esterhuizen, G.S. and Ellenberger, J.L. (2007). Effects of Weak Bands on Pillar Stability in Stone Mines: Field Observations and Numerical Model Assessment. Proceedings of 26th International Conference on Ground Control in Mining.

Everest Platinum Mine COP, (2007). Code of Practice to Combat Rock Fall and Rock Burst Accidents in Tabular Metalliferous Mines, Aquarius Platinum Pty Ltd.

Fernandes, N.D. (2020). Personal communication.

Gay, N.C., Ortlepp, W.D., Ryder, J.A., Steffen, O. and Wagner, H. (1982). The development of rock mechanics in the South African mineral industry, Proceedings of the 12th Congress of the Council of Mining and Metallurgy Institutions, Johannesburg, South Africa, 3–7 May 1982. Journal of the South African Institute of Mining and Metallurgy, Johannesburg, 1982. pp. 365–376.

Godden, S.J. (2008). Everest Platinum subsidence event. Consultancy report by S. Godden & Associates Ltd. for Aquarius Platinum (South Africa) (Pty) Ltd. December 18, 2008.

Godden, S.J. (2008). Interim Report on the December 2008 Subsidence Event, Everest Platinum. Consultancy report by S. Godden & associates Ltd. for Aquarius Platinum (South Africa) (Pty) Ltd. February 19, 2009.

Godden S J. (2009). Pillar design and cutting at Everest Mine. Consulting report by S.Godden and Associates April.

Godden and Associates (Pty) Ltd. (2009). The Sequence of Key Actions and Outcomes leading to the December 2008 Subsidence Event, Everest Platinum Mine.

Greenwald, H.P., Howard, H.C., and Hartmann, I. (1939). Experiments on the strength of small pillars of coal in the Pittsburg Bed. US Bureau of Mines, paper No. 605, 1939.

Greenwald, H.R., Howarth, H.C. and Hartman, I. (1941). Progress Report: Experiments on strength of small pillars of coal, Pittsburgh bed.

Hartzenburg, A.G, du Plessis, M, Malan, D.F. (2020). The effect of alteration layers on UG2 pillar behaviour in the Bushveld Complex, Rock Mechanics for Natural Resources and Infrastructure Development – Fontoura, Rocca and Pavon Mendoza (Eds), 2020 ISRM, ISBN 987-0-367-42284-4, (2309-2331)

Hedley, D.G.F. and Grant F. (1972). Stope pillar design for the Elliot Lake uranium mines, Journal of the Canadian Institute of Mining and Metallurgy Volume 65, pp. 37-44.

Hoek, E. (1968). Brittle fracture in rock. Chapter 4, Rock Mechanics In Engineering practice. Edited Stagg and Zienkiewicz, Wiley press, 1968.

Hoek, E., Wood, D. and Shah, S. (1992). A Modified Hoek-Brown Criterion for Jointed Rock Masses. Rock Characterization: International Society of Rock Mechanics Symposium, Chester, 14-17 September 1992, 209-213.

Iannacchione, A.T. (1990). The effects of roof and floor interface slip on coal pillar behaviour.

Laubscher, D.H. (1990) A geomechanics classification system for the rating of rock mass in mine design. Journal of the South African Institute of Mining and Metallurgy, Volume 90, no. 10, 1990. pp. 257–273.

Lombard, J., Benson, F., and Schoombee, J. (2008). Closure of the hangingwall and pillars spalling along the South Bords up dip of Strike 3 South – Everest Platinum mine. Internal company report from the mine's Rock Engineer. Report RED 33/08. March 20.

Lombard, J. (2008). Large hangingwall instability in the south bords back area up dip of Bord 4 South – Everest mine. Internal company report from the mine's Rock Engineer. Report RED 52/08. May 28.

Lombard, J. (2008). Scaling pillars up dip of Strike 3 South, creating a breaker-line of pillars for decline protection – Everest mine. Internal company report from the mine's Rock Engineer. Report RED 62/08. August 11.

Lombard, J. (2008). Pillar failure in the south bords, initial cost estimates for backfilling – Everest Platinum mine. Internal company report from the mine's Rock Engineer. Report RED 82/08. October 14.

Lombard, J. (2008). Summary of proposals for protecting the declines from possible pillar failure – Everest Platinum mine. Internal company report from the mine's Rock Engineer. Report RED 88/08. October 31.

Lombard, J. (2008). Support of the decline pillars for protection from failing pillars in the south bords – backfill option for ensuring future stability – Everest Platinum mine. Internal company report from the mine's Rock Engineer. Report RED 97/08. November 19.

Lombard, J. (2008). Accelerated closure indicted in travelling-way adjacent to Decline 3 – Everest Platinum mine. Internal company report from the mine's Rock Engineer. Report RED 100/08. November 26.

Lombard, J. (2008). Large collapse of hangingwall over the declines from Strike 0 to Strike 5 – Everest Platinum mine. Internal company report from the mine's Rock Engineer. Report RED 103/08. December 12.

Malan, D.F. (2006). Numerical modelling of the bord and pillar layout at Kroondal mine. Groundwork report TN1/0209/XE003.

Malan, D.F. (2008). Investigation of pillar design and pillar stability at Saffy and Hossy shaft, Groundwork consultancy report, Reference CR300/1008/LM052.

Malan, D.F. (2011). Pillar design in hard rock mines: can we do this with confidence? Proceeds from 2nd Australasian Ground Control in Mining Conference, Sydney, NSW, 23 - 24 November 2010

Malan, D.F. and Napier, J.A.L. (2006). Practical application of the TEXAN code to solve pillar design problems in tabular excavations, South African National Institute of Rock Engineering (SANIRE) Symposium, Facing the challenges in Rock Mechanics. Rustenburg, pp. 55-74.

Malan, D.F. and Napier, J.A.L. (2007). Numerical Modelling of the Bord and Pillar Layout at Impala no 12 Shaft. Contract report CR269/0307/IMP021 March 2007.

Malan, D.F, and Napier, J.A.L. (2011). The design of stable pillars in the Bushveld Complex mines: a problem solved? Journal of the South African Institute of Mining and Metallurgy, Volume 11, no 12 December 2011.

Malan, D.F and Napier, J.A.L. (2021). A review of the role of underground measurements in the historic development of rock engineering in South Africa, to be published: Journal of the South African Institute of Mining and Metallurgy. May 2021.

Malan, D.F and Ryder, J. (2009). Numerical modelling of the current and revised lay-out in the mechanised section at 14 Shaft. Groundwork report TN622/1009/IP044. 2009

Maritz, J.A. and Malan, D.F. (2011). The influence of shear stress and weak contacts on pillar behaviour. Harmonising rock engineering and the environment. Qian & Zhou (eds), Taylor & Francis, 599-604.

Martin, C.D. and Maybee, W.G. (2000). The strength of hard rock pillars. International Journal of Rock Mechanics and Mining Science Volume 37, 2000.

More O'Ferrall, G.C. and Malan, D.F. (2012). The effect of weak layers on pillar performance in South African chrome and platinum mines, In: C. Hawkes (ed.) Proceedings from the 21st Canadian Rock Mechanics Symposium, The Canadian Rock Mechanics Association, pp 3-10.

Napier, J.A.L. and Malan, D.F. (2007). The computational analysis of shallow depth tabular mining problems, J. S. Afr. Inst Min Metall., Volume 107, Nov 2007, pp 725-742.

Napier, J.A.L., and Malan, D.F. (2011). Numerical modelling of average pillar stress and implications for pillar design. Journal of the South African Institute of Mining and Metallurgy, Volume 11, no 12, December 2011.

Pretorius, J.W., (2000), Personal communication.

Roberts, M.K.C., (2008), Comments regarding as visit to Everest Platinum mine on the 9th October, 2008. Consultancy report for Everest Platinum. Report No. TWP 14/10/08. October 2008.

Roberts, M.K.C., and Clark-Mostert, V. (2010). Is there some commonality between the geological structures in the Bushveld Complex and the Great Dyke?. The 4th International Platinum Conference, Platinum in transition 'Boom or Bust', The Southern African Institute of Mining and Metallurgy.

Salamon, M.D.G. (1982). Unpublished report to Wankie Colliery.

Spencer, D. (1999). A case study of a pillar system failure at shallow depth in a chrome mine. Hagan, T.O. (ed.). Proceedings of SARES99, 2nd Southern African Rock Engineering Symposium, 1999. pp. 53–59.

Spencer, D. (2008) Rock engineering review, Consultancy report by Spencer Rock Mechanics Consultancy CC for Everest Platinum mine. December 08, 2008.

Stacey, T.R. and Page, C.H. (1986). Practical handbook for Underground Rock mechanics"' Series on Rock and Soil Mechanics, Volume 12 Trans Tech Publications, 1986, pp.53-63.

Stacey, T.R. and Swart, A.H. (2001). Practical rock engineering practice for Shallow and Opencast Mines, Safety in Mines Research Advisory Committee, Johannesburg, 2001.

Treloar, M. (2019). Personal communication.

Van der Merwe, N. (2006). Beyond Coalbrook: what did we really learn? Journal of the Southern African Institute of Mining and Metallurgy, Volume 106, 2006. pp. 857–868.

Van der Merwe, N. (2019). Coal pillar strength analysis based on size at the time of failure. Journal of the South African Institute of Mining and Metallurgy, Volume 119, pp 681-692.

Wagner, H. (1974). Determination of the complete load-deformation characteristics of coal pillars, Proceeds from 3rd International Congress on Rock Mechanics, International Society for Rock Mechanics, Denver, USA, Volume 2B, pp. 1076-1082.

Wagner, H. (1980). Pillar design in coal mines. Journal of the South African Institute of Mining and Metallurgy, February 1980.

Wagner, H. and Madden, B.J. (1984). Fifteen years' experience with the design of coal pillars in shallow South African collieries. Design and Performance of Underground Excavations. International Society for Rock Mechanics, Cambridge.

Watson, B.P., Ryder, J.A., Kataka, M.O., Kuijpers, J.S. and Leteane, F.P. (2008). Merensky pillar strength formulae based on back-analysis of pillar failures at Impala Platinum, Journal of the South African Institute of Mining and Metallurgy, Volume 108, pp. 449-461.

APPENDICES

Table 1. Summary of using the simulated APS to determine the K values for Hedley and Grant, Platmine and the Linear formula for the collapsed area simulated in Chapter 6.

Collapsed Area															
Pillar	APS	FoS	PS	Area	w	h	Hedley and Grant			Platmine - UG2			Linear		
							α	β	K	α	β	K	A	B	K
P1	13.02054	1	13.02054	26.05	5.10392	2	0.5	0.75	**9.69**	0.67	0.32	**10.91**	0.3	0.6	**31.07**
P2	16.9212	1	16.9212	23.36	4.833218	2	0.5	0.75	**12.94**	0.67	0.32	**14.70**	0.3	0.6	**38.78**
P3	14.9563	1	14.9563	31.96	5.653318	2	0.5	0.75	**10.58**	0.67	0.32	**11.70**	0.3	0.6	**38.57**
P4	19.34388	1	19.34388	19.6	4.427189	2	0.5	0.75	**15.46**	0.67	0.32	**17.82**	0.3	0.6	**41.58**
P5	17.31132	1	17.31132	28.78	5.364699	2	0.5	0.75	**12.57**	0.67	0.32	**14.02**	0.3	0.6	**42.89**
P6	17.69784	1	17.69784	30.68	5.538953	2	0.5	0.75	**12.65**	0.67	0.32	**14.03**	0.3	0.6	**44.93**
P7	22.12629	1	22.12629	15.96	3.994997	2	0.5	0.75	**18.62**	0.67	0.32	**21.84**	0.3	0.6	**44.21**
P8	19.15118	1	19.15118	22.13	4.704253	2	0.5	0.75	**14.85**	0.67	0.32	**16.94**	0.3	0.6	**43.02**
P9	17.87445	1	17.87445	23.6	4.857983	2	0.5	0.75	**13.64**	0.67	0.32	**15.48**	0.3	0.6	**41.12**
P10	11.70487	1	11.70487	56.25	7.5	2	0.5	0.75	**7.19**	0.67	0.32	**7.58**	0.3	0.6	**37.75**
P11	16.61415	1	16.61415	35.65	5.970762	2	0.5	0.75	**11.43**	0.67	0.32	**12.53**	0.3	0.6	**44.69**
P12	19.48971	1	19.48971	36.96	6.079474	2	0.5	0.75	**13.29**	0.67	0.32	**14.52**	0.3	0.6	**53.16**
P13	16.58077	1	16.58077	72.48	8.513519	2	0.5	0.75	**9.56**	0.67	0.32	**9.86**	0.3	0.6	**59.35**
P14	24.11736	1	24.11736	27.55	5.248809	2	0.5	0.75	**17.70**	0.67	0.32	**19.83**	0.3	0.6	**58.78**
P15	23.42411	1	23.42411	37.15	6.09508	2	0.5	0.75	**15.96**	0.67	0.32	**17.42**	0.3	0.6	**64.02**
P16	26.41663	1	26.41663	21.32	4.617359	2	0.5	0.75	**20.68**	0.67	0.32	**23.66**	0.3	0.6	**58.54**
P17	22.07788	1	22.07788	33.53	5.790509	2	0.5	0.75	**15.43**	0.67	0.32	**16.99**	0.3	0.6	**57.99**
P18	25.39085	1	25.39085	19.2	4.38178	2	0.5	0.75	**20.40**	0.67	0.32	**23.56**	0.3	0.6	**54.17**
P19	16.57737	1	16.57737	43.62	6.604544	2	0.5	0.75	**10.85**	0.67	0.32	**11.68**	0.3	0.6	**48.27**

P20	19.13799	1	19.13799	31.9	5.648008	2	0.5	0.75	**13.54**	0.67	0.32	**14.98**	0.3	0.6	**49.31**
P21	25.19111	1	25.19111	22.03	4.693613	2	0.5	0.75	**19.56**	0.67	0.32	**22.32**	0.3	0.6	**56.50**
P22	33.20399	1	33.20399	13.81	3.716181	2	0.5	0.75	**28.97**	0.67	0.32	**34.40**	0.3	0.6	**63.11**
P23	29.33212	1	29.33212	19.64	4.431704	2	0.5	0.75	**23.43**	0.67	0.32	**27.01**	0.3	0.6	**63.10**
P24	31.05352	1	31.05352	17.4	4.171331	2	0.5	0.75	**25.57**	0.67	0.32	**29.78**	0.3	0.6	**63.97**
P25	24.00982	1	24.00982	34.32	5.858327	2	0.5	0.75	**16.68**	0.67	0.32	**18.34**	0.3	0.6	**63.64**
P26	28.76131	1	28.76131	20.18	4.492215	2	0.5	0.75	**22.82**	0.67	0.32	**26.24**	0.3	0.6	**62.48**
P27	25.02007	1	25.02007	28.63	5.350701	2	0.5	0.75	**18.19**	0.67	0.32	**20.31**	0.3	0.6	**61.87**
P28	23.32271	1	23.32271	29.53	5.434151	2	0.5	0.75	**16.83**	0.67	0.32	**18.73**	0.3	0.6	**58.35**
P29	18.86027	1	18.86027	40.55	6.367888	2	0.5	0.75	**12.57**	0.67	0.32	**13.62**	0.3	0.6	**53.35**
P30	26.63478	1	26.63478	14.11	3.756328	2	0.5	0.75	**23.11**	0.67	0.32	**27.40**	0.3	0.6	**51.00**
P31	33.13306	1	33.13306	14.85	3.85357	2	0.5	0.75	**28.39**	0.67	0.32	**33.50**	0.3	0.6	**64.57**
P32	37.93958	1	37.93958	12.88	3.588872	2	0.5	0.75	**33.68**	0.67	0.32	**40.24**	0.3	0.6	**70.42**
P33	27.65064	1	27.65064	26.65	5.162364	2	0.5	0.75	**20.47**	0.67	0.32	**22.99**	0.3	0.6	**66.55**
P34	29.16856	1	29.16856	21.48	4.634652	2	0.5	0.75	**22.79**	0.67	0.32	**26.06**	0.3	0.6	**64.82**
P35	29.91287	1	29.91287	20.64	4.543127	2	0.5	0.75	**23.60**	0.67	0.32	**27.09**	0.3	0.6	**65.51**
P36	26.2183	1	26.2183	25.87	5.086256	2	0.5	0.75	**19.55**	0.67	0.32	**22.01**	0.3	0.6	**62.40**
P37	30.46439	1	30.46439	17.43	4.174925	2	0.5	0.75	**25.07**	0.67	0.32	**29.20**	0.3	0.6	**62.79**
P38	26.36477	1	26.36477	24.75	4.974937	2	0.5	0.75	**19.88**	0.67	0.32	**22.47**	0.3	0.6	**61.73**
P39	24.70966	1	24.70966	25.08	5.007994	2	0.5	0.75	**18.57**	0.67	0.32	**20.96**	0.3	0.6	**58.14**
P40	18.32574	1	18.32574	36.06	6.004998	2	0.5	0.75	**12.58**	0.67	0.32	**13.77**	0.3	0.6	**49.51**
P41	27.97854	1	27.97854	20.93	4.574932	2	0.5	0.75	**22.00**	0.67	0.32	**25.22**	0.3	0.6	**61.59**
P42	29.50522	1	29.50522	21.26	4.610857	2	0.5	0.75	**23.11**	0.67	0.32	**26.46**	0.3	0.6	**65.32**
P43	30.8728	1	30.8728	23.74	4.872371	2	0.5	0.75	**23.52**	0.67	0.32	**26.68**	0.3	0.6	**71.17**
P44	29.09331	1	29.09331	23.14	4.810405	2	0.5	0.75	**22.31**	0.67	0.32	**25.36**	0.3	0.6	**66.44**
P45	32.66516	1	32.66516	18.03	4.246175	2	0.5	0.75	**26.66**	0.67	0.32	**30.95**	0.3	0.6	**68.14**
P46	27.05428	1	27.05428	26.49	5.146844	2	0.5	0.75	**20.06**	0.67	0.32	**22.54**	0.3	0.6	**64.97**
P47	32.10375	1	32.10375	16.59	4.073082	2	0.5	0.75	**26.75**	0.67	0.32	**31.28**	0.3	0.6	**65.03**

P48	19.41695	1	19.41695	31.27	5.591959	2	0.5	0.75	**13.81**	0.67	0.32	**15.30**	0.3	0.6	**49.65**
P49	24.12709	1	24.12709	27.49	5.243091	2	0.5	0.75	**17.72**	0.67	0.32	**19.85**	0.3	0.6	**58.75**
P50	25.88551	1	25.88551	28.2	5.310367	2	0.5	0.75	**18.89**	0.67	0.32	**21.11**	0.3	0.6	**63.64**
P51	32.31579	1	32.31579	17.35	4.165333	2	0.5	0.75	**26.63**	0.67	0.32	**31.02**	0.3	0.6	**66.50**
P52	32.08566	1	32.08566	19.17	4.378356	2	0.5	0.75	**25.79**	0.67	0.32	**29.78**	0.3	0.6	**68.42**
P53	34.96959	1	34.96959	16.32	4.039802	2	0.5	0.75	**29.26**	0.67	0.32	**34.26**	0.3	0.6	**70.43**
P54	24.77095	1	24.77095	37.83	6.15061	2	0.5	0.75	**16.80**	0.67	0.32	**18.31**	0.3	0.6	**68.19**
P55	28.76491	1	28.76491	23.17	4.813523	2	0.5	0.75	**22.05**	0.67	0.32	**25.06**	0.3	0.6	**65.72**
P56	27.292	1	27.292	22.68	4.762352	2	0.5	0.75	**21.03**	0.67	0.32	**23.95**	0.3	0.6	**61.87**
P57	19.78266	1	19.78266	39.17	6.258594	2	0.5	0.75	**13.30**	0.67	0.32	**14.45**	0.3	0.6	**55.20**
P58	31.15475	1	31.15475	46.1	6.789698	2	0.5	0.75	**20.11**	0.67	0.32	**21.55**	0.3	0.6	**92.73**
P59	28.33915	1	28.33915	15.23	3.902563	2	0.5	0.75	**24.13**	0.67	0.32	**28.41**	0.3	0.6	**55.71**
P60	29.04279	1	29.04279	23.14	4.810405	2	0.5	0.75	**22.27**	0.67	0.32	**25.31**	0.3	0.6	**66.32**
P61	29.67737	1	29.67737	23.7	4.868265	2	0.5	0.75	**22.62**	0.67	0.32	**25.66**	0.3	0.6	**68.37**
P62	29.02587	1	29.02587	22.62	4.756049	2	0.5	0.75	**22.38**	0.67	0.32	**25.49**	0.3	0.6	**65.73**
P63	34.66608	1	34.66608	26.92	5.188449	2	0.5	0.75	**25.60**	0.67	0.32	**28.72**	0.3	0.6	**83.75**
P64	25.88592	1	25.88592	17.32	4.16173	2	0.5	0.75	**21.34**	0.67	0.32	**24.86**	0.3	0.6	**53.24**
P65	27.30648	1	27.30648	36.66	6.05475	2	0.5	0.75	**18.66**	0.67	0.32	**20.40**	0.3	0.6	**74.25**
P66	24.6965	1	24.6965	19.09	4.36921	2	0.5	0.75	**19.87**	0.67	0.32	**22.96**	0.3	0.6	**52.58**
P67	21.94317	1	21.94317	18.38	4.28719	2	0.5	0.75	**17.82**	0.67	0.32	**20.66**	0.3	0.6	**46.09**
P68	29.66262	1	29.66262	22.79	4.773887	2	0.5	0.75	**22.83**	0.67	0.32	**25.99**	0.3	0.6	**67.36**
P69	29.30576	1	29.30576	16.97	4.119466	2	0.5	0.75	**24.28**	0.67	0.32	**28.34**	0.3	0.6	**59.84**
P70	31.224	1	31.224	20.37	4.513314	2	0.5	0.75	**24.72**	0.67	0.32	**28.40**	0.3	0.6	**68.06**
P71	30.967	1	30.967	21.27	4.611941	2	0.5	0.75	**24.25**	0.67	0.32	**27.76**	0.3	0.6	**68.57**
P72	31.56899	1	31.56899	20.12	4.485532	2	0.5	0.75	**25.07**	0.67	0.32	**28.83**	0.3	0.6	**68.50**
P73	28.11666	1	28.11666	20.89	4.570558	2	0.5	0.75	**22.12**	0.67	0.32	**25.36**	0.3	0.6	**61.85**
P74	26.59028	1	26.59028	27.39	5.233546	2	0.5	0.75	**19.55**	0.67	0.32	**21.90**	0.3	0.6	**64.66**
P75	22.72663	1	22.72663	23.41	4.838388	2	0.5	0.75	**17.38**	0.67	0.32	**19.73**	0.3	0.6	**52.12**

P76	23.88721	1	23.88721	29.73	5.452522	2	0.5	0.75	**17.20**	0.67	0.32	**19.14**	0.3	0.6	**59.92**
P77	21.21945	1	21.21945	19.93	4.464303	2	0.5	0.75	**16.89**	0.67	0.32	**19.44**	0.3	0.6	**45.89**
P78	26.93137	1	26.93137	22.5	4.743416	2	0.5	0.75	**20.80**	0.67	0.32	**23.69**	0.3	0.6	**60.87**
P79	34.75838	1	34.75838	22.52	4.745524	2	0.5	0.75	**26.83**	0.67	0.32	**30.57**	0.3	0.6	**78.59**
P80	27.26585	1	27.26585	14.03	3.745664	2	0.5	0.75	**23.69**	0.67	0.32	**28.10**	0.3	0.6	**52.10**
P81	28.45719	1	28.45719	26.84	5.180734	2	0.5	0.75	**21.03**	0.67	0.32	**23.60**	0.3	0.6	**68.67**
P82	30.36142	1	30.36142	25.35	5.034878	2	0.5	0.75	**22.76**	0.67	0.32	**25.67**	0.3	0.6	**71.72**
P83	26.68323	1	26.68323	19.17	4.378356	2	0.5	0.75	**21.45**	0.67	0.32	**24.77**	0.3	0.6	**56.90**
P84	19.49372	1	19.49372	23.63	4.86107	2	0.5	0.75	**14.87**	0.67	0.32	**16.87**	0.3	0.6	**44.86**
P85	21.59307	1	21.59307	62.37	7.897468	2	0.5	0.75	**12.92**	0.67	0.32	**13.50**	0.3	0.6	**72.64**
P86	18.99966	1	18.99966	23.17	4.813523	2	0.5	0.75	**14.56**	0.67	0.32	**16.55**	0.3	0.6	**43.41**
P87	24.3274	1	24.3274	32.37	5.689464	2	0.5	0.75	**17.15**	0.67	0.32	**18.95**	0.3	0.6	**63.04**
P88	27.19574	1	27.19574	26.33	5.131277	2	0.5	0.75	**20.19**	0.67	0.32	**22.70**	0.3	0.6	**65.16**
P89	26.09462	1	26.09462	21.29	4.614109	2	0.5	0.75	**20.43**	0.67	0.32	**23.39**	0.3	0.6	**57.80**
P90	27.07551	1	27.07551	21.32	4.617359	2	0.5	0.75	**21.19**	0.67	0.32	**24.25**	0.3	0.6	**60.00**
P91	25.66963	1	25.66963	22.13	4.704253	2	0.5	0.75	**19.90**	0.67	0.32	**22.71**	0.3	0.6	**57.67**
P92	24.25095	1	24.25095	23.44	4.841487	2	0.5	0.75	**18.54**	0.67	0.32	**21.05**	0.3	0.6	**55.64**
P93	21.72092	1	21.72092	25.57	5.056679	2	0.5	0.75	**16.24**	0.67	0.32	**18.31**	0.3	0.6	**51.48**
P94	18.57843	1	18.57843	30.24	5.499091	2	0.5	0.75	**13.32**	0.67	0.32	**14.80**	0.3	0.6	**46.90**
P95	18.79502	1	18.79502	22.23	4.71487	2	0.5	0.75	**14.56**	0.67	0.32	**16.60**	0.3	0.6	**42.29**
P96	18.48707	1	18.48707	28.36	5.325411	2	0.5	0.75	**13.47**	0.67	0.32	**15.05**	0.3	0.6	**45.55**
P97	19.29356	1	19.29356	19.15	4.376071	2	0.5	0.75	**15.51**	0.67	0.32	**17.92**	0.3	0.6	**41.13**
P98	14.88602	1	14.88602	20.23	4.497777	2	0.5	0.75	**11.80**	0.67	0.32	**13.57**	0.3	0.6	**32.37**
P99	19.14783	1	19.14783	32.39	5.691221	2	0.5	0.75	**13.50**	0.67	0.32	**14.91**	0.3	0.6	**49.63**
P100	19.26563	1	19.26563	22.32	4.724405	2	0.5	0.75	**14.91**	0.67	0.32	**17.00**	0.3	0.6	**43.42**
P101	20.06	1	20.06	22	4.690416	2	0.5	0.75	**15.58**	0.67	0.32	**17.78**	0.3	0.6	**44.97**
P102	19.26563	1	19.26563	20.45	4.522168	2	0.5	0.75	**15.24**	0.67	0.32	**17.50**	0.3	0.6	**42.05**
P103	19.26899	1	19.26899	20.88	4.569464	2	0.5	0.75	**15.16**	0.67	0.32	**17.38**	0.3	0.6	**42.38**

P104	15.51749	1	15.51749	32.28	5.681549	2	0.5	0.75	**10.95**	0.67	0.32	**12.10**	0.3	0.6	**40.17**
P105	15.96378	1	15.96378	27.16	5.211526	2	0.5	0.75	**11.76**	0.67	0.32	**13.19**	0.3	0.6	**38.70**
P106	16.05095	1	16.05095	20.64	4.543127	2	0.5	0.75	**12.66**	0.67	0.32	**14.54**	0.3	0.6	**35.15**
P107	22.30745	1	22.30745	55.11	7.423611	2	0.5	0.75	**13.77**	0.67	0.32	**14.54**	0.3	0.6	**71.35**
Average	**24.60439**			**25.92477**	**5.019242**				**18.81**			**21.39**			**57.19**

Table 2. Summary of using the simulated APS to determine the K values for Hedley and Grant, Platmine and the Linear formula for the collapsed area simulated in Chapter 6.

Intact Area															
Pillar	**APS**	**FoS**	**PS**	**Area**	**w**	**h**	**Hedley and Grant**			**Platmine - UG2**			**Linear**		
							α	**β**	**K**	**α**	**β**	**K**	**A**	**B**	**K**
P1	17.62101	1.5	26.43151	30.16	5.491812	2	0.5	0.75	**18.97**	0.67	0.32	**21.08**	0.3	0.6	**66.66**
P2	17.13492	1.5	25.70238	81.64	9.035486	2	0.5	0.75	**14.92**	0.67	0.32	**14.92**	0.3	0.6	**92.83**
P3	19.94105	1.5	29.91158	48.36	6.954135	2	0.5	0.75	**19.08**	0.67	0.32	**20.37**	0.3	0.6	**90.75**
P4	17.90557	1.5	26.85836	80.49	8.971622	2	0.5	0.75	**15.08**	0.67	0.32	**15.42**	0.3	0.6	**100.45**
P5	14.60222	1.5	21.90332	124.24	11.1463	2	0.5	0.75	**11.03**	0.67	0.32	**10.87**	0.3	0.6	**98.59**
P6	20.27379	1.5	30.41068	52.2	7.224957	2	0.5	0.75	**19.03**	0.67	0.32	**20.18**	0.3	0.6	**95.15**
P7	18.12524	1.5	27.18786	73.85	8.593602	2	0.5	0.75	**15.60**	0.67	0.32	**16.06**	0.3	0.6	**98.09**
P8	18.75061	1.5	28.12592	57.32	7.570997	2	0.5	0.75	**17.19**	0.67	0.32	**18.09**	0.3	0.6	**91.40**
P9	15.36931	1.5	23.05396	70.33	8.386298	2	0.5	0.75	**13.39**	0.67	0.32	**13.85**	0.3	0.6	**81.50**
P10	18.53997	1.5	27.80996	29.3	5.412947	2	0.5	0.75	**20.10**	0.67	0.32	**22.40**	0.3	0.6	**69.37**
P11	18.92667	1.5	28.39	64.63	8.039279	2	0.5	0.75	**16.84**	0.67	0.32	**17.54**	0.3	0.6	**96.92**
P12	17.32953	1.5	25.99429	81.75	9.041571	2	0.5	0.75	**14.54**	0.67	0.32	**14.84**	0.3	0.6	**97.86**
P13	22.03521	1.5	33.05282	51.75	7.193747	2	0.5	0.75	**20.73**	0.67	0.32	**22.00**	0.3	0.6	**103.05**
P14	22.20429	1.5	33.30644	74.23	8.615683	2	0.5	0.75	**19.08**	0.67	0.32	**19.64**	0.3	0.6	**120.42**
P15	28.65805	1.5	42.98708	50.14	7.08096	2	0.5	0.75	**27.17**	0.67	0.32	**28.92**	0.3	0.6	**132.33**

P16	22.14063	1.5	33.21095	142.69	11.94529	2	0.5	0.75	**16.16**	0.67	0.32	**15.74**	0.3	0.6	**158.78**
P17	21.12286	1.5	31.68429	50.51	7.107039	2	0.5	0.75	**19.99**	0.67	0.32	**21.26**	0.3	0.6	**97.82**
P18	17.15716	1.5	25.73574	63.37	7.960528	2	0.5	0.75	**15.34**	0.67	0.32	**16.01**	0.3	0.6	**87.15**
P19	19.98207	1.5	29.97311	44.51	6.671582	2	0.5	0.75	**19.52**	0.67	0.32	**20.98**	0.3	0.6	**87.97**
P20	19.24525	1.5	28.86787	63.94	7.996249	2	0.5	0.75	**17.17**	0.67	0.32	**17.90**	0.3	0.6	**98.11**
P21	19.1563	1.5	28.73445	123.99	11.13508	2	0.5	0.75	**14.48**	0.67	0.32	**14.27**	0.3	0.6	**129.23**
P22	28.50602	1.5	42.75903	58.79	7.667464	2	0.5	0.75	**25.97**	0.67	0.32	**27.27**	0.3	0.6	**140.40**
P23	28.21197	1.5	42.31796	59.2	7.694154	2	0.5	0.75	**25.66**	0.67	0.32	**26.93**	0.3	0.6	**139.35**
P24	25.29982	1.5	37.94973	62.18	7.88543	2	0.5	0.75	**22.73**	0.67	0.32	**23.75**	0.3	0.6	**127.51**
P25	22.68314	1.5	34.02471	82.95	9.107689	2	0.5	0.75	**18.96**	0.67	0.32	**19.34**	0.3	0.6	**128.88**
P26	21.52673	1.5	32.2901	53.18	7.292462	2	0.5	0.75	**20.11**	0.67	0.32	**21.30**	0.3	0.6	**101.79**
P27	19.64334	1.5	29.46501	44.52	6.672331	2	0.5	0.75	**19.18**	0.67	0.32	**20.63**	0.3	0.6	**86.49**
P28	18.51044	1.5	27.76566	76.4	8.740709	2	0.5	0.75	**15.79**	0.67	0.32	**16.22**	0.3	0.6	**101.60**
P29	22.69873	1.5	34.0481	51.68	7.18888	2	0.5	0.75	**21.36**	0.67	0.32	**22.67**	0.3	0.6	**106.10**
P30	20.68584	1.5	31.02875	41.16	6.415606	2	0.5	0.75	**20.60**	0.67	0.32	**22.30**	0.3	0.6	**88.29**
P31	20.45865	1.5	30.68797	59.81	7.733693	2	0.5	0.75	**18.56**	0.67	0.32	**19.46**	0.3	0.6	**101.48**
P32	22.80444	1.5	34.20666	82.47	9.081299	2	0.5	0.75	**19.09**	0.67	0.32	**19.48**	0.3	0.6	**129.25**
P33	35.9456	1.5	53.9184	40.18	6.33877	2	0.5	0.75	**36.02**	0.67	0.32	**39.06**	0.3	0.6	**151.97**
P34	27.31002	1.5	40.96502	69.93	8.362416	2	0.5	0.75	**23.82**	0.67	0.32	**24.65**	0.3	0.6	**144.48**
P35	24.9287	1.5	37.39305	125.44	11.2	2	0.5	0.75	**18.79**	0.67	0.32	**18.50**	0.3	0.6	**169.02**
P36	25.80813	1.5	38.71219	62.59	7.911384	2	0.5	0.75	**23.15**	0.67	0.32	**24.18**	0.3	0.6	**130.42**
P37	20.59106	1.5	30.88659	61.08	7.815369	2	0.5	0.75	**18.58**	0.67	0.32	**19.45**	0.3	0.6	**103.02**
P38	18.76032	1.5	28.14048	69.28	8.323461	2	0.5	0.75	**16.40**	0.67	0.32	**16.99**	0.3	0.6	**98.86**
P39	18.42381	1.5	27.63572	114.36	10.69392	2	0.5	0.75	**14.21**	0.67	0.32	**14.10**	0.3	0.6	**120.02**
P40	29.31235	1.5	43.96853	25.03	5.002999	2	0.5	0.75	**33.06**	0.67	0.32	**37.33**	0.3	0.6	**103.37**
P41	32.0643	1.5	48.09645	32.25	5.678908	2	0.5	0.75	**33.94**	0.67	0.32	**37.51**	0.3	0.6	**124.46**
P42	31.0129	1.5	46.51934	51.18	7.15402	2	0.5	0.75	**29.25**	0.67	0.32	**31.08**	0.3	0.6	**144.39**
P43	29.2998	1.5	43.9497	63.8	7.98749	2	0.5	0.75	**26.15**	0.67	0.32	**27.27**	0.3	0.6	**149.24**

P44	28.77379	1.5	43.16068	58.12	7.623647	2	0.5	0.75	**26.29**	0.67	0.32	**27.63**	0.3	0.6	**141.06**
P45	32.45115	1.5	48.67672	34.54	5.877074	2	0.5	0.75	**33.77**	0.67	0.32	**37.10**	0.3	0.6	**129.33**
P46	27.12344	1.5	40.68516	60.52	7.77946	2	0.5	0.75	**24.53**	0.67	0.32	**25.70**	0.3	0.6	**135.19**
P47	21.80079	1.5	32.70118	62.85	7.927799	2	0.5	0.75	**19.53**	0.67	0.32	**20.39**	0.3	0.6	**110.36**
P48	18.59065	1.5	27.88597	60.43	7.773674	2	0.5	0.75	**16.82**	0.67	0.32	**17.62**	0.3	0.6	**92.60**
P49	27.62026	1.5	41.43038	33.31	5.771482	2	0.5	0.75	**29.00**	0.67	0.32	**31.96**	0.3	0.6	**108.55**
P50	27.70038	1.5	41.55057	68.39	8.269825	2	0.5	0.75	**24.30**	0.67	0.32	**25.19**	0.3	0.6	**145.20**
P51	38.75718	1.5	58.13577	32.61	5.710517	2	0.5	0.75	**40.91**	0.67	0.32	**45.17**	0.3	0.6	**151.08**
P52	26.32151	1.5	39.48227	111.05	10.53803	2	0.5	0.75	**20.45**	0.67	0.32	**20.35**	0.3	0.6	**169.31**
P53	29.58701	1.5	44.38052	65.54	8.095678	2	0.5	0.75	**26.23**	0.67	0.32	**27.29**	0.3	0.6	**152.38**
P54	21.13406	1.5	31.70109	176.78	13.29586	2	0.5	0.75	**14.62**	0.67	0.32	**13.98**	0.3	0.6	**166.54**
P55	18.41074	1.5	27.61611	183.13	13.53255	2	0.5	0.75	**12.63**	0.67	0.32	**12.04**	0.3	0.6	**147.37**
P56	27.42101	1.5	41.13151	66.35	8.145551	2	0.5	0.75	**24.24**	0.67	0.32	**25.19**	0.3	0.6	**141.94**
P57	32.57502	1.5	48.86253	50.89	7.133723	2	0.5	0.75	**30.77**	0.67	0.32	**32.70**	0.3	0.6	**151.32**
P58	30.94118	1.5	46.41177	79.25	8.902247	2	0.5	0.75	**26.16**	0.67	0.32	**26.78**	0.3	0.6	**172.46**
P59	31.22908	1.5	46.84362	53.41	7.308215	2	0.5	0.75	**29.14**	0.67	0.32	**30.85**	0.3	0.6	**147.93**
P60	23.23398	1.5	34.85096	92.37	9.610931	2	0.5	0.75	**18.91**	0.67	0.32	**19.10**	0.3	0.6	**138.14**
P61	22.87001	1.5	34.30502	65.22	8.07589	2	0.5	0.75	**20.30**	0.67	0.32	**21.13**	0.3	0.6	**117.55**
P62	20.32661	1.5	30.48992	50.3	7.092249	2	0.5	0.75	**19.25**	0.67	0.32	**20.49**	0.3	0.6	**93.98**
P63	29.37257	1.5	44.05885	46.08	6.788225	2	0.5	0.75	**28.44**	0.67	0.32	**30.49**	0.3	0.6	**131.11**
P64	29.72587	1.5	44.58881	55.41	7.443789	2	0.5	0.75	**27.49**	0.67	0.32	**29.01**	0.3	0.6	**142.92**
P65	31.68384	1.5	47.52575	53.79	7.334167	2	0.5	0.75	**29.51**	0.67	0.32	**31.23**	0.3	0.6	**150.51**
P66	23.86957	1.5	35.80436	125.44	11.2	2	0.5	0.75	**17.99**	0.67	0.32	**17.71**	0.3	0.6	**161.84**
P67	28.7947	1.5	43.19204	62.32	7.894302	2	0.5	0.75	**25.85**	0.67	0.32	**27.01**	0.3	0.6	**145.26**
P68	27.1132	1.5	40.66979	69.74	8.351048	2	0.5	0.75	**23.67**	0.67	0.32	**24.49**	0.3	0.6	**143.27**
P69	25.53397	1.5	38.30096	51.08	7.147027	2	0.5	0.75	**24.09**	0.67	0.32	**25.60**	0.3	0.6	**118.79**
P70	18.95356	1.5	28.43034	170.24	13.04761	2	0.5	0.75	**13.24**	0.67	0.32	**12.70**	0.3	0.6	**146.89**
P71	33.19005	1.5	49.78507	38.9	6.236986	2	0.5	0.75	**33.53**	0.67	0.32	**36.46**	0.3	0.6	**138.55**

P72	33.91112	1.5	50.86668	51.85	7.200694	2	0.5	0.75	**31.88**	0.67	0.32	**33.83**	0.3	0.6	**158.72**
P73	23.52219	1.5	35.28329	125.87	11.21918	2	0.5	0.75	**17.72**	0.67	0.32	**17.44**	0.3	0.6	**159.72**
P74	28.64295	1.5	42.96442	56.45	7.513322	2	0.5	0.75	**26.36**	0.67	0.32	**27.78**	0.3	0.6	**138.76**
P75	30.44407	1.5	45.6661	54.52	7.383766	2	0.5	0.75	**28.26**	0.67	0.32	**29.87**	0.3	0.6	**145.42**
P76	37.97715	1.5	56.96573	27.9	5.282045	2	0.5	0.75	**41.69**	0.67	0.32	**46.63**	0.3	0.6	**139.49**
P77	18.95342	1.5	28.43013	154.35	12.42377	2	0.5	0.75	**13.57**	0.67	0.32	**13.12**	0.3	0.6	**140.68**
P78	26.77205	1.5	40.15808	59.33	7.702597	2	0.5	0.75	**24.33**	0.67	0.32	**25.53**	0.3	0.6	**132.36**
P79	30.20927	1.5	45.31391	71.45	8.45281	2	0.5	0.75	**26.21**	0.67	0.32	**27.07**	0.3	0.6	**161.25**
P80	22.08861	1.5	33.13292	90.35	9.505262	2	0.5	0.75	**18.07**	0.67	0.32	**18.30**	0.3	0.6	**130.11**
P81	25.92538	1.5	38.88807	64.81	8.050466	2	0.5	0.75	**23.05**	0.67	0.32	**24.00**	0.3	0.6	**132.91**
P82	27.59399	1.5	41.39099	57.96	7.613147	2	0.5	0.75	**25.23**	0.67	0.32	**26.52**	0.3	0.6	**135.13**
P83	34.33219	1.5	51.49829	30.21	5.496362	2	0.5	0.75	**36.94**	0.67	0.32	**41.05**	0.3	0.6	**129.97**
P84	21.65755	1.5	32.48632	34.17	5.845511	2	0.5	0.75	**22.60**	0.67	0.32	**24.85**	0.3	0.6	**85.96**
P85	22.67044	1.5	34.00565	37.74	6.143289	2	0.5	0.75	**23.07**	0.67	0.32	**25.16**	0.3	0.6	**93.52**
P86	20.01106	1.5	30.01659	79.17	8.897753	2	0.5	0.75	**16.92**	0.67	0.32	**17.33**	0.3	0.6	**111.49**
P87	19.44195	1.5	29.16293	79.77	8.931405	2	0.5	0.75	**16.41**	0.67	0.32	**16.79**	0.3	0.6	**108.66**
P88	17.18968	1.5	25.78451	103.88	10.19215	2	0.5	0.75	**13.58**	0.67	0.32	**13.59**	0.3	0.6	**107.45**
P89	18.09802	1.5	27.14703	74.98	8.659099	2	0.5	0.75	**15.52**	0.67	0.32	**15.96**	0.3	0.6	**98.56**
P90	18.19053	1.5	27.28579	77.86	8.823831	2	0.5	0.75	**15.45**	0.67	0.32	**15.84**	0.3	0.6	**100.64**
P91	17.98793	1.5	26.9819	73.37	8.565629	2	0.5	0.75	**15.50**	0.67	0.32	**15.98**	0.3	0.6	**97.08**
Average			**39.08515**		**8.287701**				**23.63**			**24.83**			**133.32**